EXPERIMENTAL AND THEORETICAL STUDIES OF TRANSIENT MOLECULES

A thesis
submitted in partial fulfilment
of the requirements for the degree of

Doctor of Philosophy in Chemistry

in the

University of Canterbury

by

John Andrew Harrison

University of Canterbury
1988

To my family.

"Certainly the atoms did not post themselves purposefully in due order by an act of intelligence, nor did they stipulate what movements each should perform. As they have been rushing everlastingly throughout all space in their myriads, undergoing a myriad changes under the disturbing impact of collisions, they have experienced every variety of movement and conjunction till they have fallen into the particular pattern by which this world of ours is constituted."

Titus Lucretius Carus. Circa 55 BC.

ACKNOWLEDGEMENTS

The work described in this thesis could not have been completed without the assistance and guidance of a number of people. Firstly, friend and mentor, Professor Leon. F. Phillips, deserves considerable thanks for acting as supervisor during the past few years. I am also greatly appreciative of the time and energies of Drs. Robert. G. A. R. Maclagan and Peter. W. Harland. Thanks also to Drs. Bryce Williamson, Gordon A. Rodley and Andrew Abell who have been the source of a variety of worthwhile diversions.

The skills of the department's technical staff are humbly acknowledged. In particular the abilities of R. W. Gillard, K. Gillard, R. M. McGregor, D. J. MacDonald, A. M. Fergusson and B. Reid have contributed to my sanity during many a trying problem.

The friendship, enthusiasm and sense of humour of fellow researchers: Dr. Andy Whyte, Sean Smith, Dr. Richard Simpson, Pravit Sudkeaw, Brett Cameron, Gordon Cameron, Roger Meads,David Moore and Dr. Pascal Roussel; is greatly appreciated.

I am grateful for the award of a U. G. C. Postgraduate Scholarship over the past three years.

TABLE OF CONTENTS

LIST OF FIGURES

LIST OF TABLES

ABSTRACT

Room temperature bimolecular rate constants for the reactions :

1 $NH + N_2H_4$ ---> products
$k_1 = (3.6 \pm 2.2) \times 10^{-15}$ cm^3 $molec^{-1}$ s^{-1}

2 $NH + NO$ ---> products
$k_2 = (5.78 \pm 0.64) \times 10^{-11}$ cm^3 $molec^{-1}$ s^{-1}

3 $NH + NO_2$ ---> products
$k_3 = (1.61 \pm 0.14) \times 10^{-11}$ cm^3 $molec^{-1}$ s^{-1}

4 $BH + NO$ ---> products
$k_4 = (15.6 \pm 2.3) \times 10^{-11}$ cm^3 $molec^{-1}$ s^{-1}

5 $BH + C_2H_4$ ---> products
$k_5 = (14.4 \pm 1.7) \times 10^{-11}$ cm^3 $molec^{-1}$ s^{-1}

have been measured along with upper limits for the reaction rates of :

6 $BH + O_2$ ---> products
$k_6 < 1.1 \times 10^{-11}$ cm^3 $molec^{-1}$ s^{-1}

7 $BH + CH_4$ ---> products
$k_7 < 9.4 \times 10^{-13}$ cm^3 $molec^{-1}$ s^{-1}

8 $BH + C_2H_6$ ---> products
$k_8 < 1.6 \times 10^{-12}$ cm^3 $molec^{-1}$ s^{-1}

9 $BH + CO$ ---> products
$k_9 < 1.3 \times 10^{-13}$ cm^3 $molec^{-1}$ s^{-1}

All rates were measured at 1 torr buffer pressure. The effect of temperature on the rate constants for reactions 2,3,4 and 5 has been investigated along with the effect of varying the nature of the third body. NH ($X,^3\Sigma^-$) was generated from KrF 248.5 nm excimer laser photolysis of hydrazine and detected by laser induced fluorescence at 336 nm (A --> X, Q(0,0)). BH ($X,^1\Sigma$) was produced from ArF 193 nm excimer laser photolysis of diborane and the concentration was monitored by 433.4 nm laser induced fluorescence of the A --> X, Q(0,0) transition.

Ab-initio calculations of species important on the potential energy surfaces of the systems:

$NH + NO, NO_2$
$NH_2 + NO, NO_2$
$BH + NO$
$BH_2 + NO$

have been carried out in order to compliment the data obtained in the above, and future, experiments.

Prompt emission observed in the 193 nm photolysis of diborane has been characterized. The emission bands and probable emitters (in brackets) were :

249.7, 208.9 nm (Boron atomic lines)
254 - 326 nm (BH_3^*)
320 - 340 nm (BH_2^*)
366 - 388 nm (BH_3^*)
423 - 450 nm (BH A - X)

Assignment of the probable emitter was based on band structure, thermochemistry and observed power dependence of each of the bands. The two bands attributed to BH_3^* are the first experimentally detected electronic transitions for this important species. The band attributed to BH_2^* is also a new transition.

An apparatus capable of generating a pulsed supersonic molecular beam has been constructed. Software and hardware to determine the translational temperature for species in the beam has been developed and temperatures for beams of various species have been measured.

CHAPTER 1

INTRODUCTION

The end result of any gas-phase kinetics study is an increased knowledge of the potential energy surface of all the atoms involved. This information may take the form of overall pressure or temperature dependences of the rate, representing averages of many fundamental processes occurring, or it may be more specific and focus on individual quantum states of one, or more, of the entities involved. The behaviour of all particles involved on the potential surface may be described by quantum mechanics. The ultimate aim of the kineticist must therefore be to gain a complete understanding of the processes occurring during a reaction, within the framework of quantum mechanics. The number of tools available to the kineticist are ever increasing. Advances in laser technology have facilitated the probing of chemical processes to an unheard of level [1.1]. Such studies as quantum state resolved unimolecular dissociations [1.2], real time femtosecond monitoring [1.3,1.4] and even studies of species as they undergo the bond forming and bond breaking processes [1.5] In parallel with these developments is the advancement of theoretical tools, not only *ab-initio* theories such as molecular orbital theory and valence bond approaches, but also theories describing the dynamics of the processes involved and statistical theories, such as RRKM theory. There is no doubt that the chemist's understanding of chemical reactivity depends on both experimental observation and theoretical prediction.

This thesis is concerned with the reactions of transient species produced by excimer laser photolysis of a stable precursor and has arisen from a continuing interest in gas phase kinetics in this laboratory. The fragments under study are monitored by the method of time-resolved laser induced fluorescence after production by photolysis of stable species by excimer laser radiation. The advantages of a well defined time-structure and the large concentration of radicals resulting from excimer laser photolysis do

not need expounding. Despite this, the photolysis process itself may not be well understood, and care must be taken during this type of experiment that no unexpected effects appear. The high intensity of UV light available from excimer lasers increases the probability of multi-photon processes and allows the kineticist access to an even larger variety of reactive radicals [1.6,1.7] The kinetics of two such species, NH(X) and BH(X), arising from multi-photon absorption by hydrazine (248.5 nm) and diborane (193 nm) respectively, are studied in this thesis.

To complement the experimental studies undertaken by this laboratory, the potential energy surfaces of the reactions of BH + NO, BH_2 + NO, NH + NO, NH + NO_2, NH_2 + NO and NH_2 + NO_2 have been investigated by calculating the properties of the intermediates, transition states and products. With current computer resources a complete investigation of such complex surfaces is not possible and thus only a very limited portion of the multidimensional surface may be investigated. By concentrating on the points on the surface that correspond to minima and first order saddle points (or cols) a minimum energy path may be traced out that corresponds to the more conventional notion of motion along the reaction coordinate. The use of these potential energy surfaces for dynamics calculations is very much an infant science [1.8] but with the increasing computing power and growing understanding of algorithms such studies are becoming more widespread [1.9]. There is no doubt that the ultimate goal of all experimental and theoretical work is the complete determination of that area of the potential surface that corresponds to the energies of chemical interest. The use of *ab-initio* theory to calculate the properties of the potential surface would be out of reach of most chemists were it not for the widespread distribution of such packages as GAUSSIAN 82 or GAMESS [1.10]. The dedication of a few groups to developing the software and implementing new theoretical advances, that any chemist, regardless of background, can then use is humbly acknowledged [1.11].

As theory becomes more accessible to the common chemist the ability to achieve high resolution experiments becomes more and more expensive. The usefulness of lasers to probe the potential surface is unquestioned [1.12], what is most difficult is the production of any particular point of the PES in sufficient quantity for detection. The recent developments in molecular beam technology [1.13] have allowed the study of transient

species whose lifetimes would be far too low at thermal temperatures.by laser and mass spectrometric based methods There have been many reviews on the usefulness of jet - cooled, collision free beams in the study of such species [1.14] and such an instrument has been developed as part of this study. The realization of crossed molecular beam experiments to reveal the finer details of molecular interactions and rearrangements has only been possible within the last three decades [1.15,1.16].

Although studies into the fundamental physical processes of nature need no further justification, the information gained is of practical use and may often be of commercial importance. Only through the detailed investigation into the elementary processes involved may we begin to comprehend such complex phenomena as atmospheric and combustion chemistry. Knowledge of the temperature and pressure dependences, product distributions and energetics of elementary reactions are essential if the modelling of physical phenomena [1.17] is to become anything more than an empirical past-time. The modelling of fuel combustion would seem a hopeless task in view of the enormous number of unknown parameters, but often the overall process is dependent on only a few of the elementary steps and knowledge of these particular bottlenecks can lead to a near quantitative explanation of the observed behaviour. In this respect the chemistry of Nitrogen containing species is important in a great number of combustion systems i.e. any system containing N and H will involve the reactions of NH and NH_2. The chemistry of small boranes has not received as much attention with only three recently reported studies on the gas phase reactions of BH and BH_3. Boron containing fuels have great potential due to the extremely high exothermicities and very high reaction rates. Small boron - hydrogen containing species are also ideal candidates for ab-initio calculations due to the low number of electrons. Individual boron containing species are in themselves interesting and very little about the electronic structures and geometries has been determined experimentally. During the course of these studies it was observed that the prompt emission arising from the 193 nm photolysis of diborane contained many previously unknown bands. Although this technique has been extensively used for investigation of primary photochemical processes in molecules whose electronic transitions have already been thoroughly investigated [1.18], it would seem experiments of this type have enormous, but as yet largely unrealized, potential for generation of spectra of transient species. The bands observed have been

tentatively assigned on the basis of observed laser power dependence, energetics and band shape to a new band of BH_2, two new bands of BH_3 and to the well known BH(A-X) and atomic boron emissions. BH_2 has been seen previously in absorption by other workers but despite considerable effort from many groups the electronic transitions of BH_3 had eluded detection prior to this study.

The reactions of NH_2 with NO and NO_2 have been found to be fast despite involving a considerable amount of bond breaking and bond formation. An investigation of the PES of NH_2 + NO reveals the elementary steps in the reaction may proceed essentially without any energy barriers and thus the reaction rate is dominated by effects due to initial formation of the H_2NNO intermediate and not the subsequent rearrangement. This particular reaction has some commercial importance as a key step in the patented Thermal DeNOx process, where a nitrogen containing species capable of forming NH_2 is injected into flue gases containing Nitrogen oxides and Oxygen. The ensuing reactions ultimately produce NN bonds. This process is already in use in West German power stations and several processes have been proposed use in removal of NOx in engine exhausts. NH_2 is also an important atmospheric specie and may act as either a source or sink for NOx in this system.

The rapidly expanding field of gas phase kinetics remains one of the most challenging and rewarding areas of all science

CHAPTER 2

EXPERIMENTAL

Laser photolysis was used to generate free radicals of interest in a fast flow system. The radicals were then monitored either directly, by their prompt emission (chapter 7), or in the kinetics studies (chapters 6,9), by time resolved laser induced fluorescence. Laser photolysis / laser induced fluorescence (LP/LIF) is now a standard technique for the study of fast reactions and has already been briefly discussed in chapter 1. The general descriptions, operating parameters and specifications for the equipment used in the kinetic and spectroscopic studies are given below. Discussion of the equipment unique to the molecular beam will be given in chapter 11.

2.1 Apparatus

A. Excimer Laser

The photolysis source used was a Lumonics 861-T thyratron switched Excimer Laser operating on either ArF (193.3 nm) or KrF (248.5 nm). Typical output descriptions are given in Table 2-1. The power output of the excimer laser was measured with a Scientech model 364 power/energy meter and the spectral distribution of the beam was measured by a McPherson model 218 (0.3 m) monochromator (section 2.1F). For the experiments involving production of the NH and BH radicals the output beam was focussed from its initial 2 cm x 1 cm cross section to a point approximately 2 mm x 1 mm by a 0.6 m focal length lens placed between the laser and the photolysis cell.

Table 2-1. Excimer Laser Output Characteristics.

	ArF	KrF
Wavelength (nm)	193.3	248.5
Pulse Width (ns)	10	10
Pulse Energies (mJ)	50 - 100	75 - 100
Repetition rate (Hz)	15 - 35	40
Bandwidth (FWHM, cm^{-1})	100	100

B. Dye Laser

The laser induced fluorescence excitation source was an AVCO model C4000 tunable dye laser pumped by an AVCO C5000 pulsed nitrogen laser. The nitrogen laser produced 10 ns pulses corresponding to 100 kW peak power at 337.1 nm. The dye laser output consisted of 2-8 ns pulses of between 2 and 150 μJ per pulse. The bandwidth (fwhm) of the output was < 0.1 nm when the dye laser was properly tuned. To obtain 336.1 nm light for the NH studies it was necessary to frequency double the output at 672.2 nm of a mixture of CV670 and R590 dyes with an angle-tuned potassium dihydrogen phosphate (KDP) crystal (Interactive Radiation, Inc.). The 306.4 nm light for LIF detection of OH in the NH + NO experiment was obtained by frequency doubling the output of R590 dye at 612.8 nm with a temperature phase-matched ammonium dihydrogen arsenate crystal tuned using an INRAD 5-1 temperature phase-matching system (both Interactive Radiation, Inc.). A summary of dyes used and their various properties is given in Table 2-2.

Table 2-2. Dye Laser specifications.

Species	Wavelength (nm)	Dye (a)	Conc. (mmol l^{-1})	Solvent
BH	433.4	S420	1.8	water
NH	336.1 (b)	CV670/	3.3/	
		R590	2.5	ethanol
OH	306.4 (c)	R590	5.3	ethanol

(a) All dyes supplied by Exciton Chemical Company, Inc.
(b) Frequency doubled by Angle-Tuned KDP crystal
(c) Frequency doubled by Temp. Phase-Matched ADA crystal

C. Photolysis Cell

Photolysis cells were purpose built in the glassblowing workshop of this department. Special features associated with each cell are described in the appropriate chapters. Generally there were several criteria that were borne in mind when the cell was designed and built. These were:

1) Temperature control and measurement: Temperature control was achieved by having two sidearms long enough so the gas mixture could equilibrate with the cell wall temperature. The 30 cm sidearms were therefore constructed using a double layer of glass tubing so that coolant could be flowed through the temperature jacket. Using various liquids the temperature range available was $250 < T < 350$ K. The liquid used was circulated by an in-line pump from the reservoir through the temperature jacket and back into the thermo-stated reservoir. The cell was insulated with several layers of glass wool. Under normal operating conditions the temperature of the liquid after passing through the jacket and pump was within 5 °C of the reservoir temperature. The temperature was measured using a precalibrated copper-constantin thermocouple situated just below the viewing region inside the cell. For the NH experiments the thermocouple was fed through a pinhole in the throat of the exhaust port and torr-sealed in place. In the subsequent BH experiments a purpose built B7 ground glass

joint was included so that the thermocouple could be easily removed for maintenance and calibration checks (without the simultaneous destruction of the cell as had occurred with the previous, NH cell). This technique of temperature measurement gave an accurate and reliable value of the gas temperature near the active site.

2) Pressure monitoring: In the NH experiments the pressure was measured by a Texas Instruments quartz spiral gauge, connected to the cell through a glass line blown onto the side of the cell, near the active region. The pressures of the later BH experiments were measured with a 0-10 Torr MKS Baratron. The Baratron was fitted with a B19 cone which fitted into a right angle adaptor connected to the cell.

3) Sufficient pumping speed: Pumping was provided by a two stage rotary pump (Welch 1397B, pumping speed 450 l min^{-1}). Gas was first pumped through a cold trap at -196 °C to remove corrosive gasses before passing through the pump, and to stop pump oil from getting into the reaction cell. The pumping system was upgraded for the BH experiments by using the Welch pump as the backing pump for a Heraeus R150 roots blower. The pumping speed was such that the contents were effectively swept out between laser pulses at the repetition rates used. No effect on the measured BH rate constants was noticed when the roots blower was not used, indicating that the system had sufficient pumping speed to avoid build-up of reaction and photolysis products.

4) Rugged construction: Schott Duran glass was used as the construction material. After construction the cells were annealed overnight to relieve strain. Glass construction, although inherently fragile, enabled subsequent modifications to the cells to be made with relative ease over that required with, for example, stainless steel. Quartz windows (suprasil) were epoxied (Torr-seal) onto the ends of the sidearms. B34 ground glass joints were provided for photomultiplier and monochromator attachment. All joints were lubricated with Apiezon 'N' or 'H' grade vacuum grease. Gas was introduced at both ends of the cells so that some of the gas flowed past the windows, effectively eliminating dead space and the build-up of opaque photolysis products on the windows during the course of the experiment. The minimum base pressure typically obtainable was 5-10 mTorr. Cell life varied from one week to several months.

5) Minimisation of stray light: The principle causes of stray light were :

a) Room lights. This was eliminated by painting the cell with several layers of matt black paint.

b) Window fluorescence: Although the windows were of high grade quartz (suprasil), defects and non-linear effects inside the quartz caused broad-band emission. This effect was especially noticeable with 193 nm irradiation. The emission intensity seen by the photomultiplier diminished with distance from the windows but could not be completely eliminated. This caused a minimum delay period of around 50 μs before data could be collected. In practice this was not a serious problem because a delay of this magnitude was necessary to ensure complete thermalisation of the fragments with the bath gas.

c) Scattering of photolysis and probe lasers: This was a problem with all optical elements along the laser paths. The effect was reduced by ensuring that all the optical elements were off axis, so that all reflections were directed away from the critical region. Windows were angled approximately 30 degrees from perpendicular. Scattering from the photolysis pulse into the photomultiplier was eliminated by a suitable combination of either interference or Corning glass filters to select the wavelength region of interest. Initial alignment of the cell and optical elements was achieved using a He-Ne laser directed along the paths of either the photolysis or probe beams. The probe laser was optimised with respect to the background scatter and LIF intensity before each experiment.

D. Vacuum Line

The vacuum line used for the laser experiments may be divided into two parts; the preparation line and the manifold connected to the photolysis cell. The preparation line was pumped by either a two stage glass diffusion pump or a 1" Edwards diffusion pump. Several bulbs were incorporated into this line for gas purification and storage. The diborane was produced in a purpose built vacuum line housed remotely from the main laboratory for safety and convenience. The main vacuum manifold connected to the cell included several novel features. The first of these was an array of taps that enabled any of the several gas lines to be directed into any of the available

flowmeters. Another useful feature was the ability to measure the pressure (with the MKS 0-1000 torr Baratron) in one of the many independent gas lines that comprised the system. Generally the geometry of the system was dictated by the nature of the gases in each line. The handling procedures for individual gases are given in section 2.2. The glass gas lines were continually monitored for leaks by checking the pressure and by frequent use of a Tesla coil. Taps were supplied by J. Young, Scientific Glassware Limited. All vacuum pumps, including diffusion pumps, were isolated from the vacuum lines by liquid nitrogen traps. Glass construction of the vacuum system allowed (many and varied) modifications to be made swiftly and cheaply. The vacuum systems of the molecular beam will not be described until chapter 11.

E. Photomultipliers

Two photomultipliers were used :
EMI 9813 QA - Bialkali response, high gain, low dark current, high blue response. Quantum efficiency (QE) 26% at 360 nm falling to 2% at 600 nm.
EMI 9558 QB - S20 response (trialkali - high red sensitivity). QE 22% at 400 nm falling to 2% at 800 nm.

Both photomultipliers were shielded by mu-metal. Pre-amplifiers, where used, were contained inside the same housing as the photomultiplier in order to minimise electrical noise pick-up before amplification.

F. Monochromator

Two McPherson monochromators (model 218, 0.3 m) were used for a variety of functions. These monochromators were equipped with snap-in gratings, of which there were three available for use (blazed at 500, 300 and 150 nm, all 1200 grooves / mm). For the experiments of chapter 7, care was taken to ensure the grating and photomultiplier combination with the optimum efficiency in the region of interest was used. Typical specifications for the 300 nm grating were 75% efficiency at 296.0 nm decreasing to 58% at 404.6 nm (before detection). Maximum first order resolution achievable in practice was 0.07 A (minimum entrance and exit slits). The wavelength scales of both monochromators were calibrated using a Pen Ray Hg lamp.

G. Instrumentation

(1) Boxcar Integrator

The main data acquisition device for the kinetics and emission studies was a Princeton Applied Research (PAR) model 160 Boxcar integrator. This instrument enabled signal gating and averaging either directly or as a slave device of the PDP11/23 minicomputer. In all experiments care was taken to optimise carefully the various parameters of the Boxcar so that optimum signal/noise was obtained along with ensuring that the various time constants, inherent in Boxcar operation, did not affect the data in an undesirable way. For the kinetics experiments this meant, in practise, that the gatewidth was optimised with respect to the LIF pulse and the minimum time constant was selected.

(2) Oscilloscopes

The Textronix Inc. 500 MHz 7904 oscilloscope was invaluable for monitoring the time dependent features of the kinetics experiments, and for general trouble-shooting of the experimental system. Especially useful was the dual timebase feature which allowed quick checks on the individual timing aspects of each piece of apparatus (i.e. excimer laser, dye laser, boxcar gate position and width), over the various timebases used. The 7904 mainframe was fitted with the following modules : 7A26 dual trace amplifier; 7A22 differential amplifier; 7B85 (A) delaying timebase; and 7B80 (B) timebase.

A 20 MHz dual trace (COS 5020) oscilloscope was sufficient for monitoring of signals in the molecular beam experiments. Data collection of arrival time distributions was achieved using the transient recorders described below. The LeCroy Waveform - Catalyst system, as configured in our system, effectively functions as a 32 MHz dual trace digital storage oscilloscope.

(3) Transient Recorders

The transient recorders used in the measurement of the lifetime of BH A -> X emission (chapter 7) and in the molecular beam time of flight determinations (chapter 11), were two LeCroy TR8837F 32MHz recorders situated in a LeCroy 8013A Camac crate. The input for these two recorders was first amplified by a LeCroy 6103 dual channel, programmable gain

amplifier, also situated in the crate. The amplifier also provided the source of the record stop pulse needed by the transient recorders. All modules in the crate were controlled by LeCroy's Waveform-Catalyst digital storage oscilloscope software running on a Sundox PC/XT. Communication between the camac and the computer was via IEEE Standard 488 (1978) GPIB interfaces (Camac- LeCroy 8901A; Sundox- Singular model I-7210-C interface card).

(4) Pressure Gauges

Several pressure gauges were used during the course of these studies. A high performance capacitance manometer (MKS Instruments Inc., 0-1000 torr, type 315BH-1000, control unit 270M) was attached to the vacuum manifold to enable the pressures of bulbs, the hydrazine saturator, line pressures, amongst others, to be monitored. Reference vacuum for this device was supplied at $< 10^{-6}$ torr by either a two stage glass diffusion pump or an Edwards 1" diffusion pump. For the more accurate pressure readings required for the kinetics experiments, either a Texas Instruments Inc. model 144 quartz spiral gauge (NH, chapter 6) or an MKS Instruments Inc. 0-10 torr type 222CA capacitance manometer (BH, chapter 9) were used. The 0-10 torr Baratron was calibrated before use by zeroing the display at $< 10^{-6}$ torr. The reference vacuum for this instrument is supplied internally. The reference vacuum for the Texas Instruments gauge was maintained by a 2 stage glass diffusion pump. Gas pressures in the molecular beam sample preparation and nozzle lines were measured by an MKS 221AA (10000 torr) capacitance manometer connected to an MKS PDRC-1B power- supply readout. Measurement of the high vacuum inside the molecular beam will be discussed in chapter 11. The error in all pressure readings was taken as 1%.

(5) Flowmeters

Flow rates were measured with either Hastings mass flowmeters, or for the later BH experiments, with Tylan FM360 flowmeters. Capacity of the flowmeters ranged from 5 to 1000 sccm. All flowmeters were calibrated using standard bubble tube techniques. Calibration factors were calculated from the ratios of actual flow / indicated flow and for all flowmeters other than the Hastings 500 sccm, yielded a correction factor independent of flow rate. A quadratic fit was used for the 500 sccm Hastings mass flowmeter. All flowmeters were spot-checked over the course of these experiments and no major deviations from the original calibration factors were found. The

Hastings flowmeters were connected to a digital voltmeter, adjusted for 1.5 V fsd. Readings were taken directly from the dvm and later converted into the actual flow (section 2.4). The Tylan flowmeters were connected to a RO20A readout box that gives the flowrate directly (in sccm). Flows to the 5 and 10 sccm flowmeters were controlled by a Granville-Phillips variable leak or by a Whitey needle valve. All other flows on the kinetics apparatus were controlled by Edwards needle valves. Gas flows on the molecular beam sample line were measured and controlled by an MKS mass flowmeter/controller (258/259) connected to an MKS type 250B controller. A Whitey needle valve, in series with the mass flowmeter, enabled manual control of the flow.

H. Computers and Software

(1) Kinetics experiments:

Initial data acquisition and subsequent processing of the boxcar data was performed by a Digital Equipment Corporation PDP11/23 minicomputer. Collection was via an AXV11-C interface which has 16 analogue to digital conversion channels and two digital to analogue outputs (all 12 bit). The PDP system incorporated two 8 inch floppy disk drives (RX02) for program and data storage, along with a Sundox dot matrix printer.

Data acquisition was performed by program BOXCAR. BOXCAR, an interactive program, allowed control over the time delay (as a portion of the preset boxcar timebase) and number of points to be taken, as well as the number of measurements at each point, and the settling time between measurements. The program had the facility for collection of background points (corresponding to the boxcar zero offsets) before, and after, the scan. BOXCAR stored all data to a disk file; including background values, sampling parameters and (X,Y) data points. These files were later processed by program BOXFIT; another interactive program. BOXFIT subtracted the average background values and, if desired, a stored background file. BOXFIT then extracted the fluorescence decay rate from a linear least-squares analysis of the log(intensity) vs time data points. The ratio of the sum of the RMS deviation between calculated and observed fluorescence intensities to the peak fluorescence intensity gave an indication of the quality of fit. Typically this ratio was less than 1% for fast decays (i.e. high [Reactant]) rising to 5% for zero [reactant] decays. Gas flows were calculated by program

GCOMP. GCOMP automatically subtracted the flowmeter zero offset from the indicated flow and then converted this to an actual flow using the calibration factors for each flowmeter and gas component. Heat capacity correction factors for each gas were obtained directly from the flowmeter manufacturers' data. Overall concentrations of each gas present were computed from partial flow rate, the known temperature and the absolute cell pressure. Errors in the concentrations thus calculated were estimated to be around 6%.

The [reactant concentration, fluorescence decay rate] data pairs were then linear least squares and Students t-tested by program LSQFIT. The bimolecular rate constant along with 90% and 95% confidence limits were thus obtained. BOXCAR, BOXFIT, GCOMP, and LSQFIT were written by Professor L. F. Phillips in BASIC.

(2) Spectra:

Spectra were collected via the AXV11-C by program SCANYT. This program can collect a maximum 2000 data points over a timescale defined by the user. The data file thus collected was then transferred to a Sundox PC-XT microcomputer via a RS232 link, for further processing. The sending program was FISEND the receiving program a version of KERMIT. Once transferred to the PC the file was processed using program PSPEC. PSPEC allowed visual observation of the spectrum and had some processing ability (cursor selection of regions of interest, automatic calibration from two known features, etc.). Final hardcopy resolution was 800 x 600 pixels/screen. SCANYT and FISEND were written in BASIC by Professor L. F. Phillips. KERMIT is public domain software. PSPEC was written in Microsoft Fortran by the author.

(3) Molecular Beam:

Data acquisition through the LeCroy Catalyst system will be described, along with the data processing program (ATD), in chapter 11.

2.2 Gases

Gases used can be described in three categories: buffer gases, radical precursors and reactants. Table 2-3 summarizes the source and purification methods of the various gases used. The purity of the diborane used varied with the length of time from manufacture. The given purity of >95% is estimated from mass spectrometric analysis of a sample taken after the emission experiments, described in chapter 7, with impurities being H_2 and higher boranes.

Table 2-3. Gas source and purification methods.

Gas	Use (a)	Source (b)	Grade	Nominal Purity %	Purification Method (c)
Ar	B	NZIG	Welding	>99.99	BASF-BTS 150 EtOH/Dry Ice
B_2H_6	RP	Synth(d)	-	>95	Distillation
CH_4	R	NZIG	UHP	>99.97	-
C_2H_4	R	NZIG	CP	>99.5	-
C_2H_6	R	Math	CP	>99	-
CO	R	Math	CP	>99.5	-
He	B	NZIG	Scientific	>99.993	BASF-BTS 150 Liq N_2
N_2	B	NZIG	O_2 Free	>99.995	BASF-BTS 150 EtOH/Dry Ice
NH_3	RP	GCC	-	>99.9	Distillation
N_2H_4	RP	Fluka	Purum(I)		-
NO	R	Math	CP	>99.0	EtOH/Dry Ice
NO_2	R	Synth(e)			-
N_2O	B	NZIG	Medical	>99	BASF-BTS 100
O_2	R	Math	UHP	>99.99	-
SF_6	B	AP	Instrument	>99.99	-

(a) B = Buffer gas
R = Reactant
RP = Radical precursor

(b) AP = Air Products.
GCC = Christchurch Gas, Coal and Coke Co.
Math = Matheson Gas Products.
NZIG = New Zealand Industrial Gases

(c) BASF-BTS catalyst in reduced form, heated to temperature indicated (°C), followed by passing through a cold trap at either -78°C (EtOH/Dry Ice) or -196°C (liq N_2)

(d) Preparation of Diborane, B_2H_6.

Diborane was produced by the method described by Jeffers [2.1]. This involved heating pre-dried $SnCl_2$ and $NaBH_4$ to approximately 350°C in a vacuum system. The gases produced were separated by passing through three cold traps: ice/salt, dry ice/ethanol and liquid nitrogen. The diborane freezes in the liquid nitrogen trap (m.p.= -164.86°C, b.p.= -92.53°C [2.2]) with the higher boranes remaining trapped in the dry ice/ethanol trap. All non-condensables produced, notably H_2, are pumped away. Once the reaction was complete, as indicated by the cessation of frothing in the reaction vessel, the diborane was transferred by distillation into the cold finger of a 5 l glass bulb. The pressure in the vacuum line was kept below 10 Torr, to reduce the proportion of higher boranes formed, by controlling the temperature of the reactants. Yields were typically 90% of theoretical with sufficient quantity produced to fill the 5 l pyrex bulb with 0.5 atm of B_2H_6. To avoid polymerisation, which is rapid at room temperature, it was necessary to keep the diborane frozen at liquid nitrogen temperature until required. Disposal of surplus and waste diborane was carried out under vacuum by reaction with water sucked into the vessel where the diborane was situated. This method proved to be an efficient and safe way of disposing of diborane, and reaction mixtures containing diborane, producing relatively harmless boric acid.

(e) Preparation of Nitrogen dioxide, NO_2.

Nitrogen dioxide was prepared by the reaction of excess O_2 with NO in a 10 litre glass bulb. The mixture was then purified by freezing with liquid

nitrogen, pumping and then thawing. A pure sample was indicated by the absence of any blue or green colour in the frozen sample.

2.3 Experimental Procedures

This section contains a description of general methodology used in the kinetics and emission experiments. Molecular beam procedures will be briefly described in chapter 11.

The optimisation of the parameters and behaviour of all equipment used was completed before any data was collected. This usually involved several parameters that were optimised once for any given experiment and other parameters that had to be monitored continuously during the several weeks of experimentation. Parameters that fall into the first category were: the boxcar timebase, boxcar gatewidth, boxcar gain and time constant, initial and final fractions of the timebase over which the scan occurred, excimer laser (and hence overall) repetition rate, gross dye laser tuning, geometry of the laser pathways, and preparation of reaction gases. Parameters in the second category were: fine tuning of the above list - especially dye laser tuning and purification of the reaction gases, fluorescence optimisation and careful monitoring of all delays (in particular elimination of delay between the boxcar gate and dye laser pulse). The system was checked thoroughly for leaks before any days' experimentation, any anomaly with any of the various pieces of the equipment was rectified before continuing.

Most of the boxcar parameters were dictated by the nature of the experiment and signal to noise ratio. The timebase was decided upon from the rate of reaction and the concentration range of reactant necessary for reliable data. The repetition rate (17-40 Hz) was a compromise between the total time for an experiment (typically data acquisition lasted 2-3 hours) and the excimer laser lifetime (which decreases with increase in repetition rate). The experiments themselves involved collecting data for various concentrations of reactant (usually 20) and a series of zero reactant runs. Backgrounds were either collected for each concentration or, as was the case in the NH experiments, a couple of representative curves were averaged. In any run 500 individual fluorescence measurements were taken usually configured in the following way: 10 points at random, linearly spanning the selected timebase fractions, each with 50 fluorescence

measurements. Sufficient settling time was allowed for the boxcar to recover from the previous measurement before initiating data collection again. Data thus collected was then processed by the suite of programs available, as described above.

CHAPTER 3

AB-INITIO CALCULATIONS

3.1 Introduction

In this chapter a brief discussion of the elementary theory behind modern ab-initio molecular orbital calculations will be presented. There are many excellent texts on this subject and it is not intended to give anything other than a brief outline of some aspects of ab-initio theory that are relevant to this study [11.1,11.2].

Molecular Orbital theory requires that each electron within the molecule is placed within its own spin orbital. To take account of the symmetry properties of the many electron wavefunction these one electron orbitals are combined in a Slater determinant to give the overall electronic wavefunction. If the electronic wavefunction is assumed to be a single determinant this level of approximation to the true wavefunction is called Hartree-Fock theory.

A Hartree-Fock Theory.

The spin orbitals are comprised of a linear combination of one electron orbitals, usually these are the atomic orbitals of the constituent atoms (LCAO-MO). The variational theorem is invoked to determine the coefficients of the atomic basis functions, the best combination is that which minimises the electronic energy. This is achieved via the self-consistent field (SCF) approach which results in the best wavefunction possible for the basis set used at the single determinant level. The n electrons are placed in the desired orbitals such that the ground-state wavefunction corresponds to filling the n molecular orbitals with the lowest orbital energies. If the spin-orbitals are constrained to have the same spatial parts for both a and ß spins this level is termed restricted Hartree-Fock theory (RHF) and if different

spatial orbitals are used unrestricted Hartree-Fock theory (UHF). RHF theory is used for closed-shell species and UHF for open-shell. The best attainable wavefunction (that has an infinite basis set) will give the electronic energy at the Hartree-Fock limit.

The Hartree-Fock limit is not generally reached due to basis set truncation to give computationally manageable wavefunctions. The basis sets relevant to the calculations in sections 4, 5, 8, and 10 are discussed in section C. In general wavefunctions at the HF limit (or close to it) give good representations of the geometry and moderately good predictions for vibrational frequencies. They are not good enough for calculation of thermochemistry or when extremely accurate predictions of molecular parameters are required. This deviation away from the true molecular wavefunction is due to the neglect of the so-called correlation energy. Correlation energy arises from the correlated motion of electrons with different spin (the single determinant level includes correlation between electrons of the same spin). To include correlation effects in the wavefunction either other electron configurations are included via adding a linear combination of Slater determinants to the wavefunction, (Configuration Interaction -CI) and then using the variational theorem to determine the contribution of each determinant to the wavefunction, or by including the effects as perturbations on the reference determinant.

B Moller-Plesset Perturbation Theory (MPPT).

The first application of Rayleigh-Schrodinger perturbation theory to molecular systems was described by Moller and Plesset in 1934. MPPT involves starting with the reference HF wavefunction and including the effects of other configurations as a perturbation upon it. Usually this takes the form of a convergent series expansion involving a perturbation parameter with the series being truncated at the desired level. The HF wavefunction is taken as the zeroth approximation; inclusion of the first order correction corresponds to the MP2 wavefunction; second to MP3; third to MP4. Currently the truncation of the perturbation expansion to a level corresponding to inclusion of single, double and quadruple excitations from the reference configuration, (MP4SDQ) is a state of the art calculation readily available as part of Gaussian 82. With the advent of Gaussian 86, the ability

to include (important) effects of triple excitations (MP4SDTQ) has only recently, become available to the non-specialist.

C Basis Sets.

The two most frequently used types of basis set are those using Slater type atomic orbitals (STO) and those using Gaussian type descriptions for the atomic orbitals (GTO). Slater type orbitals are based on the wavefunctions for the Hydrogen atom and thus include a term exp-(zeta.r), where zeta is the orbital exponent, in the spatial portion. Guassian type orbitals, as the name suggests, have as the exponential term exp-(zeta.r^2) and because of this are favoured over STO's due to the analytic expressions for the resulting integrals. In general a greater number of GTO's than STO's are required to give the same accuracy mainly due to the failure of the GTO's to give the required cusp at the origin. As implied by the name, the package used for the studies reported here, utilises GTO's for basis functions.

A STO-NG basis set approximates each STO with N gaussians and are termed minimal basis sets since the number of orbitals used is the same as the number of electrons in the system. The most common of these is the STO-3G set. A double-zeta basis set is that which has each STO of a minimal basis replaced by two STO's differing in their orbital exponents. There have been several improvements made to these basis sets. The first is to introduce a split into the valence atomic orbital. An example of this basis set is the 4-31G set, where each core atomic orbital is comprised of a linear combination of four gaussians and the valence orbitals comprise two independent parts: an inner of three gaussians; and an outer single gaussian. This enables greater flexibility in the optimisation stages of the MO's. The valence orbitals may be subjected to a further split resulting in basis sets such as 6-311G. A further improvement results in the addition of polarisation functions to the atoms (d-type functions for non-Hydrogen atoms and a set of p-type functions for H). An example of this which is used extensively in this work, is the 6-31G* basis set. This basis has a set of d-type functions located on each heavy atom. The related basis set, 6-31G**, includes a set of p-type functions on the H atoms.

D Notation.

In addition to the notation introduced above there is a conventional sequence for writing the level of theory. A "//" separates the level at which the geometry has been optimised (right hand side) from the level at which the energy has been calculated. Thus a MP4SDQ/6-31G* //HF/6-31G* calculation is one in which the energy has been calculated at the MP4 (including contributions from all single, double and quadruple excitations) level with the 6-31G* basis set, at the optimised HF/6-31G* geometry.The unit of energy used here is the hartree, where 1 hartree = 2625.502 kJ mol^{-1}.

E Gaussian 82.

Gaussian 82 [11.3] is a general purpose package and is probably the most widely used of all the quantum chemistry programs. This program is designed to be user friendly in that the user need only supply the minimum data needed for any calculation. Data on the basis sets atomic masses etc. is contained internally to the program. For a geometry optimisation this consists of: the spin multiplicity; the level of theory of the calculation; charge of the species; and an initial guess for the geometry. Frequencies are calculated from the second derivatives of the energy with respect to displacement of the nuclei.

F Potential Energy Surface (PES) Calculations.

Because for any molecule there are 3N-6 (linear 3N-5) independent degrees of freedom, then the possible arrangements of the nuclei span a multidimensional space. It is currently not possible to calculate the entire potential energy surface for all but the simplest of molecules, and thus we must concentrate on calculating the potential energies of the important critical points on the surface. This means selecting possible intermediate and products and doing geometry optimisations at these local minima. Transition states can be calculated by constraining one coordinate to be a local maximum with respect to the energy and all other coordinates local minima (i.e. saddle points, convex in one coordinate). The vibrational frequencies of a transition state include one imaginary frequency corresponding to the coordinate of the local potential energy maximum.

3.2 Discussion

A number of studies, mainly from the Pople group, have focussed on the reliability of various levels of theory for calculation of molecular energies, structures and harmonic vibrational frequencies [11.4-11.9]. Conclusions from the studies relevant to the levels of theory used in later chapters are given below.

A Geometries.

The geometries calculated at the HF level are known to underestimate bond lengths. Agreement is particularly bad with bonds involving electronegative atoms.

The results of a study of AH_n molecules at the HF/6-31G* and MP2/6-31G* levels showed that inclusion of electron correlation effects lengthens AH bonds giving better agreement with experimental values [11.10]. The same study indicated that HAH bond angles changed only slightly on inclusion of correlation effects at the MP2 level. In a more extensive study, DeFrees et al [11.11] noted the following trends between HF/6-31G* and MP2/6-31G* geometries:

1) Calculations at the HF/6-31G* level on molecules containing a single 2nd row atom gave a mean deviation to experiment for AH bond lengths of 0.013 A improving to 0.011 A at the MP2/6-31G* level (17 comparisons). For molecules with two heavy atoms (i.e. non-hydrogen) the corresponding deviations are 0.011 A (HF) and 0.008 A (MP2).

2) HAH bond angles in AH_n systems were similarly improved with a mean absolute deviation of 1.4° at MP2/6-31G* compared to 2.2° at the HF/6-31G* level.

3) AB bond lengths improved from a mean absolute deviation of 0.036 A at HF/6-31G* to 0.017 A at MP2/6-31G*.

4) In all cases the MP2/6-31G* calculations overestimated the lengths of multiple bonds whereas the HF level underestimated these lengths.

B Energies.

It has proven difficult to gauge the success of ab-initio calculations of energies, mainly because of the absence of good quality experimental data for comparison. An estimate of ± 20 kJ mol^{-1} is not unreasonable for MP4SDQ/6-31G*//HF/6-31G* energies. In practice, relative energies from calculations on compounds that contain similar bonding, such as those on a reaction PES, often have errors very much less than this due to cancellation of basis set truncation effects and other systematic errors. In any case, experimental thermochemistry of many of the species discussed in the following chapters, is unknown and an ab-initio calculation is the only way to estimate the thermochemistry with any degree of accuracy. This is particularly true for the boron containing species discussed in chapters 8 and 10. The 6-31G* basis set has been shown to give energies close to the HF limit [11.12].

C Harmonic Vibrational Frequencies.

At the HF/6-31G* level the harmonic vibrational frequencies calculated by Gaussian 82, have been shown in an extensive study by DeFrees and McLean [11.13], to be greater than their anharmonic experimental counterparts by around 12%. DeFrees et al's study suggested that application of an empirical scaling factor of 0.89 results in a mean error of only 49 cm^{-1}. The overestimation of the frequencies is due to neglect of correlation effects in the wavefunction, basis set truncation errors and anharmonicity of the experimentally observed frequencies.

D General Considerations.

The objectives of the ab-initio studies reported here, were to suggest explanations for observed kinetic data and to predict the possible important intermediates, transition states and product sets involved in the reaction PES. Where the calculations were carried out without knowledge of the rate or products involved (as in the case of BH + NO) the predictive power has been excellent. Although emphasis must be placed on what has been observed, theoretical calculations such as these, not only provide useful data but indeed provide essential data for analysis of any experimental data.

The 6-31G* basis set was chosen not only because of its predictive power with energies, geometries and frequencies, but also because it is an economical basis set (both computer time and disk space). Even so, the computations described herein represent many months of computer time, and for this we thank the Department of Civil Engineering for the use of their VAX 780 at no charge.

CHAPTER 4

AB-INITIO POTENTIAL ENERGY SURFACES OF THE REACTIONS OF NH_2 WITH NO AND NO_2

4.1 Introduction

The reactions of NH_2 with NO and NO_2 have aroused considerable interest recently. These reactions have been found to be fast, even though the major products appear to involve substantial rearrangement of the collision complex.

A NH_2 + NO:

Since 1939 when Bamford first reported that the products of Hg lamp irradiated ammonia/nitric oxide mixtures were exclusively N_2 and H_2O the reaction between amidogen (NH_2) and NO has attracted a great deal of interest. Both NH_2 and NO are common species in combustion and the atmosphere, and because the reaction between these two species is fast, the possible products from this reaction could also be important in these systems. It is now generally accepted that despite being extremely fast the reaction proceeds through a nitrosamide (H_2NNO) intermediate to products, after substantial rearrangement. The following elementary reactions have been proposed for the reaction of NH_2 with NO:

$NH_2 + NO \rightarrow H_2NNO^* \rightarrow$ products			(1)
$\rightarrow N_2 + H_2O$	ΔH=-522±7	kJ/mol	(2)
$\rightarrow N_2H + OH$	ΔH=?		(3)
$\rightarrow N_2 + H + OH$	ΔH=-29±8	kJ/mol	(4)
$\rightarrow N_2O + H_2$	ΔH=-198±6	kJ/mol	(5)

A chronological survey of both experimental and theoretical studies of reaction (1) is given in Table 4-1. The structures referred to are given in Figure 4.1.

The spread of values for the rate constants evident in Table 4-1, at both room temperature and higher temperatures, along with the controversy over the value for the branching coefficient, a, (which has reported values spanning nearly the complete range of possibilities) indicate, that despite over 30 studies in the last 10 years, this reaction is still not well understood. The anomalous factor of two between the rates determined by flash studies and those measured in a discharge flow system is also of concern, especially from an experimentalists point of view. (The same effect has been noticed in the $NH_2 + NO_2$ reaction). The experimental studies do agree on a zero pressure dependence for the rate constant, and the few studies applying various statistical models to the reaction have been able to explain this, despite the reaction involving substantial rearrangement through possibly several intermediates.

The motivation for an ab-initio study of the reaction potential surface would not seem particularly great, especially considering several studies along this line have already been published. It was intended to carry out calculations on the various intermediates and products in order to supply data for use in RRKM type calculations. The data needed for such a study includes, not only geometries and energies, but also vibrational frequencies; no one study had reported all three. After finding that a planar N-Nitrosamide corresponds to a transition state, a more extensive study on the effects of basis sets and inclusion of correlation energy was decided upon. This is described in section 4.3. Section 4.4 presents the study on the $NH_2 + NO$ potential energy surface.

Table 4-1. Summary of previous studies on the reaction of NH_2 with NO.

Rate constants are at T=298 K unless stated otherwise and are expressed in cm^3 $molec^{-1}$ s^{-1} units.
Abbreviations: f branching parameter = $k_3/(k_3 + k_2)$

RA Resonance Absorption; DF Discharge Flow; AS Absorption Spectroscopy; FP Flash Photolysis; LIF Laser Induced Fluorescence; IRS Intra-cavity Resonance Spectroscopy; LP Laser Photolysis; IRMPD IR Multi-Photon Dissociation; CARS Coherent Anti-Stokes Raman Spectroscopy; IRAS IR Laser Absorption Spectroscopy.

Year [Ref]	Authors, Description of work.
1939 [4.1]	C. H. Bamford. Product analysis of Hg lamp irradiated NH_3/NO mixtures. N_2 and H_2O determined to be final products of reaction (1).
1959 [4.2]	A. Serewicz and W. A. Noyes. Product analysis of Hg lamp irradiated NH_3/NO mixtures. Proposed mechanism involving NH_2 and HNO as key intermediates.
1960 [4.3]	R. Srinivasan. ^{15}N labelling of NH_3. $^{15}N^{14}N$ > 95% ,$N^{14}{}_2O$ 100%. Anomalous $^{14}N_2$ at high NO pressures.
1961 [4.4]	C. P. Fenimore and G. W. Jones. NH_3/NO flame study. 1700-1900 K, NO decay only if NH_3 added to flame. $k_1=(4.8 \pm 1.6)\times10^{-11}$.
1971 [4.5]	S. Gordon, W. Mulac and P. Nangia. Pulse radiolysis of NH_3 mixtures (250-1520 torr). RA of NH_2 at 597.6 nm. $k_1=2.7\times10^{-11}$
1971 [4.6]	L. Radom, W. J. Hehre and J. A. Pople. HF/4-31G Energies at estimated geometries for I-V.

1972 M. Gehring, K. Hoyermann, H. Schacke and J. Wolfrum.
[4.7] DF/AS $k_1=(0.83 \pm 0.17)x10^{-11}$.ESR detection of H atoms negative. IR H_2O emission proportional to [NO]. Mass spectrum peaks at 45, 46 attributed to NH_2NO.

1975 G. Hancock, W. Lange, M. Lenzi and K. H. Welge.
[4.8] FP/LIF (1 Torr Ar) $k_1=(2.1 \pm 0.2)x10^{-11}$.

1975 R. Lesclaux, P. V. Khe, P. Dezauzier and J. C. Soulignac.
[4.9] FP/AS No pressure effect over 0-700 torr N_2
$k_1=(1.8 \pm 0.3)x10^{-11}$ (T = 298K)
For $300<T<500$ K $k_1 = 2.1x10^{-8} T^{-1.25}$.

1976 R. K. M. Jayanty, R. Simonaitis and J. Heicklen.
[4.10] 213.9 nm irradiation of NH_3/NO mixtures.
Quantitative NH_3 --> N_2(93%) + N_2O(7%)

1976 R. K. Lyon.
[4.11] $NO/NH_3/O_2$ reaction. Observed quantitative reduction of NO by NH_3. T = 1255 K. Needed $0.25 < f < 0.5$ to explain observations.

1977 C. Thomson, D. Provan and S. Clark.
[4.12] Chemical carcinogenesis ab-initio study. STO-3G and STO-4G optimized geometries of I-V. Energy profiles for I-II-III and for I-XIII-V.

1977 R. Cimiraglia, M. Persico and J. Tomasi.
[4.13] CI+SCF/STO-3G, STO-3G+sp energies of150 points in the 9 dimensional conformational space (ground and 1st excited state), including XIII-XVI.

1978 O. M. Sarkisov, S. G. Cheskis and E. A. Sviridenkov.
[4.14] FP/IRS $k_1=(1.7 \pm 0.4)x10^{-11}$, 0.1-1.0 torr(Ar)

1979 R. K. Lyon and D. Benn.

[4.15] $NO/NH_3/O_2$ reaction kinetics. NO found to be both consumed and produced in reaction. $1145 < T < 1227$ K.

1979 W. Hack, H. Schacke, M. Schroter and H. Gg. Wagner.
[4.16] DF/LIF $210 < T < 500$ K 0.6-4.0 torr $k_1 = 4.5 \times 10^{-7} T^{-1.85}$.

1981 J. A. Miller, M. C. Branch and R. J. Kee.
[4.17] $NH_3/NO/O_2$ modelling study using 82 elementary reactions. (1) found to be of primary importance. For good agreement with experimental studies need (1) to be chain branching and proposed (3) as a major channel.

1981 T. R. Roose, R. K. Hanson and H. C. Kruger.
[4.18] $NO/NH_3/H_2/Ar$ shocks. IR emission, IR laser Abs. of NO, N_2O, NH_3, NH_2 and NH. $1680 < T < 2850$ K 0.3 - 0.8 atm. $k_1 = (5 + 5, -3) \times 10^{-11} e^{-7900/T}$ $k_5 = (11 + 11, -7) \times 10^{-11} e^{-14000/T}$.

1982 L. J. Steif, W. D. Brobst, D. F. Nava, R. P. Borkowski and
[4.19] J. V. Michael.
FP/LIF, $216 < T < 480$ K, 2.5 - 20 torr. $a << 0.22$
$k_1 = (2.77 \pm 0.89) \times 10^{-7} T^{(-1.67 \pm 0.05)}$.

1982 J. A. Silver and C. E. Kolb.
[4.20] DF/LIF, $294 < T < 1215$ K, $f = 0.4 \pm 0.1$.
$k_1 = [(4.38 \pm 0.70) \times 10^{-5}] T^{-(2.3 \pm 0.02)} e^{(-5712 \pm 504/RT)}$.

1982 L. J. Steif, W. D. Brobst, D. F. Nava, R. P. Borkowski and
[4.21] J. V. Michael.
Further report from previous study. RRK study gave $T^{-1.73}$, adduct lifetime too short for collisional stabilisation.

1982 P. Andresen, A. Jacobs, C. Kleinermanns and J. Wolfrum.
[4.22] LP/RA (NH_2), IR Emission (H_2O), LIF (OH).
$k_4 = (1.7 \pm 0.5) \times 10^{-11}$
importance of channels: (2) ≥ 0.29, (3) ≥ 0.65, (5) ≤ 0.01.

1982 C. J. Casewit and W. A. Goddard III.
[4.23] Optimised HF/4-31G geometries and thermochemistry from GVB CI (DZP) for I - V, XIII, XIV, reactants and products.

1983 J. A. Miller, M. D. Smooke, R. M. Green and R. J. Kee.
[4.24] NH_3/O_2, $NH_3/H_2/O_2$ flame modelling study using 98 reaction model. (1) one of the four most important reactions. Needed f of around 0.4 to model T dependence.

1983 A. R. Whyte and L. F. Phillips.
[4.25] LP/LIF, $k_1 = (1.81 \pm 0.12)\times10^{-11}$.

1984 J. B. Jeffries, J. A. McCaulley and F. Kaufman.
[4.26] IRMPD (SF_6 sensitized, N_2H_4)/LIF. 0.5-5.0 torr
$k_1 = 0.9\times10^{-11}$

1984 T. K. Ha, M. T. Nguyen and P. Ruelle.
[4.27] Chemical Carcinogenesis ab-initio study. SCF/3-21G optimized geometries of I. Energies at 3-21G, 4-31G and 6-31G* for I along with one electron properties.

1984 K. H. Gericke, L. M. Torres and W. A. Guillory.
[4.28] IRMPD/LIF 0.5 - 130 torr.
k_1 $NH_2(0,0,0) = 1.4\times10^{-11}$, k_1 $NH_2(0,1,0) = 3.2\times10^{-11}$

1984 H. Abou-Rachid, C. Pouchan and M. Chaillet.
[4.29] Ab-Initio SCF/4-31G optimisation and CI energies for intermediates and products for (2), (3) and (4). (i.e. I-VI and XII). RRKM study of dubious quality.

1984 C. F. Melius and J. S. Binkley.
[4.30] BAC-MP4 (split-valence + polarisation) Heats of formation and free energies for I-V, XIV, XIII, reactants, transition states and products. Reaction pathway (2) thermoneutral, (3) endothermic.

1984 T. Dreier and J. Wolfrum.

[4.31] LP/CARS (N_2,NH_2) IR Emission (H_2O), H_2O circa 10^4 K.
$k_1 = 1.7 \times 10^{-11}$, k_2 (from H_2O) = $(1.3 \pm 0.4) \times 10^{-11}$

1985 H. Abou-Rachid and C. Pouchan.
[4.32] IR spectrum calculated for I SCF/4-31G. Claim that addition of 3d polarisation functions (on N and O) confirms the planar nature of I.

1986 R. G. Gilbert, A. R. Whyte and L. F. Phillips.
[4.33] RRKM Master equation to include collision effects. Assumed a single loose transition structure. Anharmonicity was found to play a significant role in rearrangement.

1986 J. L. Hall, D. Zeitz, J. W. Stephens, J. V. V. Kasper,
[4.34] G. P. Glass, R. F. Curl and F. K. Tittel.
LP/IRAS (OH, H_2O^*) 3-20 Torr, OH $13 \pm 2\%$, H_2O (85 ± 9), $(66 \pm 3)\%$.

1986 M. A. Kimball-Linne and R. K. Hanson.
[4.35] Flow Reactor studies of Thermal De NOx. Optimum fit for $f = 0.48$ at 1050 K, ≥ 0.8 at 1400 K (55 reaction model) noted extreme coupling between modelling parameters, especially a and (3).

1986 J. A. Harrison, A. R. Whyte and R. G. A. R. Maclagan.
[4.36] Ab-Initio study of I at various levels, found minimum energy structure to be non-planar. (Section 4.3 of this study).

1986 D. A. Dolson.
[4.37] Flow reactor/ Mass spec. $a < 0.13$.

1987 L. F. Phillips.
[4.38] A Priori rate for (1) using semiclassical trajectory calculations. Lifetime of intermediate estimated at 10^{-11}s (from ab-initio potential surface data).

1987 J. N. Crowley and J. R. Sodeau.
[4.39] FTIR Product analysis of photolysed NH_3/NO mixtures in Ar, N_2, Ne matrices. N_2O observed and $^{15}N^{14}NO$ from $^{15}NH_3$.

1987 J. A. Silver and C. E. Kolb.
[4.40] Re-evaluation of a from earlier work. Production of NH accounted for in DF experiment. f now 0.12.

1987 J. A. Harrison, A. R. Whyte and R. G. A. R. Maclagan.
[4.41] Optimised structures, MP4SDQ energies and vibrational frequencies for reactants, products Ia-XI. (Section 4.4 of this study).

1988 J. N. Crowley.
[4.42] FTIR studies of H_2NNO, D_2NNO and $H_2{}^{15}N^{14}NO$ trapped in Ar and N_2 at 4 K.

N-Nitrosamide

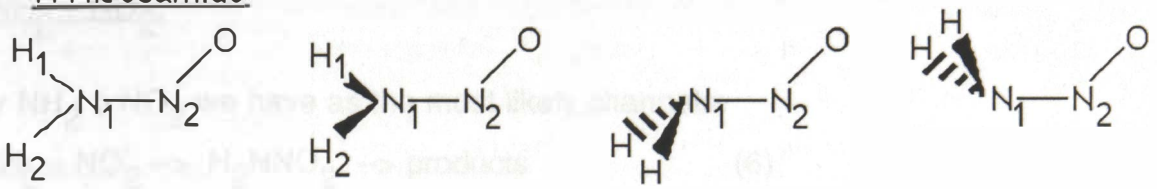

Planar I | Non-planar Ia | Trans Ib | Cis Ic

Hydroxydiimides

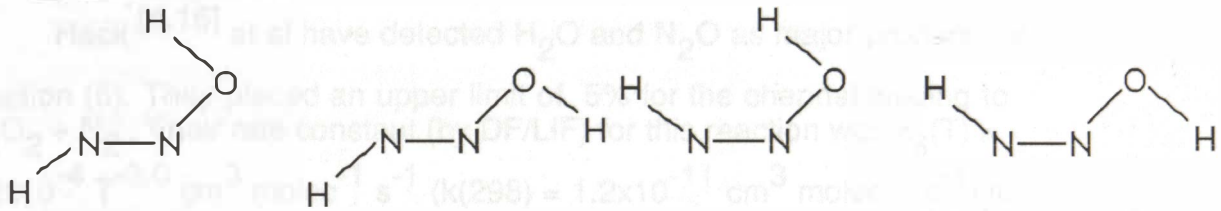

II III IV V

Transition States

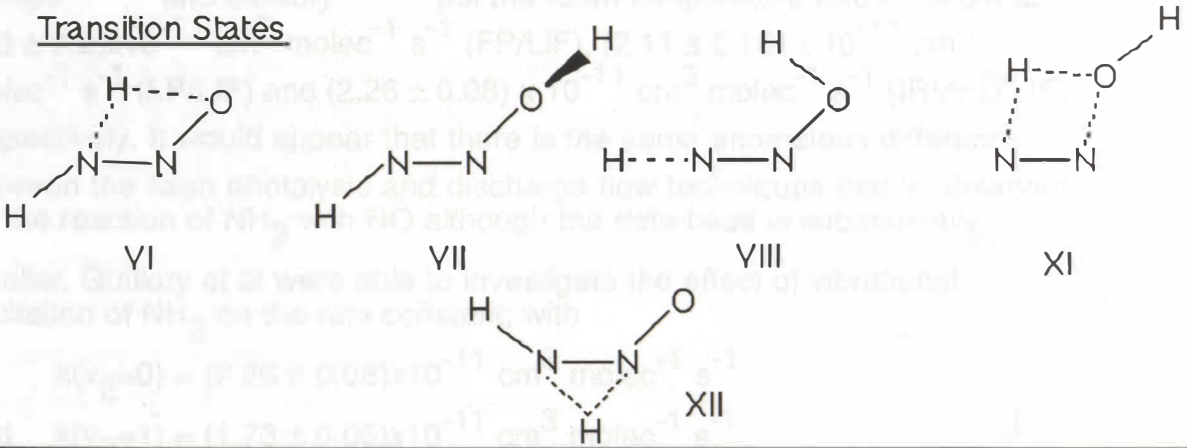

VI VII VIII XI XII

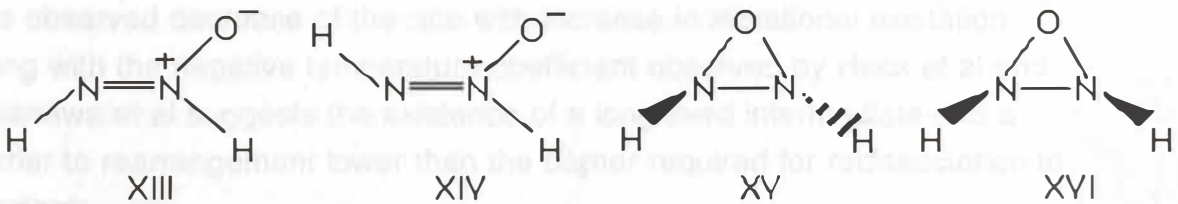

XIII XIV XV XVI

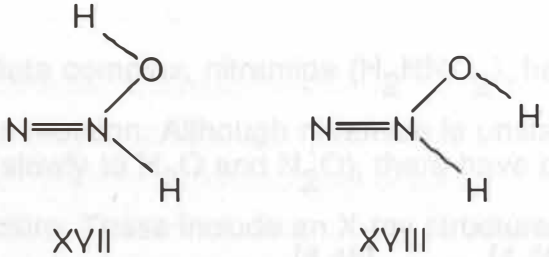

XVII XVIII

Figure 4.1. Key to H_2N_2O isomers.

B $NH_2 + NO_2$:

For $NH_2 + NO_2$ we have as the most likely channels:

$$NH_2 + NO_2 \rightarrow H_2NNO_2^* \rightarrow \text{products} \quad (6)$$

$$\rightarrow H_2NNO_2 \quad (7)$$

$$\rightarrow H_2O + N_2O \quad (8)$$

Hack [4.16] et al have detected H_2O and N_2O as major products of reaction (6). They placed an upper limit of 5% for the channel leading to $H_2O_2 + N_2$. Their rate constant (by DF/LIF) for this reaction was $k_6(T) = 3.2 \times 10^{-4} T^{-3.0}$ cm^3 $molec^{-1}$ s^{-1} ($k(298) = 1.2 \times 10^{-11}$ cm^3 $molec^{-1}$ s^{-1}) for the temperature range $250 < T < 500$ K. The studies of Kurasawa [4.43], Phillips [4.25] and Guillory [4.44] put the room temperature rate constant at $(2.3 \pm 0.2) \times 10^{-11}$ cm^3 $molec^{-1}$ s^{-1} (FP/LIF), $(2.11 \pm 0.18) \times 10^{-11}$ cm^3 $molec^{-1}$ s^{-1} (LP/LIF) and $(2.26 \pm 0.08) \times 10^{-11}$ cm^3 $molec^{-1}$ s^{-1} (IRMPD/LIF) respectively. It would appear that there is the same anomalous difference between the flash photolysis and discharge flow techniques that is observed for the reaction of NH_2 with NO although the data base is substantially smaller. Guillory et al were able to investigate the effect of vibrational excitation of NH_2 on the rate constant; with

$$k(v_2=0) = (2.26 \pm 0.08) \times 10^{-11} \text{ cm}^3 \text{ molec}^{-1} \text{ s}^{-1}$$

and $$k(v_2=1) = (1.73 \pm 0.06) \times 10^{-11} \text{ cm}^3 \text{ molec}^{-1} \text{ s}^{-1}.$$

The observed decrease of the rate with increase in vibrational excitation along with the negative temperature coefficient observed by Hack et al and Kurasawa et al suggests the existence of a long lived intermediate and a barrier to rearrangement lower than the barrier required for redissociation to reactants.

The possible intermediate complex, nitramide (H_2NNO_2), has, to date, not been detected in the reaction. Although nitramide is unstable at room temperature (decaying slowly to H_2O and N_2O), there have been a number of studies on its structure. These include an X-ray structure [4.45], UV absorption [4.46,4.47], microwave absorption [4.48] and IR [4.49]. The study reported in section 4.5, represents the preliminary results of a more complete study being carried out by Dr. R. G. A. R. Maclagan and the author.

NH_2 is thought to act as both a natural source and sink of NO in the troposphere and stratosphere. The range of temperatures and pressures existing in the atmosphere (troposphere 0 km: 760 Torr, 290 K; 10 km: 150 Torr, 220 K; Stratosphere 45 km: 1 Torr, 270 K [4.50]) require that to understand the possible roles reactions (1) and (6) play in the atmospheric NO_x budget the rate constants and product distributions must be measured over vastly different conditions than those that apply for combustion systems. It would appear from Table 4-1 that even though measurements for atmospheric-type conditions are easier to do than those at elevated temperatures, there is still great confusion over what products are formed and the value of the rate constants.

4.2 Details of Calculations

The geometries of the nitrosamide conformers were optimised at levels ranging from RHF/STO-3G to RHF/6-311G** and a post-HF optimisation at the MP2/6-31G** level. The geometries of the other species were optimised at the HF/6-31G* level (RHF for closed shell, UHF for open shell species). Harmonic vibrational frequencies and MP2 to MP4SDQ/6-31G* energies were calculated at the optimised geometries. All calculations were done using the Gaussian 82 program [4.51]. Harmonic vibrational frequencies for isotopically substituted (^{15}N,D) Nitrosamide were obtained using the F-G matrix method of Wilson et al [4.52]. F matrices were obtained directly from the output of Gaussian 82. These calculations were achieved with the assistance and software of Dr. B. E. Williamson of this department.

4.3 The Structure of Nitrosamide

A. Introduction

N-Nitrosamines have attracted considerable interest recently due to their mutagenic and carcinogenic properties. Upon metabolic activation dimethylnitrosamine generates intermediates capable of alkylating nucleic acids, thus causing tumours. There is some evidence that N-Nitrosamines are important environmental carcinogens. The molecule Nitrosamide (I), as the prototypical nitrosamine, has been extensively studied by ab-initio theoreticians, primarily in order to test the effects of increasing the level of ab-initio theory on molecular geometry and other properties [4.12,4.53].

Nitrosamide (I) is also of great interest as an important transient intermediate in the reaction of amidogen and nitric oxide. The role that (I) plays in this reaction, along with other intermediates and transition states potentially involved, will be discussed in section 4.4 of this chapter. A summary of previous ab-initio studies on nitrosamide is included in Table 4-1. Of particular note is that until our study reported here, the planar structure (I) appears to have been favoured over the non-planar structure (Ia) as the theoretical lowest energy conformer. Very recently Crowley has recorded the FTIR spectrum of nitrosamide (and some isotopomers) trapped in low temperature matrices of N_2 and Ar. A comparison of Crowley's study with the theoretical predictions is given below (4.3C).

B. Results and Discussion.

Optimisation of (I) at the HF/STO-3G level using the structural parameters obtained by Casewit and Goddard as starting parameters, resulted in a transition state structure (one imaginary frequency). Restarting the optimisation using an initial structure with the hydrogen atoms out of plane gave the lowest energy conformation as (Ia). Several basis sets were then used to test the effect of changing the level of theory. All optimisations were started at a non-planar geometry and energies of planar structures were obtained to make sure the calculation was not converging to a false minimum. Optimised geometries (RHF), SCF, MP2 and relative energies at the various levels of theory are given in Table 4-2. The MP2 energies include contributions from the core electrons. E_{SCF} refers to the difference between the non-planar and planar structures at each level of theory. Note that the 4-31G basis set does indeed give the planar structure as the lowest energy conformation. Retrospectively this is not surprising as a double zeta basis set predicts a planar ammonia, whereas addition of polarisation functions to the DZ basis results in a pyramidal structure [4.54-4.56]. The energy differences between (I) and (Ia) with basis sets of near double zeta quality is very small, even if a triple-split-valence basis set is used.

Increasing the size of the basis set from STO-3G to one of near double-zeta quality results in significantly reduced bond lengths, larger bond angles and smaller dihedrals; as tabulated in Table 4-2. Addition of a set of d polarisation functions on the heavy atoms has a marked effect on the bond

angles, especially the dihedrals. A further set of p polarisation functions on the hydrogens changes the angles only slightly.The alteration in geometry on introducing a triple split in the valence orbitals, is very small. The dipole moment calculated with the HF/6-311G** wavefunction is 3.61D. Inclusion of correlation energy effects on the optimised geometry was investigated by a single optimisation at the MP2/6-31G** level (core contributions neglected). The optimised MP2/6-31G** structure was: R(N-N) = 1.340 Å; R(N-O) = 1.236 Å; R(N-H_1) = 1.012 Å; R(N-H_2) = 1.004 Å; (NNO) = 112.9 ; (NNH_1) = 118.2 ; (NNH_2) = 116.3 ; ($ONNH_1$) = -8.8 ; ($ONNH_2$) = 190.2 . The MP2 energy for this structure was -185.361602 compared with -185.356473 for the MP2//HF structure (6-31G**). At the MP2 level the bond lengths have been increased and the NNO bond angle decreased. The NNH bond angles and dihedrals are not significantly different from the HF/6-31G** values. These trends were to be expected from the MP2 studies of DeFrees et al [4.57]. Further inclusion of correlation effects would not be expected to predict a planar conformation as the minimum energy isomer.

At MP4SDQ/6-31G**//HF/6-31G** (core contributions not included) the non-planar structure is lowest in energy by merely 0.33 kJ mol^{-1}. The predicted barrier to inversion is thus only of the order of 30 cm^{-1}. The value of the NH_2 wagging vibration is around 200cm^{-1} and because of the very flat potential energy surface, would be significantly affected by anharmonicity.

Structures for the cis and trans isomers were also optimised at the HF/6-31G* level. Energies and geometries of I, Ia, Ib and Ic, are listed in Table 4-3, with vibrational frequencies tabulated in 4-4. A complete rotation of the NH_2 group about the NN bond is represented by the process Ia-Ib(trans)-Ia'-Ic(cis)-Ia. Ib and Ic are both transition states (one imaginary frequency). At the MP2+ZPVE//HF (6-31G*, core contributions included) the trans structure Ib, is 90.0 kJ mol^{-1} above the minimum energy, non-planar structure, and the cis conformer is 87.8 kJ mol^{-1} above. All structures I, Ia-Ic, are below the energy of NH_2 + NO at MP2+ZPVE/6-31G*//HF/6-31G*.

Application of the empirical scaling factor of 0.89 has been shown to give a mean absolute error of 49 cm^{-1} for a series of molecules containing first row atoms at the HF/6-31G* level. Use of the scaling factor 0.87, which minimises the deviations for NH_2 and NO, should improve the estimates.

Using two scale factors; 0.875 for the NH_2 frequencies and 0.857 for the frequencies involving the NO force constant, should further reduce the error. Comparison of theoretically predicted and experimental frequencies for the related molecule, NH_2NO_2, indicate this to be the case (section 4.5).

Frequencies scaled in this manner should be reliable enough to be used in RRKM type calculations and to assign any observed IR spectrum (see the following section).

Table 4-2. Nitrosamide (structure Ia) optimised (RHF) geometries SCF, MP2, and relative energies for different basis sets. Distances in Å.

	STO-3G	4-31G	6-31G*	6-31G**	6-311G**
R(N-N)	1.450	1.312	1.316	1.312	1.313
R(N-O)	1.230	1.212	1.184	1.185	1.176
$R(N-H_1)$	1.036	0.995	1.000	0.998	0.999
$R(N-H_2)$	1.033	0.987	0.994	0.991	0.991
(NNO)	110.9	115.4	114.5	114.5	114.8
(NNH_1)	110.3	119.9	117.3	118.3	118.3
(NNH_2)	107.5	117.3	115.4	116.4	116.2
$(ONNH_1)$	-28.0	0.0	-13.4	-8.9	-10.2
$(ONNH_2)$	212.6	180.0	195.2	190.5	190.9
-E (hartree)					
SCF	182.39392	184.53866	184.82648	184.83448	184.88197
MP2	182.57192	184.89763	185.33730	185.35647	185.48562
ΔE_{SCF}					
(kJ/mol)	17.31	0.0	0.51	0.07	0.23
(cm^{-1})	1447.3	0.0	42.8	6.1	19.6

Table 4-3. Nitrosamide (structures I, Ia, Ib, Ic) optimised geometries, SCF, MP2 and relative energies (6-31G* basis set). Distances in Å.

	I	Ia	Ib	Ic
R(N-N)	1.307	1.316	1.438	1.439
R(N-O)	1.186	1.184	1.160	1.164
$R(N-H_1)$	0.999	1.000	1.008	1.008
$R(N-H_2)$	0.992	0.994	1.008	1.008
(NNO)	114.6	114.5	111.5	113.6
(NNH_1)	119.4	117.3	104.0	105.7
(NNH_2)	117.4	115.4	104.0	105.7
$(ONNH_1)$	180.0	-13.4	125.6	55.8
$(ONNH_2)$	0.0	195.2	125.6	55.8
-E (hartree)				
SCF	184.82629	184.82648	184.79807	184.79582
MP2	185.33731	185.33730	185.30509	185.30300
ΔE (kJ/mol)				
SCF	0.51	0.00	74.60	80.50
MP2	-0.02	0.00	84.55	90.04
MP2+ZPVE	-2.0	0.00	90.0	87.8

Table 4-4. Nitrosamide HF/6-31G* harmonic vibrational frequencies (cm^{-1}).

Assignment (structure Ia)	I	Ia	Ib	Ic
NH a-str	A' 3984	3955	A" 3746	A" 3753
NH s-str	A' 3788	3772	A' 3666	A' 3657
NO str/NNH_2 bend	A' 1862	1882	A' 2025	A' 1988
NH_2 scissors	A' 1769	1781	A' 1795	A' 1773
NNH_1 bend/NNH_2 bend	A' 1372	1392	A" 1279	A" 1300
NNH_2 bend/NN str	A' 1264	1251	A' 1235	A' 1244
NH_2 torsion	A" 759	744	A' 1016	A' 1028
NH_2 rock	A' 706	690	A' 738	A' 717
NH_2 wag	A' 268i	370	A' 421i	A" 548i

C Comparison with Experiment.

There have been two theoretical studies of the infrared spectrum of nitrosamide; our own and that of Abou-Rachid and Pouchan [4.32]. Recently Crowley has studied nitrosamide trapped in an inert matrix at 4.2 K by FTIR [4.42]. To assist in assigning his observed frequencies of matrix isolated $H_2{}^{14}N^{14}NO$, $H_2{}^{15}N^{14}NO$ and $D_2{}^{14}N^{14}NO$ the ab-initio force constants were obtained directly from Gaussian 82 and were used to calculate the frequencies for the various isotopically substituted nitrosamides. These were then supplied to Crowley as requested. The scaled frequencies are given in Table 4-5 along with those of ref. [4.32] and Crowley's experimental data. The experimental assignments are those suggested by Crowley based mainly on comparison with the expected shifts upon isotope substitution, along with comparison of the experimental and theoretically predicted shifts of the analogous substitutions in the isoelectronic molecule formamide (NH_2CHO). The scaled frequencies predicted from our HF/6-31G* planar structure should be more reliable than the scaled HF/4-31G frequencies calculated by Abou-Rachid et al. A comparison of the scaled frequencies for the planar and non-planar structures with the experimental data is not sufficient to decide on the experimental geometry. Crowley however, tentatively suggested that the quartet structure observed around 1200 cm^{-1} was due to a combination of site effects and inversion doubling of the NH_2 group, consistent with our prediction of a non-planar equilibrium geometry.

Table 4-5. Comparison of HF/6-31G* (scaled by 0.87) and experimental frequencies of the IR spectrum of Nitrosamide (cm^{-1})

Planar (I) $H_2{}^{14}N^{14}NO$	ref [4.32]	This study
NH_2 a-str(80), NH_2 s-str(20)	A' 3849	3466
NH_2 s-str(77), NH_2 a-str(23)	A' 3546	3296
NH_2 scissors(85), NN str(15)	A' 1750	1620
NO str(100)	A' 1525	1539
NH_2 rock(76), NN str(24)	A' 1095	1194
NN str(64), NH_2 bend(13), NH_2 rock(22)	A' 1073	1100
NNO bend(100)	A" 685	660
NH_2 oop bend(100)	A" 502	614
NNO oop bend(100)	A" 83	233

Non-Planar (Ia)	$H_2{}^{14}N^{14}NO$		$H_2{}^{15}N^{14}NO$		$D_2{}^{14}N^{14}NO$	
	calc	expt	calc	expt	calc	expt
NH a-str	3440		3429		2552	
NH s-str	3281		3277		2368	
NO str/	1637	1521.2	1636	1518.3	1625	1505.3
NNH_2 bend		1514.5		1513.0		
NH_2 scissors	1550		1543		1227	
NNH_1 bend/	1211	1210.0	1204	1203.5	1059	1232.4
NNH_2 bend		1207.3		1200.6		1227.6
		1202.3		1195.8		1223.2
		1200.1		1193.8		1088.7
NNH_2 bend/	1088	1077.1	1075	1063.6	938	
NN str		1058.8		1046.8		
NH_2 torsion	647		645		549	
NH_2 rock	600		598		487	
NH_2 wag	322		319		248	

4.4 The Potential Energy Surface of NH_2NO

Previous studies have shown that at room temperature the most energetically feasible pathways are (2), (3) and (4), while at high temperatures other pathways could occur [4.12,4.27,4.29,4.30]. Reaction (2) has been postulated to occur by rearrangement of a N_2H_2O intermediate and final 1,2 elimination of H_2O, while N_2H (reaction (3)) could be formed from decomposition of one of several of the same intermediates involved in the reaction scheme for (2). Our reaction scheme for (2) is qualitatively equivalent to that used by Melius and Binkley [4.30], differing in that rotation of OH about the NO bond, after the initial 1,3 H migration, is formally included. The optimized HF/6-31G* geometric parameters for the N_2H_2O isomers and transition states as well as those for the reactants and products are given in Table 4-6.

The structures of the intermediates and transition states are those of Figure 4.1. Structure IX is similar to VII with H_2 cis to O; structure X is similar to VIII with H_1 trans to N_1. The HF/6-31G*//HF/6-31G*, MP2/6-31G*//HF/6-31G* and MP4SDQ/6-31G*//HF/6-31G* total energies are given in table 4-7, relative energies in Table 4-8. The relative MP4SDQ/6-31G*//HF/6-31G* energies are plotted in Figure 4.2. The MP2 energies include core contributions, the MP4SDQ energies do not.

Intermediate I has been discussed in the previous section. In going from N-Nitrosamide (I) to the hydroxydiimide isomers (II-V), the NN bond shortens as it goes from a single to a double bond, and the NO bond lengthens in going from a double to a single bond. The geometric parameters for the transition state VI are intermediate between those of I and II, except that the NNO bond angle is about 10 degrees less than in both I and II. In the transition states the NO bond lengths are slightly longer and the NNO bond angles slightly larger than in the intermediates.

In the final transition state H_2 is still relatively strongly attached to N_1. At high temperatures this transition state could lead to the formation of N_2H + OH rather than N_2 + H_2O. The geometric parameters for isomers II-V are in good agreement with published HF/4-31G optimised structures [4.23,4.29]. The only noticeable differences between the 4-31G and 6-31G* geometries for I-V are a shortening (about 0.05 A) in the NO bond length, and a

decrease (about 3 degrees) in the NNH and NOH bond angles, both of which can be attributed to the inclusion of d polarisation functions in the 6-31G* basis set. The STO-4G bond lengths of Thompson [4.12] are longer for the transition state VI, and the NO bond length is 0.06 A longer in the 4-31G structure than in the 6-31G* structure, the rest of the parameters being in reasonable agreement.

Table 4-8 shows that at the HF/6-31G* level the activation energy barriers to rearrangement are large. Inclusion of correlation substantially lowers the energies of the transition states and intermediates relative to the reactants. While at the MP2/6-31G*//HF/6-31G* level our results imply that reaction (1) can proceed without an activation barrier, in accord with the BAC-MP4 study of Melius and Binkley, the MP4SDQ/6-31G*//HF/6-31G* calculations actually give a small activation barrier. It is interesting to note that, although structures I-V have their energies lowered by between 122 and 133 kJ mol^{-1} when the HF and MP4SDQ energies are compared, the effect on the transition states VI-XI is far more erratic, with relative energies lowered by between 120 and 183 kJ mol^{-1}. The HF level is known to describe bonds between electronegative elements poorly, so the importance of correlation noted above is not without precedent. The activation barriers are also lowered when zero point vibrational contributions are added. After addition of the thermal energies the barrier heights are in reasonable agreement with those of Melius and Binkley: the barrier for I -> VI -> II is 141.0 kJ mol^{-1} at 0 K compared with 118.8 kJ mol^{-1}; the barrier III -> X -> V is 169.1 kJ mol^{-1} compared with 161.1 kJ mol^{-1}; and the barrier V -> XI -> N_2 + H_2O is 114.8 kJ mol^{-1} c.f. 92.0 kJ mol^{-1}. Relative to the reactants, the enthalpies at 0 K of the intermediates calculated by us are about 52-56 kJ mol^{-1} higher than those reported by Melius and Binkley. The other major systematic error in these calculations is the quality of the 6-31G* basis set. The existence of the comparison by DeFrees and McLean [4.58] between experimental vibrational frequencies and harmonic frequencies computed at the HF/6-31G* level of theory was a major factor in the choice of basis set for this study.

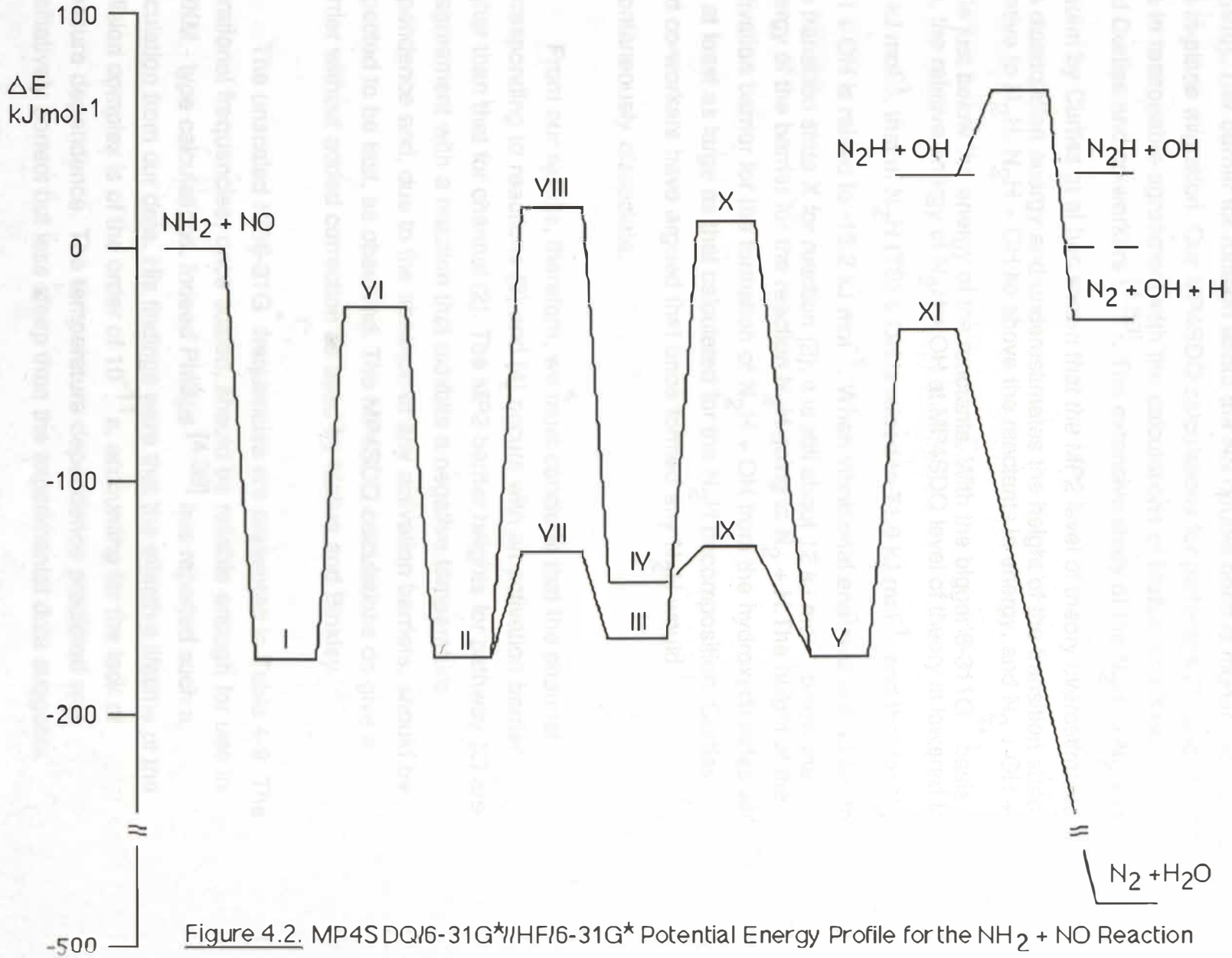

Figure 4.2. MP4SDQ/6-31G*//HF/6-31G* Potential Energy Profile for the NH_2 + NO Reaction

As was found by Melius and Binkley, the major barrier to rearrangement for pathway (2) is the in-plane migration of the H atom (TSVIII). The barrier for rotation about the NN double bond is higher than for the in-plane migration. Our MP4SDQ calculations for pathways (3) and (4) are in reasonable agreement with the calculations of Melius and Binkley, and Curtiss and co-workers [4.59]. The extensive study of the $N_2H \rightarrow N_2 + H$ system by Curtiss et al has shown that the MP2 level of theory overestimates the dissociation energy and underestimates the height of the transition state relative to N_2H. N_2H + OH lie above the reactants in energy, and N_2 + OH + H lie just below the energy of the reactants. With the bigger 6-311G** basis set, the relative energy of N_2H + OH at MP4SDQ level of theory is lowered to 30 kJ mol^{-1}, that of N_2H (TS) + OH is raised to 71.6 kJ mol^{-1}, and that for N_2 + H + OH is raised to -16.2 kJ mol^{-1}. When vibrational energies are added to the transition state X for reaction (2), it is still about 12 kJ mol^{-1} below the energy of the barrier for the reaction N_2H going to N_2 + H.The height of the activation barrier for the formation of N_2H + OH from the hydroxydiimides will be at least as large as that calculated for the N_2H decomposition. Curtiss and co-workers have argued that once formed any N_2H would spontaneously dissociate.

From our results, therefore, we must conclude that the channel corresponding to reactions (3) and (4) occurs with an activation barrier higher than that for channel (2). The MP2 barrier heights for pathway (2) are in agreement with a reaction that exhibits a negative temperature dependence and, due to the absence of any activation barriers, should be expected to be fast, as observed. The MP4SDQ calculations do give a barrier without added correction as used by Melius and Binkley.

The unscaled HF/6-31G* frequencies are presented in Table 4-9. The vibrational frequencies, once scaled, should be reliable enough for use in RRKM - type calculations. Indeed Phillips [4.38] has reported such a calculation from our data. His findings were that the effective lifetime of the collision complex is of the order of 10^{-11} s, accounting for the lack of pressure dependence. The temperature dependence predicted was qualitatively correct but less steep than the experimental data suggests.

The Thermal DeNOx reaction, which has attained some commercial importance as an effective method of eradicating waste NOx from exhaust

gases [4.60,4.61] appears to include reaction (1) as a key step. In order to successfully model data obtained from studies on the Thermal DeNOx reaction, it has been necessary to use a value for the branching ratio, f, of around 0.4. The most recent and reliable experimental measurements of this quantity suggest it is circa. 0.13. There would thus appear to be some problem with the modelling mechanisms, although it has been noted that there is a strong inverse relationship between f and k_3 [4.35]. Use of equation (4) has not been favoured in the modelling studies mainly because of the experimental evidence against it (failure to detect H atoms in several studies). The evidence against the existence of N_2H would appear to be equally strong. There is thus a major problem with modelling this reaction, which is not entirely surprising when one considers the number of elementary reactions occurring in such a system, and the number of coupled parameters.

Table 4.6 Optimized HF/6-31G* geometric parameters for the NH_2 + NO reaction. (Bond lengths in Å, angles in degrees). The key to the structures and labelling is given in Figure 4.1.

Reactants and Products			
NH_2	N_1-H_1 = 1.013	N_1-H_2 = 1.013	H_1-N_1-H_2 = 104.3
NO	N_2-O = 1.127		
N_2	N_1-N_2 = 1.078		
H_2O	O-H_1 = 0.947	O-H_2 = 0.947	H_1-O-H_2 = 105.5
OH	O-H_1 = 0.958		
N_2H	N_1-N_2 = 1.179	N_1-H_2 = 1.029	H_2-N_1-N_2 = 113.0
N_2H TS	N_1-N_2 = 1.119	N_1-H_2 = 1.386	H_2-N_1-N_2 = 113.3

	Intermediates				
	Ia	II	III	IV	V
N_1-N_2	1.316	1.206	1.203	1.202	1.199
N_1-H_1	1.000				
N_1-H_2	0.994	1.007	1.008	1.020	1.017
N_2-O	1.184	1.334	1.351	1.347	1.366
O-H_1		0.958	0.949	0.957	0.949
N_2-N_1-H_1	117.3				
N_2-N_1-H_2	115.4	107.0	106.0	113.4	111.0
N_1-N_2-O	114.5	112.8	110.4	118.6	112.8
N_2-O-H_1		107.5	104.6	110.8	105.4
O-N_2-N_1-H_1	-13.4				
O-N_2-N_1-H_1	195.2				

Table 4.6. Continued

	Transition States					
	VI	VII	VIII	IX	X	XI
N_1-N_2	1.240	1.201	1.179	1.199	1.172	1.128
N_2-H_1	1.638					
N_1-H_1	1.285					
N_1-H_2	1.002	1.011	0.982	1.017	0.981	(1.14)
N_2-H_2						1.724
N_2-O	1.260	1.383	1.380	1.391	1.460	1.837
O-H_1	(1.327)	0.951	0.956	0.953	0.950	0.953
N_2-N_1-H_2	118.6	106.0	179.9	111.9	176.9	(98.9)
N_1-N_2-H_1	50.8					
N_2-N_1-H_1	80.8					
N_1-N_2-H_2						40.8
N_1-N_2-O	103.3	110.6	115.2	114.8	111.7	90.0
N_2-O-H_1	(78.5)	106.3	107.4	107.8	103.9	139.8
N_1-N_2-O-H_1		8.75		65.0		

Table 4-7. HF/6-31G*, MP2/6-31G* and MP4SDQ/6-31G* Total energies (//HF/6-31G* geometry).

		- HF	- MP2 (hartree)	- MP4SDQ
	NH_2 + NO	184.805586	185.256365	185.274534
I	NH_2NO	184.826480	185.337296	185.341926
	HNNOH			
II	trans-cis	184.825151	185.334729	185.341571
III	trans-trans	184.822464	185.331126	185.338654
IV	cis-cis	184.810008	185.322680	185.329480
V	cis-trans	184.822198	185.333654	185.340984
	transition states			
VI	I --> II	184.747581	185.284015	185.283406
VII	II --> III	184.809332	185.315552	185.324125
VIII	II --> IV	184.744409	185.262915	185.267914
IX	IV --> V	184.804977	185.315405	185.323416
X	III --> V	184.746270	185.264672	185.270022
XI	V --> products	184.750187	185.289940	185.290197
	products			
	N_2H + OH	184.807677	185.236141	185.262669
	TS --> N_2 + H + OH	184.786185	185.226567	185.248575
	N_2 + H + OH	184.825503	185.276760	185.287050
	N_2 + H_2O	184.954696	185.453037	185.457825

Table 4-8. HF/6-31G*, MP2/6-31G* and MP4SDQ/6-31G* relative energies (//HF/6-31G* geometry).

	HF	MP2	MP4SDQ
		(kJ mol^{-1})	
NH_2 + NO	0.0	0.0	0.0
I NH_2NO	-54.9	-212.5	-176.9
HNNOH			
II trans-cis	-51.4	-205.7	-176.0
III trans-trans	-44.3	-196.3	-168.3
IV cis-cis	-11.6	-174.1	-144.3
V cis-trans	-43.6	-202.9	-174.5
transition states			
VI I --> II	+152.3	-72.6	-23.3
VII II --> III	-9.8	-155.4	-130.2
VIII II --> IV	+160.6	-17.2	+17.4
IX IV --> V	+1.6	-155.0	-128.3
X III --> V	+155.7	-21.8	+11.8
XI V --> products	+145.5	-88.2	-37.2
products			
N_2H + OH	+5.5	+53.1	+31.2
TS --> N_2 + H + OH	+50.9	+78.2	+68.2
N_2 + H + OH	-52.3	-53.5	-32.9
N_2 + H_2O	-391.5	-516.4	-481.2

Table 4-9. HF/6-31G* Harmonic vibrational frequencies. (cm^{-1}).

	NH_2	A_1 1712	A_1 3605	B_2 3705	
	NO	Σ 2221			
I	NH_2NO	370	690	741	1251
	1392	1781	1882	3772	3955
	HNNOH				
II	trans-cis	A" 668	A' 738	A" 1080	A' 1136
	A' 1547	A' 1618	A' 1925	A' 3710	A' 3953
III	trans-trans	A" 498	A' 735	A" 1096	A' 1107
	A' 1510	A' 1618	A' 1966	A' 3692	A' 4108
IV	cis-cis	A" 475	A' 761	A" 1089	A' 1100
	A' 1455	A' 1635	A' 1937	A' 3505	A' 3946
V	cis-trans	A" 475	A' 711	A' 1060	A" 1147
	A' 1477	A' 1607	A' 1975	A' 3576	A' 4101
	transition states				
VI	I --> II	A' 2444i	A" 705	A' 1058	A" 1282
	A' 1343	A' 1507	A' 1693	A' 2316	A' 3811
VII	II --> III	539i	746	1066	1074
	1462	1592	1939	3663	4058
VIII	II --> IV	A' 1561i	A" 544	A" 613	A' 727
	A' 971	A' 1508	A' 2001	A' 3976	A' 4103
IX	IV --> V	461i	725	1030	1103
	1441	1585	1943	3559	4035
X	III --> V	A' 1554i	A" 500	A" 631	A' 717
	A' 898	A' 1482	A' 2036	A' 4088	A' 4120
XI	V --> products	A' 1615i	A" 91	A' 616	A' 859
	A" 1131	A' 1184	A' 2122	A' 2326	A' 4048
	products				
	N_2H	A' 1264	A' 1661	A' 3276	
	TS --> N_2 + H	A' 1919i	A' 896	A' 2136	
	OH	Σ 3997			
	N_2	Σ 2758			
	H_2O	A_1 1827	A_1 4070	B_2 4189	

4.5 The Potential Energy Surface of NH_2NO_2

The optimised HF/6-31G* structure of nitramide, along with the microwave and crystal structures, is given in Figure 4.3. Table 4-10 lists the total and relative MP4SDQ/6-31G*//HF/6-31G* energies for the reactants, intermediate nitramide and possible products in the reaction of NH_2 with NO_2. The optimised structures, energies, and harmonic vibration frequencies for all species other than nitramide can be found in the previous section of this chapter, or in the following chapter.

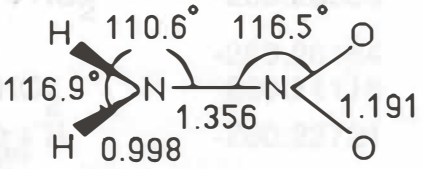

Ab-Initio HF/6-31G*

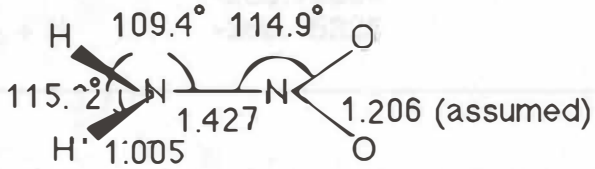

Microwave Structure (ref.[4.48])

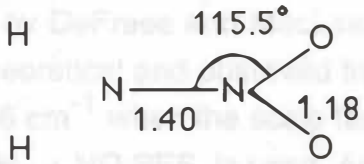

Crystal Structure (ref.[4.45])

Figure 4.3. Experimental and Ab-Initio Geometries for Nitramide. (all distances in Å).

Table 4-10. MP4SDQ/6-31G*//HF/6-31G* relative and absolute energies for NH_2NO_2 species.

	MP4SDQ//HF (hartree)	Relative E (kJ mol^{-1})
$NH_2 + NO_2$	-260.25621	0.0
(7) H_2NNO_2	-260.33770	-214.0
(8) $N_2O + H_2O$	-260.39015	-351.7
(9) $N_2 + 2OH$	-260.32230	-173.5
(10) $N_2 + H + HO_2$	-260.26555	-24.5
(11) 2HNO	-260.26164	-14.3
(12) $N_2H + HO_2$	-260.24116	+40.5
(13) $H_2NNO + H$	-260.23721	+50.9
(14) HNNO + OH	-260.23268	+61.8
(15) HNO + HON	-260.22924	+70.8
(16) 2HON	-260.19684	+155.9
(17) $HNNO_2 + H$	-260.15325	+270.3

As can be seen from Table 4-11 the HF/6-31G* level of theory significantly over-estimates the vibrational frequencies (the reasons for this have been given in chapter 3). Application of the scale factor of 0.89 recommended by DeFrees and MacLean gives a mean absolute deviation between the theoretical and observed frequencies of 43 cm^{-1}. This decreases to 36 cm^{-1} when the scale factor of 0.87, as suggested by our study on the NH_2 + NO PES, is used. Agreement is even better (26 cm^{-1}) when the NH and NO frequencies are scaled independently by 0.875 and 0.857, respectively. Two of the three frequencies with deviations greater than 20 cm^{-1} have been noted to be very dependent on the matrix supporting environment [4.49].

The torsional vibrational frequency ν_{12} is much larger than that for the isoelectronic H_3CNO_2, which has been found to have nearly free internal rotation [4.62]. The higher frequency reflects the partial multiple bond character of the NN bond. This is reflected by the shorter bond length than that for hydrazine (1.427 A [4.48] c.f. hydrazine 1.46 A [4.63]) and in the NN stretching force constant (3.6 mdyn A^{-1} H_2NNH_2 [4.64], 6.3 mdyn A^{-1}

H_2NNO_2 [4.49]). The predicted HF/6-31G* dipole moment is 4.18 D compared to the experimental value of 3.75 D [4.65].

From the energies in Table 4-10 the most likely channels are paths (7) to (11). For the reaction to be as fast as observed the products must be exothermic, indeed the whole pathway must be exothermic. From an estimation of barrier heights for H migration from the NH_2NO study, all barrier heights for channel (8) would be below the energies of the reactants by at least 30 kJ mol^{-1}. The transition states involving the migration of both Oxygen atoms (e.g. H_2O_2 formation) would almost certainly lie above the reactants. The results of this preliminary study are in agreement with the observed products and the rate of reaction, however until the barrier heights have been calculated a detailed discussion is not possible.

Table 4-11. Experimental and HF/6-31G* vibrational frequencies for nitramide. (cm^{-1})

	Expt[a]	Expt[b]	Calc[c]	Calc[d]	Calc[e]	PED[f]
a' 1	3359.3	3361	3794	3301	3320	NH_2 s str(97)
2	1558.1	1581	1794	1561	1570	NH_2 sciss(86)
3	1349.6	1367.5	1634	1422	1400	NO_2 s str(51)
					-NN str(25)	$-NO_2$ bend(17)
4	950.9	unobs	1171	1019	1004	NN str(36)
					$-NO_2$ s str	$+NO_2$oopbend(15)
5	797.9	776	925	805	793	NO_2oopbend(50)
						-NN str(37)
6	692.5	713.5	807	702	706	NO_2 bend(50)
						$-NH_2$ wag(25)
7	628.5	587	713	620	624	NH_2 wag(40)
					$+NH_2$ s str(27)	-NN str(19)
a" 8	3478.0	3474	3931	3420	3440	NH_2 a str(100)
9	1612.8	1610.5	1902	1655	1630	NO_2 a str(78)
10	1226.7	1238.5	1382	1202	1184	NH_2 twist(74)
						$+NO_2$ a str(24)
11	484.5	unobs	639	556	548	NO_2 ip rock(79)
12	401.5	433.8	470	409	411	Tors(88)
Mean abs deviation (Ar matrix)				36	26	

[a] Ar matrix of ref. [4.49]

[b] N_2 matrix of ref. [4.49]

[c] Unscaled HF/6-31G* harmonic vibrational frequencies

[d] Theoretical frequencies scaled by 0.87

[e] Theoretical frequencies: N-H frequencies x 0.875
N-O frequencies x 0.857

[f] Potential Energy Distribution from the normal coordinate analysis of ref. [4.49].

4.6 Summary

The study reported here of the structure and vibrational frequencies of NH_2NO (section 4.3), has been previously reported as reference [4.36]. Our findings that a non-planar structure for nitrosamide is the lowest energy conformer have some tentative experimental backing from recent matrix isolation IR spectra.

The study described in section 4.4 suggests that:
(i) the pathway corresponding to the production of $N_2 + H_2O$ via intramolecular rearrangement of the stable (with respect to $NH_2 + NO$) species can occur with a small, or no, activation barrier;
(ii) the channel to $N_2H + OH$ will be at most, a secondary pathway, with the N_2H species dissociating rapidly to $N_2 + H$, and would thus not be an important intermediate at low temperatures. $N_2 + OH + H$ would be the most important source of chain branching at combustion temperatures.
(iii) The harmonic vibrational frequencies, once scaled, and the energy data presented here will be adequate for the calculation of the various rates of intramolecular rearrangement and of the overall rate constant.

The study of the $NH_2 + NO$ potential energy surface has been reported as reference [4.41].

The rearrangement of the initial nitramide adduct for the reaction of $NH_2 + NO_2$ to give the products N_2O and H_2O as the final products would seem to be able to proceed in an entirely analogous route to the reaction with NO. The molecular structure and vibrational frequencies predicted by ab-initio calculation at the HF/6-31G* level are in excellent agreement with the experimental values.

There remains one unanswered question, that of the factor of two in the rate between flash and discharge flow systems. In the past this has been attributed to formation of an intermediate complex of sufficient lifetime to diffuse out of the viewing region in a flash experiment but short enough to dissociate in a discharge flow system. Calculations on the lifetime of the H_2NNO complex indicate that this will not be the case and for reaction (1) the absence of any pressure effect on the rate would tend to rule out any stable intermediate being formed. For the analogous reaction of NH_2 with

NO_2 the same is probably true. There would thus seem to be scope for further work on these two interesting reactions.

CHAPTER 5

AB-INITIO POTENTIAL ENERGY SURFACES OF THE REACTIONS OF NH WITH NO AND NO_2

5.1 Introduction

The reaction of NH with NO has been found to proceed at the dipole - dipole collision rate [5.1] (see chapter 6). This implies that either the collision complex HNNO is sufficiently long lived that it does not redissociate back to reactants during the timescale of the experimental observations, or products are formed with no activation barrier. The rate of reaction between NH and NO does not exhibit any pressure or temperature dependence, which tends to favour the latter possibility. In contrast the reaction with NO_2 does not proceed at the dipole - dipole rate (which is theoretically faster than for NO due to the larger dipole moment) and although no pressure dependence has been observed, the rate constant does have a weak negative temperature dependence. The possible intermediate and product channels for both reactions have not, as yet, been observed directly. There have been previous theoretical studies on the NH + NO system but to date no such studies have been reported on the NH + NO_2 reaction. The ab-initio study reported here was undertaken in order to compliment the experimental data of the next chapter.

5.2 Calculational Method

All molecules were optimised at the HF/6-31G* (RHF for closed shell, UHF for open shell species) and in the case of the molecules involved in the HNNO PES, were further optimised at the MP2/6-31G* level. MP4SDQ/6-31G*//MP2/6-31G* energies contain contributions from the core electrons, MP4SDQ/6-31G*//HF/6-31G* energies do not. Harmonic vibrational frequencies were calculated at the HF/6-31G* level and are included in the

zero point energies without scaling. All calculations were done using Gaussian 82 [5.2].

5.3 Results and Discussion

The optimised HF/6-31G* geometries are given in Table 5-1. Total and relative energies for both the HNNO and $HNNO_2$ systems are given in Tables 5-2 and 5-3 respectively. HF/6-31G* harmonic vibrational frequencies for the species are listed in Table 5-4.

Table 5-1 HF/6-31G* optimised geometries. Distances in Å.

NH	NH 1.024		
OH	OH 0.959		
N_2	NN 1.078		
NO	NO 1.127		
NO_2	NO 1.165	ONO 136.1°	
N_2O	NN 1.092	NO 1.179	NNO 180°
HO_2	HO 0.953	OO 1.309	HOO 105.6°
HN_2	HN 1.029	NN 1.179	HNN 113.0°
HN_2TS_3	HN 1.386	NN 1.119	HNN 113.3°
HNNO	HN 1.015	NN 1.234	NO 1.206
	HNN 109.4°	NNO 132.4°	
$HNNOTS_1$	HN 1.289	NN 1.204	NO 1.419
	HNN 90.0°	NNO 95.5°	
$HNNOTS_2$	HN 1.548	NN 1.141	NO 1.180
	HNN 108.8°	NNO 161.3°	
$HNNO_2$	HN 1.010	NN 1.348	NO(cis) 1.217
	NO(trans) 1.252	HNN 113.6°	NNO(cis) 123.4°
	NNO(trans) 113.6°	(planar)	
$HNNO_2TS_4$	HN 1.679	NN 1.253	NO(cis) 1.355
	NO(trans) 1.189	HNN 49.3°	NNO(cis) 99.7°
	NNO(trans) 135.6°		

Table 5-2 HF/6-31G*//HF/6-31G*, MP2/6-31G*//MP2/6-31G*, MP4SDQ/6-31G*//HF/6-31G*, MP4SDQ/6-31G*//MP2/6-31G* total energies for reactants, transition states and products for the reaction of NH with NO and NO_2.

	-HF//HF	-MP2//MP2	-MP4SDQ //HF	-MP4SDQ //MP2
			(hartree)	
H	0.49823	0.49823	0.49823	0.49823
N	54.38544	54.45945	54.47280	54.47510
O	74.78393	74.88200	74.89528	74.89708
NH	54.95942	55.06142	55.07669	55.07950
OH	75.38228	75.52321	75.53453	75.53702
N_2	108.94395	109.26157	109.25324	109.26288
NO	129.24788	129.56446	129.56652	129.57336
N_2H	109.42540		109.72813	
N_2H TS_3	109.40391		109.71405	
HON	129.79722		130.09842	
HNO	129.78607		130.13082	
HO_2	150.17053		150.51303	
N_2O	183.68012	184.21368	184.18556	184.19985
NO_2	204.03149		204.54819	
HNNO	184.20851	184.69606	184.69815	184.70987
HNNO TS_1	184.14113	184.62760	184.63917	184.64845
ONNH TS_2	184.15030	184.65353	184.65138	184.66273
$HNNO_2$	259.01399		259.65397	
$HNNO_2$ TS_4	258.91916		259.60246	

Table 5-3. HF/6-31G*//HF/6-31G*, MP2/6-31G*//MP2/6-31G*, MP4SDQ/6-31G*//HF/6-31G*, MP4SDQ/6-31G*//MP2/6-31G* relative energies for reactants, transition states and products for the reactions of NH with NO and NO_2. All values include ZPVE correction.(kJ mol^{-1}).

	HF// HF	MP2// MP2	MP4SDQ// HF	MP4SDQ// MP2
		NH + NO		
NH + NO	0.0	0.0	0.0	0.0
HNNO	+18.2	-162.8	-122.9	-128.3
HNNO->N_2+OH (TS_1)	+175.8	-2.5	+13.0	+13.6
N_2+OH	-305.2	-410.2	-372.6	-379.1
HNNO->H+N_2O (TS_2)	+148.0	-74.3	-23.2	-27.6
H+N_2O	+76.3	-225.6	-106.1	-118.5
O+N_2H	-1.6		+55.7	
O+N_2H->O+H+N_2(TS_3)	+35.8		+73.6	
O+H+N_2	-64.9	-57.3	-24.9	-24.8
HNO+N	+102.8		+112.7	
HON+N	+71.2		+195.5	
		$NH + NO_2$		
NH + NO_2	0.0		0.0	
$HNNO_2$	-37.5		-53.3	
$HNNO_2$(TS_4)	+196.9		+67.4	
N_2O+OH	-179.2		-284.8	
HNNO+O	+3.8		+90.4	
N_2+HO_2	+313.7		-360.5	
N_2+O+OH	-319.7		-159.3	
N_2O+O+H	+60.5		+106.9	
NO+HNO	-104.5		-181.7	
NO+NOH	-136.1		-99.0	
2NO+H	-28.5		-35.8	
N+O+HNO	+88.3		+326.0	

Table 5-4. HF/6-31G* Harmonic vibrational frequencies. (cm^{-1}).

	Frequencies (cm-1)			ZPVE kJ mol^{-1}
NH ($^3\Sigma$)	Σ 3527			21.1
OH ($^2\Pi$)	Σ 3997			23.9
N_2 ($^1\Sigma$)	Σ 2758			16.5
NO ($^2\Pi$)	Σ 2222			13.3
N_2H ($^2A'$)	A' 1264	A' 1661	A' 3276	37.1
N_2H TS_3 ($^2A'$)	A' 1919i	A' 896	A' 2136	18.1
HON ($^3A''$)	A' 1286	A' 1372	A' 4011	39.9
HNO (^1A)	A' 1736	A' 1970	A' 3343	42.2
HO_2 ($^2A''$)	A' 1251	A' 1623	A' 4017	41.2
N_2O ($^1\Sigma$)	Π 689	Σ 1393	Σ 2633	32.3
NO_2 ($^2A_1$)	A_1 832	A_1 1613	B_2 1880	25.9
HNNO ($^2A'$)	A' 363	A' 942	A' 1171	54.8
	A' 1452	A' 1642	A' 3592	
HNNO TS_1 ($^2A'$)	A' 2716i	A' 528	A' 903	35.4
	A" 1072	A' 1435	A' 1980	
ONNH TS_2 ($^2A'$)	A' 1442i	A' 420	A" 661	31.7
	A' 851	A' 1315	A' 2049	
$HNNO_2$ ($^2A''$)	A" 489	A' 629	A" 636	70.1
	A' 719	A' 1051	A' 1155	
	A' 1510	A' 1822	A' 3705	
$HNNO_2$ TS_4 ($^2A'$)	A' 2841i	A' 611	A" 632	55.5
	A' 783	A" 880	A' 989	
	A' 1337	A' 1848	A' 2203	

A. NH + NO:

The MP4SDQ+ZPVE/6-31G*//MP2/6-31G* energies listed in Table 5-3 for the NH + NO reaction, are plotted in Figure 5.1. From the figure it would appear that the most likely pathway is that to N_2O + H. The channel to N_2 + OH has a transition state marginally higher than the reactants but at the level of theory used here should be considered to be essentially thermoneutral. It should be noted that the transition state TS_1, could result directly from the collision as this transition state corresponds to both ends of the dipoles colliding simultaneously in a broadside attack, rather than end on attack which will give the HNNO intermediate. Whether or not this is an important effect can not a-priori be assessed without extensive molecular dynamics calculations. One cannot, therefore, rule out N_2 + OH as the major channel. Indeed, there would seem to be some experimental evidence that this is the case. Mulvihill and Phillips [5.3] concluded that in their $N_2/H_2/O_2$ flame the reaction between NH and NO gave not more than 10% N_2O + H as reaction products. However these workers suggested that the major channel was that leading to N_2 + O + H which from Fig 5.1 would seem even less likely. Whyte and Phillips [5.4] also failed to detect any H atoms as products in their LP/RF of systems where NH and NO were present. Additional evidence comes from a recent study on the rate of reaction of H atoms with N_2O by Marshall et al [5.5]. These workers, from consideration of the reverse rate of NH + NO and the energy barriers involved, suggested that at room temperature the channel leading to N_2O + H may indeed be a secondary pathway for NH + NO. If the reaction does proceed to N_2 and OH then this would also affect some determinations of the product branching coefficient for the NH_2 + NO reaction. Recently Silver and Kolb [5.6] have adjusted their earlier estimation of the branching coefficient for this reaction (NH_2 + NO) and, by assuming OH and N_2 as the only products from secondary NH produced in their DF system, obtained a value consistent with more recent determinations.

There have been three previous ab-initio studies of this reaction. The first of these, by Melius and Binkley [5.7] using their BAC-MP4 method, reported thermochemistry for the species and transition states involved. Melius and Binkley found that NH and NO can combine with no activation barrier to form the stable HNNO intermediate. If the H atom undergoes a 1,3 shift the resulting unstable intermediate then dissociates to N_2 + OH, or the H atom can readily leave the HNNO intermediate (with a lower energy

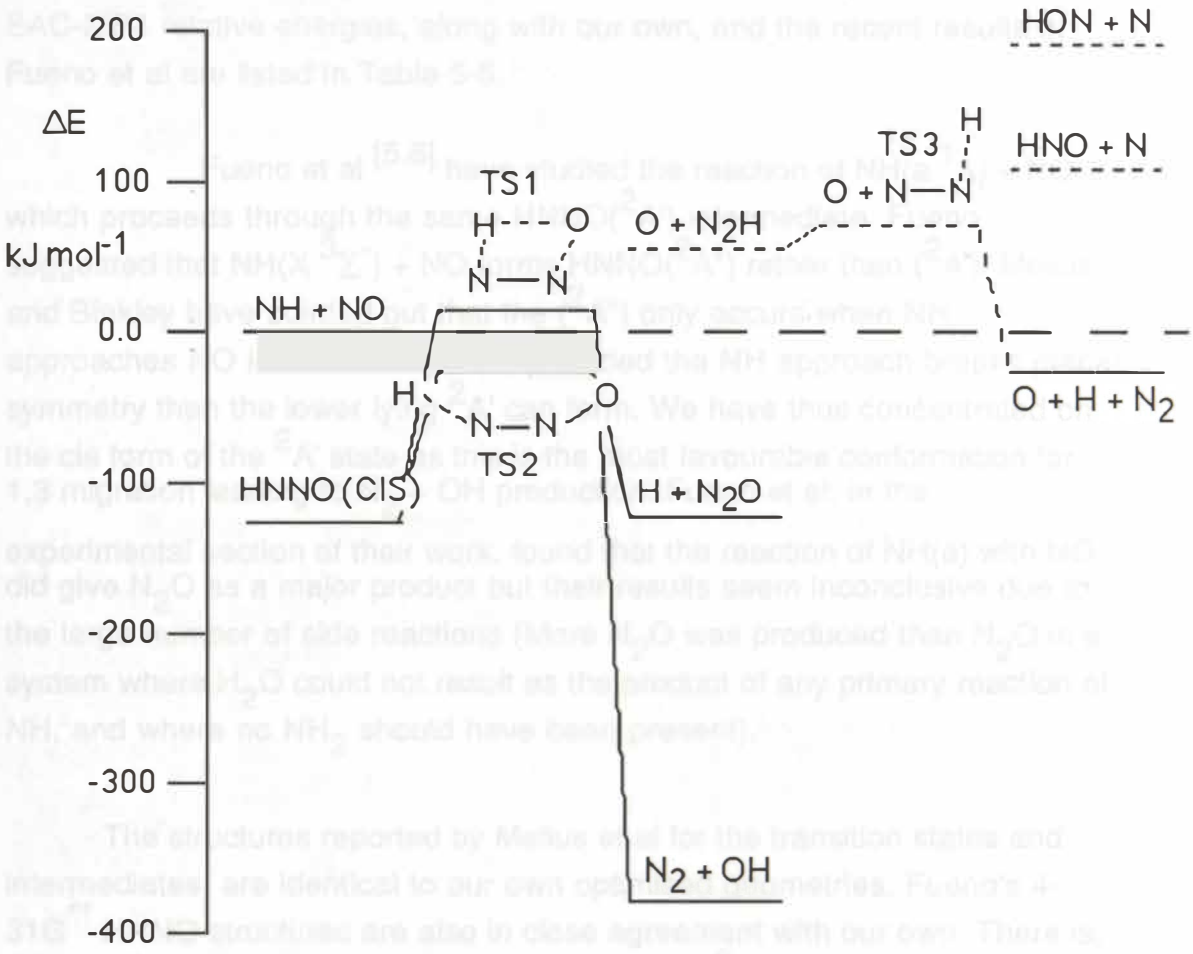

Figure 5.1 MP4SDQ+ZPVE//MP2 (6-31G*) Potential Energy profile for the NH + NO reaction. (dotted lines are MP4//HF).

barrier than the migration) to give N_2O + H. The second pathway was predicted to be dominant due to the greater density of states above this transition state than for the one leading to N_2 + OH. Marshall in association with Melius have reported a study on the H + N_2O reaction which occurs on the same PES as that for NH + NO. The BAC-MP4 predictions were used in conjunction with a tunnelling correction to model their observed H + N_2O data, over the temperature range 800 to 2500 K. In this later work an additional correction due to spin contamination of the wavefunctions was

included as well as their Bondwise Additive Corrections (BAC). Unfortunately in neither of these works did the authors report details of the basis sets used, making comparison with the present study difficult. Melius' BAC-MP4 relative energies, along with our own, and the recent results of Fueno et al are listed in Table 5-5.

Fueno et al [5.8] have studied the reaction of NH($a\ ^1\Delta$) + NO which proceeds through the same HNNO(^{2}A') intermediate. Fueno suggested that NH($X\ ^3\Sigma^-$) + NO forms HNNO(^{2}A") rather than (^{2}A'). Melius and Binkley have pointed out that the (^{2}A") only occurs when NH approaches NO in the same plane; provided the NH approach breaks planar symmetry then the lower lying ^{2}A' can form. We have thus concentrated on the cis form of the ^{2}A' state as this is the most favourable conformation for 1,3 migration leading to N_2 + OH production. Fueno et al, in the experimental section of their work, found that the reaction of NH(a) with NO did give N_2O as a major product but their results seem inconclusive due to the large number of side reactions (More H_2O was produced than N_2O in a system where H_2O could not result as the product of any primary reaction of NH, and where no NH_2 should have been present).

The structures reported by Melius et al for the transition states and intermediates, are identical to our own optimised geometries. Fueno's 4-31G** HNNO structures are also in close agreement with our own. There is, however, an anomaly with the energy for HNNO(^{2}A') intermediate. Our calculations indicate that the cis isomer of HNNO is 90 kJ mol^{-1} less exothermic than the calculations of Melius et al and 124 kJ mol^{-1} less exothermic than predicted by Fueno et al. Without details of the calculational method used by Melius and Binkley, any possible explanation for this descrepancy cannot be discussed, but, the difference between the level of theory used in Fueno et al's and our own calculations would not seem sufficiently great to be the source of such a large difference. This is serious as far as any potential modelling of this reaction, although will not alter any of the conclusions made in this discussion.

Table 5-5. Summary of recent ab-initio results for the NH + NO reaction. Values in brackets are from MP4SDQ/6-31G*//HF/6-31G* calculations.

Author	Melius [5.7]	Fueno [5.8]	This study
Level	BAC-MP4//HF	MRD-CI//HF	MP4//MP2
Basis set	unspecified	4-31G**	6-31G*
NH(X) + NO	0.0	0.0	0.0
HNNO(^{2}A') cis	-210.	-252.1	-128.3
TS_1	-17.3	-37.6	+13.6
N_2 + OH	-406.	-386.8	-379.1
TS_2	-27.7	-50.9	-27.6
N_2O + H	-155.	-129.1	-122.6
N_2H + O	+46.0	+26.	(+55.7)
O + TS_3	+74.1	+95.	(+73.6)
O + H + N_2	+3.4	+20.	-28.9

B. NH + NO_2:

As there have been no published studies on this system then no comparison of structures or energies at other levels of theory are possible. The only significant data on this system are the observations of the negative temperature dependence and the absence of any pressure effects on the rate. The negative temperature dependence is consistent with a transition state to products lower in energy than the level of the NH + NO_2 reactants. Because the rate measured is less than the expected dipole - dipole rate then this is an indication that processes occurring on the PES significantly effect the rate. The more direct abstraction mechanisms may play significant roles with the channel leading to NO + HNO being the most likely of these (on the grounds of exothermicity alone).

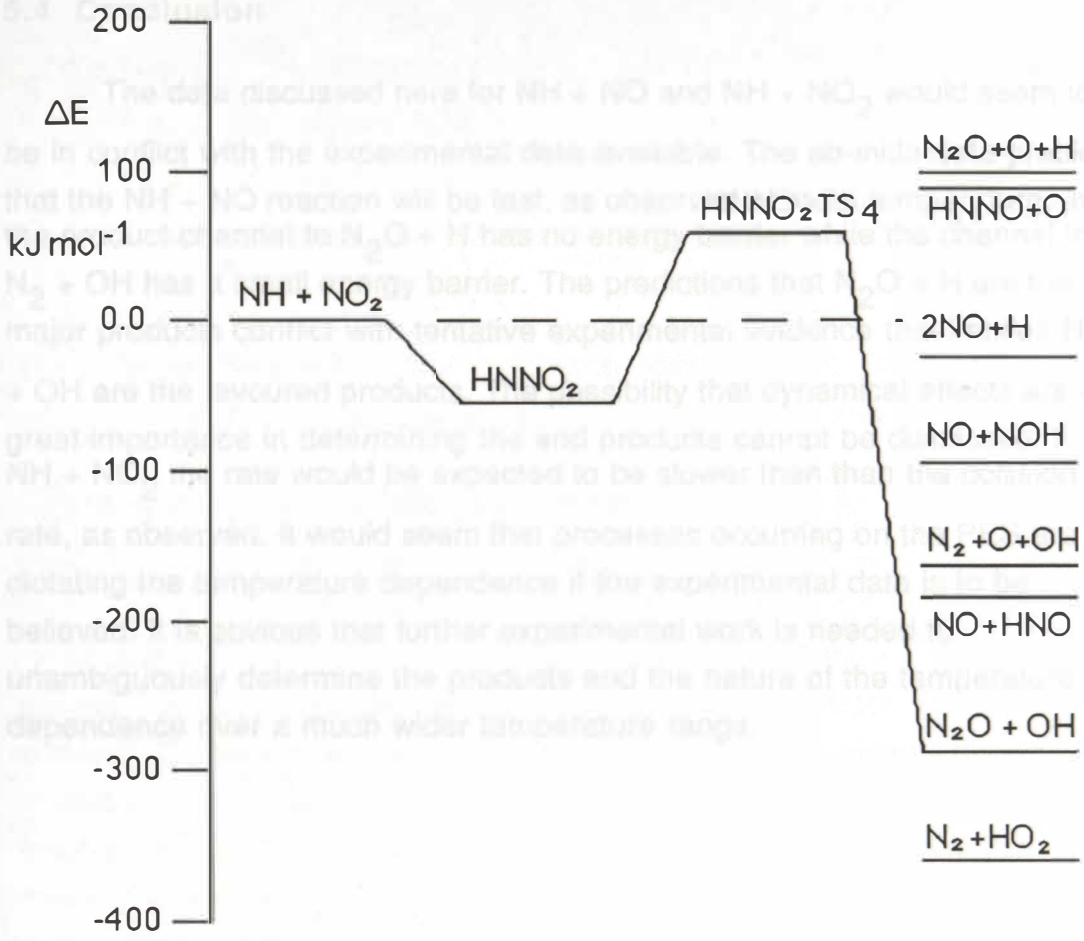

Figure 5.2. MP4SDQ+ZPVE/6-31G*//HF/6-31G* potential energy profile for the reaction of NH + NO_2

Figure 5.2 displays the relative MP4SDQ+ZPVE//HF (6-31G*) energies for the NH + NO_2 system. If the lifetime of the intermediate $HNNO_2$ is of the order of one vibration then a pressure effect would not be noticeable over the range investigated (see chapter 6). Assuming that the reaction does pass through a $HNNO_2$ intermediate, the ab-initio data predicts a positive temperature dependence, in contrast to the experimentally determined negative dependence.

5.4 Conclusion

The data discussed here for NH + NO and NH + NO_2 would seem to be in conflict with the experimental data available. The ab-initio data predicts that the NH + NO reaction will be fast, as observed at room temperature, and the product channel to N_2O + H has no energy barrier while the channel to N_2 + OH has a small energy barrier. The predictions that N_2O + H are the major products conflict with tentative experimental evidence that implies N_2 + OH are the favoured products. The possibility that dynamical effects are of great importance in determining the end products cannot be dismissed. For NH + NO_2 the rate would be expected to be slower than than the collision rate, as observed. It would seem that processes occurring on the PES are dictating the temperature dependence if the experimental data is to be believed. It is obvious that further experimental work is needed to unambiguously determine the products and the nature of the temperature dependence over a much wider temperature range.

CHAPTER 6

REACTIONS OF NH WITH NO, NO_2 AND N_2H_4

6.1 Introduction

Little is known about reactions involving NH($X\ ^3\Sigma$). Previous to this study, the bimolecular rates of reaction with NO [6.1-6.3], O_2 ($^3\Sigma$) [6.4-6.6], $O_2(^1\Sigma)$ [6.5], NH [6.6], HO_2 [6.6], NH_2 [6.6] and NH_3 [6.7-6.9], had been reported over a range of temperature and pressure conditions. Four of these studies [6.6] relied on extraction of the rate constant from computer simulation of the reactant concentration profiles, observed in a pulse radiolysis study of ammonia / oxygen mixtures. NH has been observed in emission in a variety of N/H containing flames [6.10,6.11] and is presumably an important combustion species.

The reactions of NH($X\ ^3\Sigma$) with NO and NO_2 are of interest as examples of fast reactions involving an initial adduct which can potentially undergo arrangement, similar to the NH_2 + NO system, before dissociating into one, or more, product channels. Our own and the three previous theoretical studies [6.12-6.14] on the HNNO system, have been discussed in chapter 5. The room temperature rate constant for the reaction between NH and NO is well established and was used by us, to ensure our experimental system was operating properly before looking at the reactions with NO_2 and N_2H_4. We report here the room temperature bimolecular rate constants of:

$$NH + N_2H_4 \xrightarrow{k_1} \text{products} \qquad (1)$$

$$NH + NO \xrightarrow{k_2} \text{products} \qquad (2)$$

$$NH + NO_2 \xrightarrow{k_3} \text{products} \qquad (3)$$

in Ar, at total pressures around one Torr. The pressure dependence of k_2 and k_3 was probed by altering the nature of the third body (hence altering the collision efficiency). The temperature dependences of k_2 and k_3 over the range 270-380 K, were measured. The reactions with NO and NO_2 are discussed in terms of rearrangement of intermediate HNNO and $HNNO_2$ complexes.

6.2 Experimental

The experimental system has been described in chapter 2. The essential features of the photolysis cell shown in Figure 6.1 have been discussed in section 2.1C. Pressure inside the cell was measured with the Texas Instruments quartz spiral gauge. Preliminary determinations of the NH + NO rate constant, using 193.3 nm (ArF) photolysis of either NH_3 or N_2H_4 as the source of NH, indicated that NH was being generated by secondary processes during the reaction time. This was evident in the measured rate constant, which was lower than the accepted literature value by a factor of ten. An acceptable source of NH was obtained from the 248.5 (KrF) photolysis of Hydrazine (75-100 mJ/pulse, focussed, 40 Hz). Hydrazine was introduced into the cell by passing a portion of the carrier gas flow through a saturator containing anhydrous hydrazine. The saturator pressure was maintained at around 500 Torr, as indicated by the MKS Baratron. Hydrazine concentrations were calculated from the saturator temperature and pressure from the vapour pressure data of Scott et al [6.15]. Variation in hydrazine concentration for the measurement of reaction (1) was achieved by varying the saturator pressure (Ar) between 100 and 200 torr, corresponding to N_2H_4 concentrations between 1.02 and 2.20 x 10^{15} molec cm^{-3}. For the NO and NO_2 experiments, typical concentration ratios were $[M]:[N_2H_4]:[R]$ = 300:28:0-10 where M = Ar, He, N_2, N_2O and R = NO or NO_2. Gas purities and handling procedures are given in section 2.2. Using the Scientech model 364 power/energy meter, no detectable absorption of the 248.5 nm photolysis pulse by the hydrazine could be measured. From the combined uncertainties in the power readings an upper limit of $5x10^{-19}$ cm^2 is

obtained for the absorption cross section, consistent with the single photon cross section of 8.4×10^{-20} cm^2 reported by Willis et al [6.16].

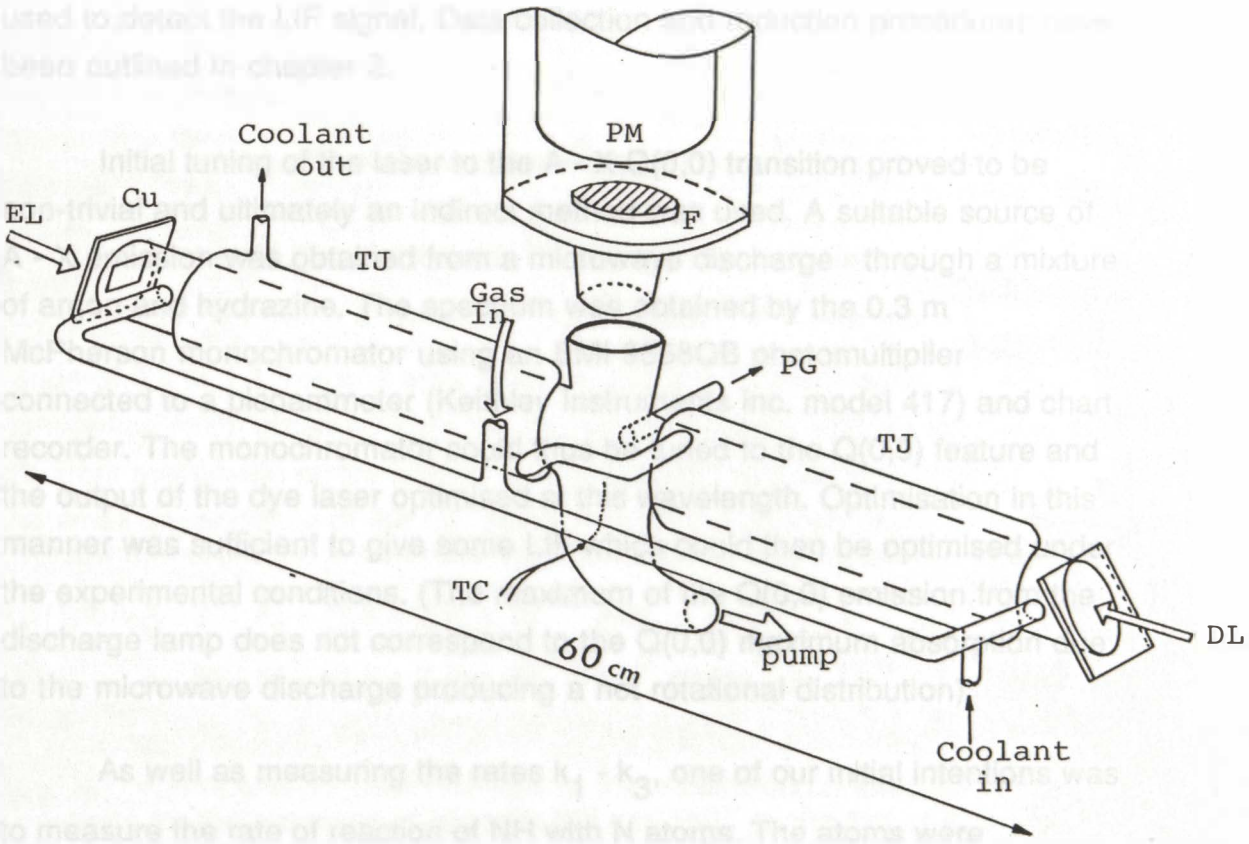

Figure 6.1 Photolysis Cell

EL Excimer Laser pulse
Cu Copper Shield
TJ Temperature Jacket
PG Pressure Gauge
TC Thermocouple
PM Photomultiplier
F Filter
DL Dye Laser pulse

NH was detected by LIF of the Q(0,0) $A(^3\Pi) - X(^3\Sigma)$ transition at 336.1 nm. Excitation light was obtained by frequency doubling (KDP angle-tuned) the output of the AVCO nitrogen-pumped dye laser operating with a mixture of cresyl violet and rhodamine 590. The output of the KDP crystal was suitably filtered to remove the transmitted fundamental at 672.2 nm. The fluorescence was observed perpendicular to the excitation beam through an interference filter (Corion Instrument Corporation, FWHM = 18 nm at 328nm) to remove the effects of prompt emission and the photolysis pulse. The low intensity of the doubled dye laser output coupled with low filter transmittance and low radical concentration, resulted in very small fluorescence signals. An EMI 9813QA photomultiplier connected to a fast preamp (10x gain) was used to detect the LIF signal. Data collection and reduction procedures have been outlined in chapter 2.

Initial tuning of the laser to the A - X Q(0,0) transition proved to be non-trivial and ultimately an indirect method was used. A suitable source of A - X emission was obtained from a microwave discharge through a mixture of argon and hydrazine. The spectrum was obtained by the 0.3 m McPherson monochromator using an EMI 9558QB photomultiplier connected to a picoammeter (Keithley Instruments Inc. model 417) and chart recorder. The monochromator could thus be tuned to the Q(0,0) feature and the output of the dye laser optimised at this wavelength. Optimisation in this manner was sufficient to give some LIF which could then be optimised under the experimental conditions. (The maximum of the Q(0,0) emission from the discharge lamp does not correspond to the Q(0,0) maximum absorption due to the microwave discharge producing a hot rotational distribution).

As well as measuring the rates k_1 - k_3, one of our initial intentions was to measure the rate of reaction of NH with N atoms. The atoms were generated upstream of the cell by microwave discharge and the concentration determined by photometric titration with NO in the standard fashion. It was found, however, that the N atoms were being removed by rapid reaction with hydrazine, before reaction with NH could occur.

6.3 Results

Data was collected at ten evenly spaced points over times ranging from 125 and 400 μs after the photolysis pulse. The 125 μs delay was necessary to avoid collection of data with a large window fluorescence component. Figure 6.2 shows a representative semi-logarithmic decay plot of NH LIF intensity for the reaction with four different concentrations of NO. The linearity of the decay plots indicate that the reaction obeyed pseudo-first order kinetics under the conditions used, as would be expected from the low cross section of hydrazine at 248.5 nm. Figures 6.3 and 6.4 are plots of the fluorescence decay rate against the concentration of reactant NO or NO_2, in various buffer gases. From these plots it is evident that there is no significant effect of the nature of the third body on the decay rate implying that both bimolecular rate coefficients for reactions (2) and (3) are pressure independent. Using the data available from all carrier gases, a least squares fit gives

k_2 (301 ± 2 K) = (5.78 ± 0.64) x 10^{-11} and

k_3 (299 ± 1 K) = (1.61 ± 0.14) x 10^{-11} cm^3 $molec^{-1}$ s^{-1} over the pressure range of 0.9 to 1.1 Torr. All error limits quoted are a combination of the 95% confidence limits obtained from the regression analysis and an estimated 6% from systematic errors (mainly due to reactant flow uncertainties). From the small dependence of the LIF decay rate on the concentration of hydrazine present the bimolecular rate constant k_1 was measured to be

k_1 (1 torr Ar, 301 K) = (3.6 ± 2.2) x 10^{-15} and

k_1 (1 torr Ar, 362 K) = (3.0 ± 2.5) x 10^{-15} cm^3 $molec^{-1}$ s^{-1}.

The temperature dependences of the measured bimolecular rate constants for the reactions of NH with NO and NO_2 in one torr of Ar are shown in Figure 6.5. From Figure 6.5 it is clear that for the reaction of NH with NO there is no significant temperature dependence over the range of temperatures studied. The bimolecular rate for the reaction of NH with NO_2 does exhibit a slight negative temperature dependence. Because of the large error limits on k_1 nothing can be said about the temperature dependence of the reaction with hydrazine.

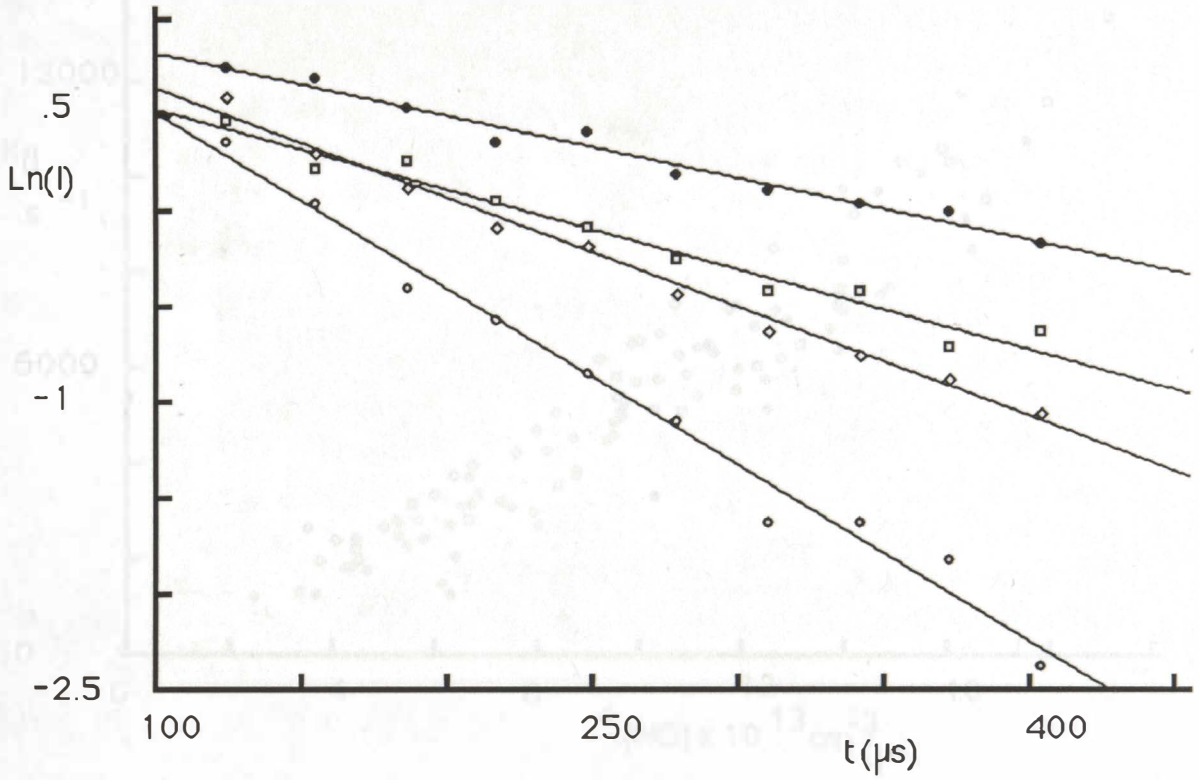

Figure 6.2. Pseudo-first-order decay plots of NH fluorescence in the presence of NO at T = 300 K, P = 1 Torr (Ar), with [NO] (10^{13} cm^{-3}) = 0 (solid dots), 3.4 (squares), 6.31 (diamonds), 12.7 (circles).

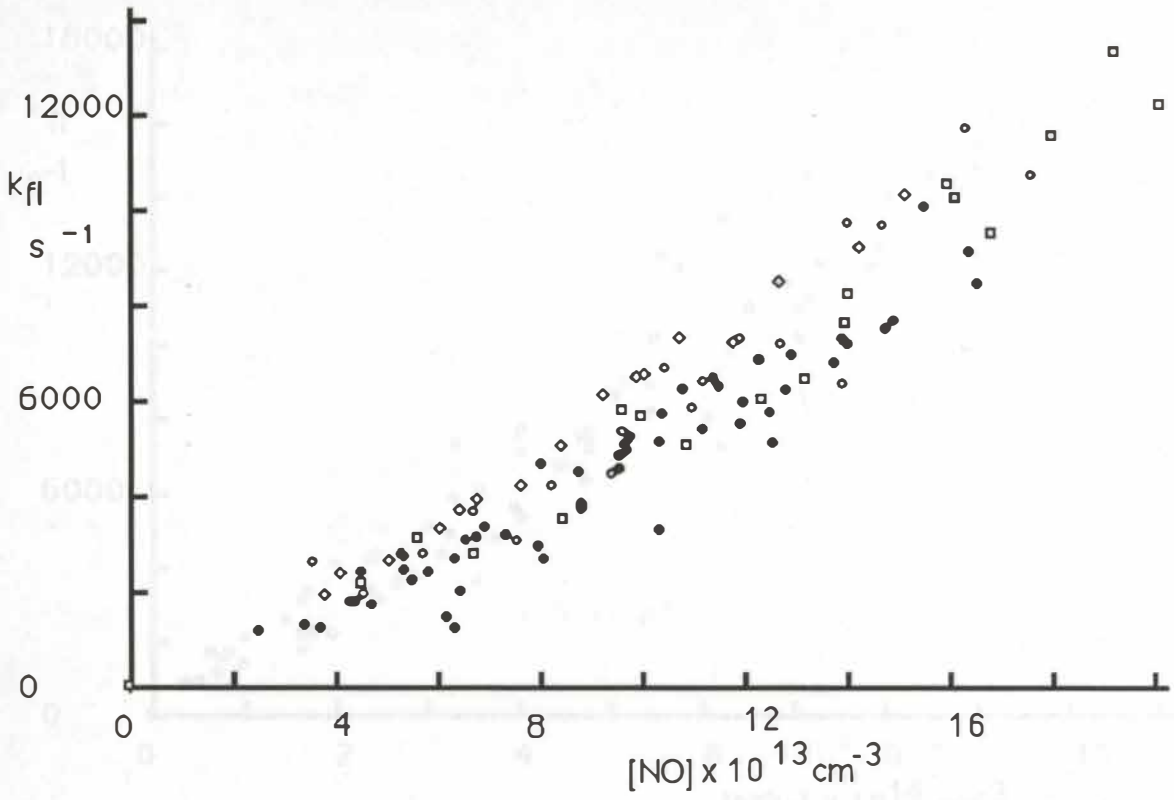

Figure 6.3. Slopes of first-order plots at 299 ± 1 K versus NO.concentration. Solid dots Ar carrier; diamonds He; circles N_2; squares N_2O.

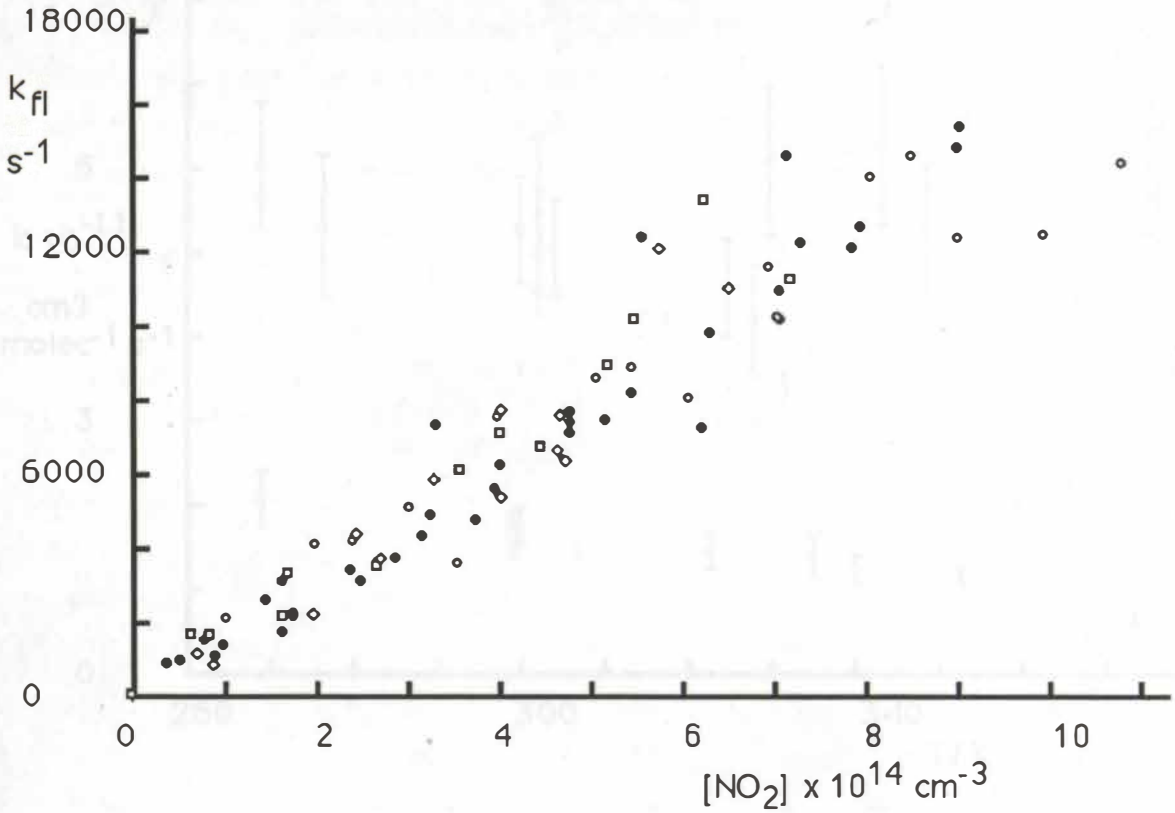

Figure 6.4. Slopes of first-order plots at 299 ± 1 K versus NO_2 concentration. Solid dots Ar carrier; diamonds He; squares N_2; circles N_2O.

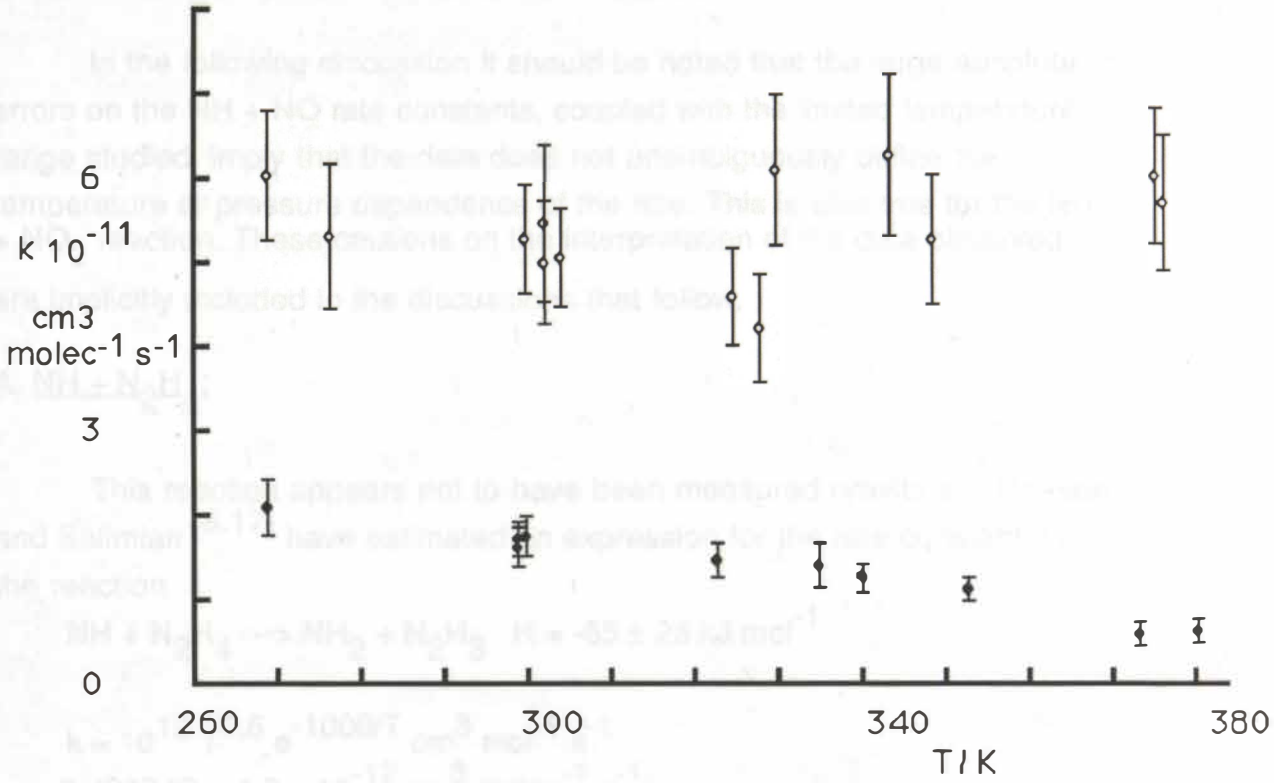

Figure 6.5. Temperature dependence of rate constants for Ar carrier. Hollow circles NH + NO; solid dots NH + NO_2

6.4 Discussion

In the following discussion it should be noted that the large absolute errors on the NH + NO rate constants, coupled with the limited temperature range studied, imply that the data does not unambiguously define the temperature or pressure dependence of the rate. This is also true for the NH + NO_2 reaction. These cautions on the interpretation of the data observed are implicitly included in the discussions that follow.

A. NH + N_2H_4:

This reaction appears not to have been measured previously. Hanson and Salimian [6.17] have estimated an expression for the rate constant for the reaction

$$NH + N_2H_4 \text{ ---> } NH_2 + N_2H_3 \quad H = -65 \pm 25 \text{ kJ mol}^{-1}$$

$$k = 10^{12}\, T^{0.5}\, e^{-1000/T} \text{ cm}^3 \text{ mol}^{-1} \text{ s}^{-1}$$

$$(k\,(298\text{ K}) = 1.0 \times 10^{-12} \text{ cm}^3 \text{ molec}^{-1} \text{ s}^{-1})$$

which clearly overestimates the room temperature rate, measured in our study to be k_1 (301 K) = (3.6 ± 2.2) x 10^{-15} cm^3 $molec^{-1}$ s^{-1}. No comparison of the temperature dependence of k_1 can be made due to the large error limits of the measured rate constants. These large errors reflect the small concentration range of N_2H_4 used.

The reaction presumably proceeds through a hydrogen abstraction, as written above. Although this reaction is exothermic, the energy barrier to H abstraction would probably be large enough to significantly slow the rate, in agreement with our measured value. The rate measured here for k_1 is comparable in magnitude to the rate of 3 x 10^{-16} cm^3 $molec^{-1}$ s^{-1} for reaction with NH_3 (H = +49 ± 29) [6.7-6,9].

B. NH + NO:

A summary of previous determinations of the rate constant of NH(X) with NO over a variety of experimental conditions is given in Table 6-1. From the table, it is obvious that the room temperature measurements have been consistent, whereas the high temperature data is not. The absence of any

pressure effect observed in our study is also evident from the studies of Hansen et al and Cox et al over the combined pressure range of 5 to 700 torr.

Table 6-1. Previous kinetic studies of NH($X\ ^3\Sigma^-$) with NO.

LP	Laser Photolysis
LIF	Laser Induced Fluorescence
FP	Flash Photolysis
RA	Resonance Absorption
PR	Pulse Radiolysis
S	Shock Tube
TOFMS	Time Of Flight Mass Spectrometry

T (K)	P (Torr)	$k_2 \times 10^{11}$ (cm^3 $molec^{-1}$ s^{-1})	Method	Ref
301	0.9-1.1	(5.78±0.64)	LP/LIF	a
270-370	1 (Ar)	$6.2\ e^{-0.048/T}$	LP/LIF	a
300	30-700 (He)	(4.7±1.2)	FP/RA	[6.1]
300	5 (He)	(4.8±0.2)	LP/LIF	[6.2]
420	250-1000 (NH_3)	3.8	PR/RA	[6.3]
1600-2100	-	$0.18\ e^{-230/T}$	S/TOFMS	[6.17]
1760-2850	-	$3.7\ e^{-10600/T}$	S/(various)	[6.17]
670-1480	-	$0.2\ e^{+960/T}$		[6.17]

[a] This work.

Phillips [6.18] has calculated the dipole - dipole capture rates using an approximate semiclassical trajectory method that includes the effect of intramolecular vibrational relaxation on the rate. These calculations indicated that the reaction proeeds at the dipole - dipole collision rate; implying subsequent rearrangement and dissociation of the collision complex were not the rate limiting steps. The absence of any temperature or pressure dependence on the rate implies that the lifetime of the $HNNO^*$ collision complex must be very small, essentially decomposing to products immediately. The ab-initio study of the previous chapter suggested that the barrier involved in the process

$HNNO \rightarrow H + NNO$ (4)

is well below the initial energy of the reactants (at 0 K). However, even though the barrier for

$HNNO \rightarrow N_2 + OH$ is calculated to lay some 13.6 kJ mol^{-1} above the reactants at 0 K, the combination of reactant thermal energy, hydrogen tunnelling and collision dynamics on the potential surface, may make this an important channel.

There have been no experimental determinations of the products for this reaction. A preliminary search in this laboratory using LIF detection of OH was inconclusive. Mulvihill and Phillips [6.19] in their $NH_3/H_2/N_2/O_2$ flame at 1500 K assigned an upper limit for the contribution of reaction (4) of 10%. Whyte and Phillips [6.20] failed to observe any increase in Hydrogen atom concentration in their 193 nm photolysis studies of NH_3/NO mixtures, such that NH would have been present in reasonable concentration.

C. $NH + NO_2$

The ab-initio results of the previous chapter suggest that both channels leading to N_2O +OH and HNNO + O have transition states lying above the energies of the initial reactants and are thus consistent with a measured rate slower than the dipole-dipole rate. The intermediate complex is calculated to be less strongly bound than the corresponding intermediate HNNO. The possibility of other channels having lower transition states than the two calculated here cannot be dismissed. Clearly, further work is necessary on this reaction to unambiguously determine the major product channels.

6.5 Summary

NH ($X\ ^3\Sigma$) radicals were generated by 248.5 nm (KrF) laser photolysis of hydrazine and their concentration was monitored by LIF at 336 nm (A-X Q(0,0)). Bimolecular rate coefficients for the reactions with N_2H_4, NO and NO_2 were measured at room temperature and 1 torr total pressure (Ar).

Room temperature bimolecular rate constants measured were :

$NH + N_2H_4$ ---> products (1)

$k_1 = (3.6 \pm 2.2) \times 10^{-15}$ cm^3 $molec^{-1}$ s^{-1}

$NH + NO$ ---> products (2)

$k_2 = (5.78 \pm 0.64) \times 10^{-11}$ cm^3 $molec^{-1}$ s^{-1}

$NH + NO_2$ ---> products (3)

$k_3 = (1.61 \pm 0.14) \times 10^{-11}$ cm^3 $molec^{-1}$ s^{-1}

k_2 was found to be independent of temperature over $270 < T < 380$ K; k_3 exhibited a small negative temperature dependence over this range. k_2 and k_3 are both independent of the choice of carrier gas at 300 K and total pressures around 1 torr. Reaction (1) probably proceeds via a hydrogen abstraction from N_2H_4. Reactions (2) and (3) are discussed in terms of either a direct mechanism or initial formation of HNNO and $HNNO_2$ intermediates followed by rearrangement and decomposition.

This work has been reported as ref [6.21]

CHAPTER 7

EMISSION FROM BH_n (n=0-3) FRAGMENTS IN THE 193.3 nm PHOTOLYSIS OF DIBORANE

7.1 Introduction

Excimer laser photolysis of stable precursors is widely used as a means of generating transient ground-state free radicals in order to study their kinetics and spectroscopy. Analysis of the prompt emission due to the initial formation of excited states of the transient species produced can yield information about the energetics and dynamics of the photofragmentation process, as has been done in the 193.3 nm photolysis of ammonia and hydrazine by Stuhl, Donnelly et al [7.1-7.4]. The aim of this section of work was to characterise the various emission bands seen as prompt emission in the 193.3 nm photolysis of Diborane by identifying the species responsible for each emission band. The amount of experimental information on the excited electronic states of BH_2 and BH_3 is limited. At the time of our experiments, the only gas phase spectra of BH_3 were those reported by Hirota et al [7.5] from the infra-red diode laser absorption study of the ν_2 band. For BH_2 the only spectrum was the absorption study by Herzberg and Johns [7.6] of the A-X transition between 600-840 nm. In the study reported here, emissions observed in the regions 254.5 to 326 nm and 366 to 386 nm are assigned to previously unknown transitions of BH_3, and emission observed between 320 and 345 nm is assigned to a new transition of BH_2, and the known A-X system of BH and with the ^2S-^2P and ^2D-^2P atomic Boron lines are also observed. The emissions observed are initially characterised on the basis of their laser power dependence and thermochemistry of BH_n species.

The photochemical decomposition of diborane has not been extensively investigated. The ultraviolet absorption spectrum of diborane has been reported by Blum and Herzberg [7.7] and by Price [7.8]. The reported

absorption consists of two continua; one with a maximum around 182 nm and a stronger absorption with maximum around 155 nm. Early experiments by Hirata and Gunning [7.9] in the 1950's, using mercury sensitized decomposition at 253.7 nm, suggested that B_2H_5 and H were the primary products of the photolysis step. Further studies by Kreye and Marcus [7.10] as well as Bufalini and Todd [7.11] in the 1960's, using the 184.9 nm Hg line as the photolysis source, also suggested that absorption in the A-X region resulted in formation of B_2H_5 and H. These conclusions were based on analysis of kinetic data obtained principally in the form of time dependent pressure changes, and on product analyses during the course of the photolysis. BH_3 was necessary to explain the production of B_5H_{11} in these experiments, but was thought to be formed with a quantum yield an order of magnitude lower than that for B_2H_5. In 1978 Clark and Anderson [7.12] proposed a photochemical purification scheme for silane contaminated with B_2H_6, using an ArF laser, and discussed the process in terms of the previous findings of Kreye et al.

Irion and Kompa [7.14] in 1982 found that the observed kinetics of the reaction of deuterium with diborane, photochemically initiated with ArF 193 nm laser radiation, could be explained in terms of the production of BH_3 as the primary reactive intermediate and not B_2H_5. More direct evidence for the production of BH_3 from the ArF laser photolysis of diborane came from Irion and Kompa's [7.15] subsequent PF_3, radical trapping experiments where they measured the quantum yield for BH_3 production to be 2.0 ± 0.25. None of this early work refers to the excited species produced in the primary photolysis step.

7.2 Experimental

Diborane was prepared by the method described earlier (section 2.2) and kept frozen at liquid nitrogen temperature until required. Mass spectrometric analysis showed that no higher hydrides were present. The photolysis cell is the same as that used for the kinetic studies of BH, described in chapter 9. Diborane flowed slowly through the cell at pressures between 7 and 20 mTorr. The photolysis source was the Lumonics TE 861-T excimer laser (section 2.1A) which under typical operating conditions produced 70 mJ, 10 ns pulses at 193.3 nm. This corresponds to a fluence of 35 mJ cm^{-2} unfocussed and at most 3 J cm^{-2} focussed. Laser intensities were measured with a Scientech model 364 power/energy meter. Spectra were measured in first and second orders of a McPherson model 218 (0.3 m) monochromator mounted adjacent to the photolysis region. Photomultipliers used were EMI 9558QB and EMI 9813QA. The signal was gated (gatewidth 0.5 μs) and amplified by a PAR model 160 Boxcar integrator before digitising and storing on a DEC LSI11/23 minicomputer. Lifetime measurements were made by amplifying the photomultiplier output (LeCroy 6103) and digitising the resulting signal with a 32 MHz transient recorder (LeCroy TR8837F), both in a Camac crate (LeCroy 8013A) controlled by a PC-XT computer. All the emissions were seen only as prompt emission on a sub microsecond timescale; no detectable emission was observed on longer timescales. Discharge spectra were obtained by passing diborane, either pure or diluted in Ar or He, through a microwave or Tesla discharge. For these measurements the signal was amplified by a Keithley model 417 picoammeter and recorded on a chart-recorder. Various combinations of Corning filters were used to select the region of interest and remove second or higher order spectra. All spectra described here are uncorrected for the wavelength response of the monochromator and photomultiplier combination.

7.3 Results

The observed spectra (an overall spectrum is shown in Figure 7.1) comprise 5 distinct emissions:

1) Atomic boron lines at 249.7 and 208.9 nm, with intensity proportional to the 193 nm laser intensity raised to a power of about 3.

2) A series of narrow, line - like features between 254 and 326 nm (Fig. 7.2), here attributed to BH_3^*, with intensity proportional to the first power of the laser intensity.

3) A structured band between 320 and 340 nm (shown at higher resolution in Fig. 7.3), here attributed to BH_2^*, with intensity proportional to the square of the laser intensity.

4) A structured region between 366 and 388 nm (also shown in Fig. 7.2), attributed to a second transition of BH_3^*, with intensity proportional to the first power of the laser intensity.

5) The A-X transition of BH [7.16] (Fig. 7.4.a), with a highly non-Boltzmann rotational distribution in the upper state and intensity proportional to the square of the laser intensity. The measured value of the BH A-X Q(0,0) emission lifetime was 540 ns, considerably longer than the literature value of 125 ± 5 ns [7.17], which implies that the v'=0 level was being repopulated by cascade processes.

The A-X bands of BH_2, which are a prominent feature of the microwave discharge spectrum, were not detectable in our laser excitation spectra. The emission from a weak tesla discharge through diborane-rare gas mixtures was also examined; only the A-X BH (Fig. 7.4.c) system was detectable. The power dependences given above were found to be within 10% of the stated integral values, generally erring on the low side except for the atomic boron lines and for the 366-388 nm emission, where the deviation could be as great as 20%. For all of the band systems there was no appreciable variation of band shape with laser intensity. The absence of any emission when a KrF (248.5 nm) laser was used as the photolysis source was attributed to the negligible single photon absorption coefficient at this wavelength.

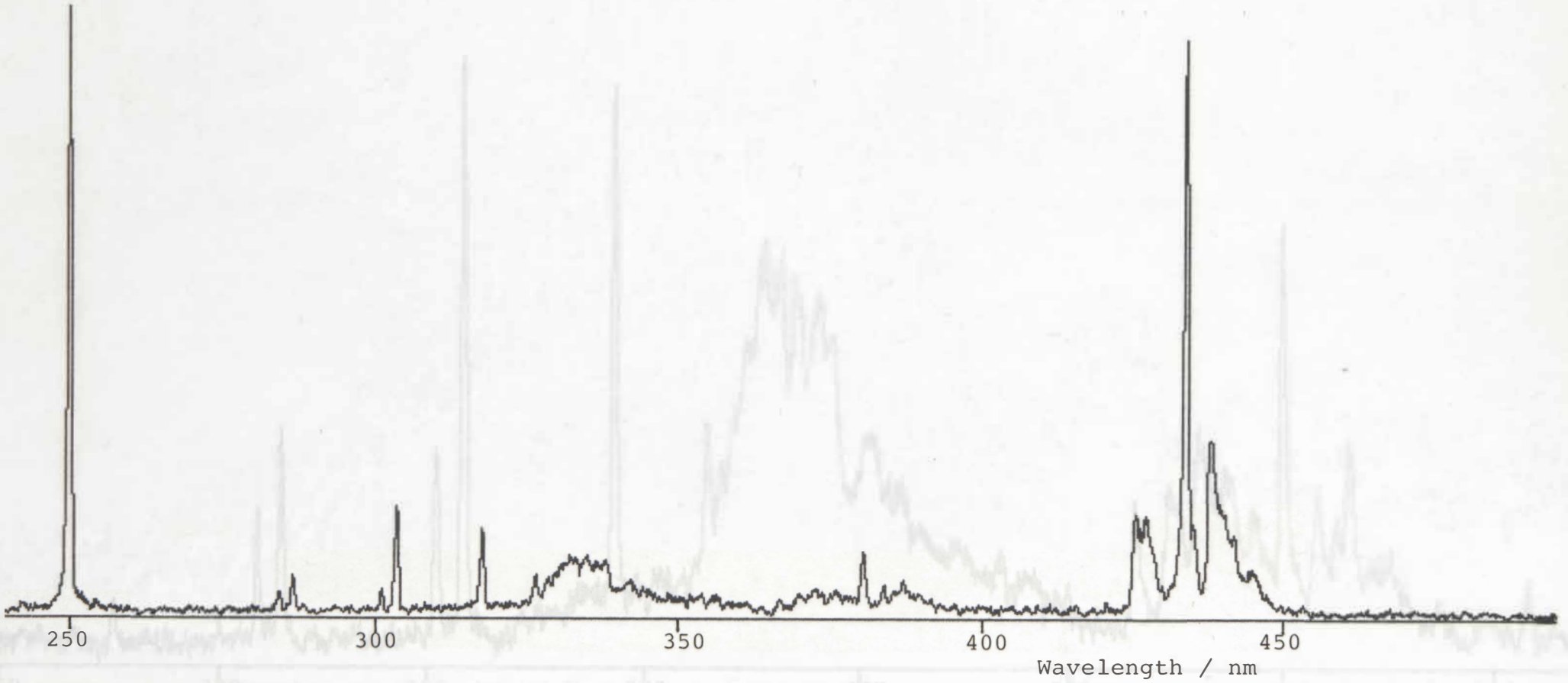

Figure 7.1 Emission spectrum at high 193.3 nm laser power.

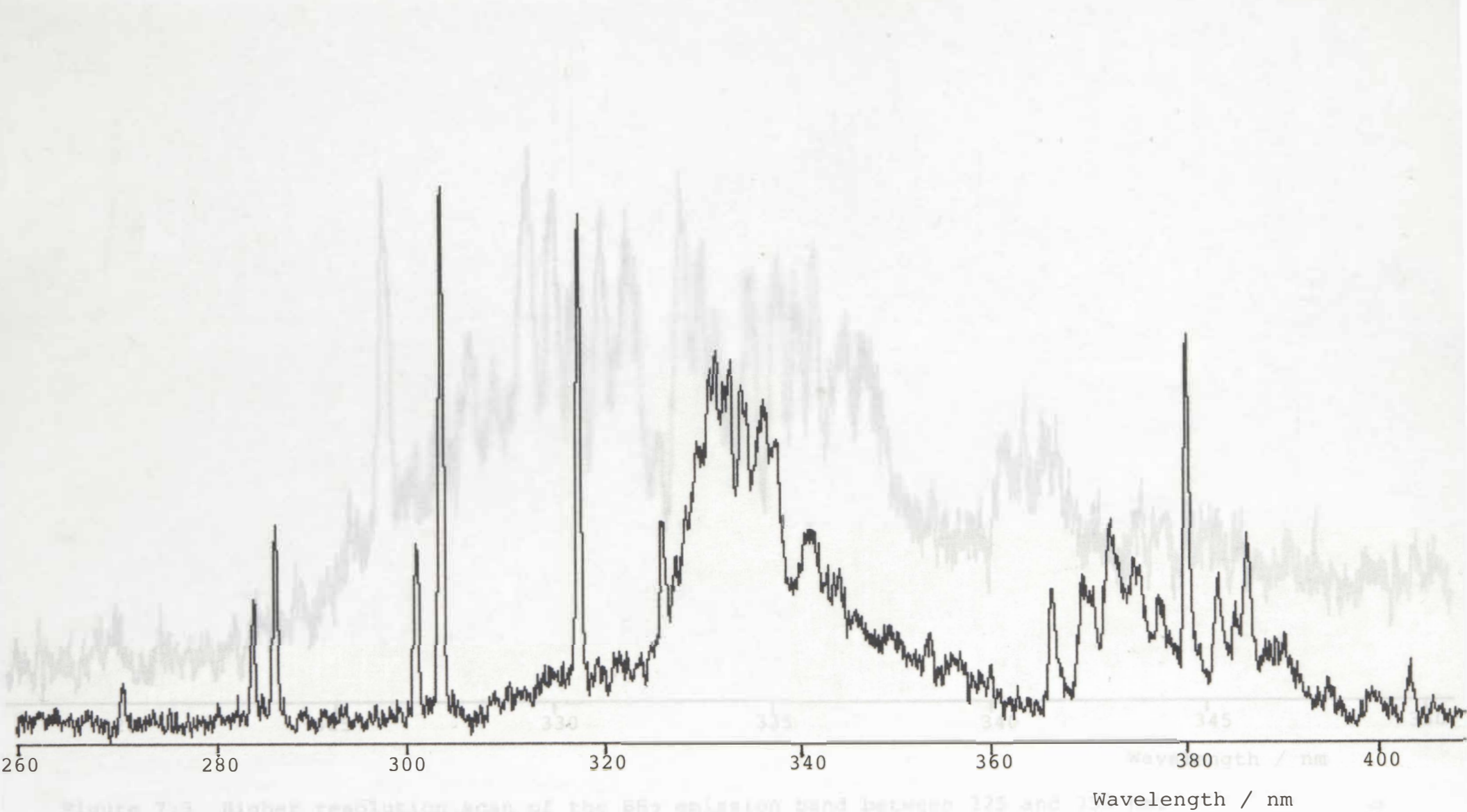

Figure 7.2 The rotationally cold BH_3 progression below 326 nm, the highly non-Boltzmann BH_2 emission band between 325 and 345 nm, and the BH_3 transition between 366 and 386 nm.

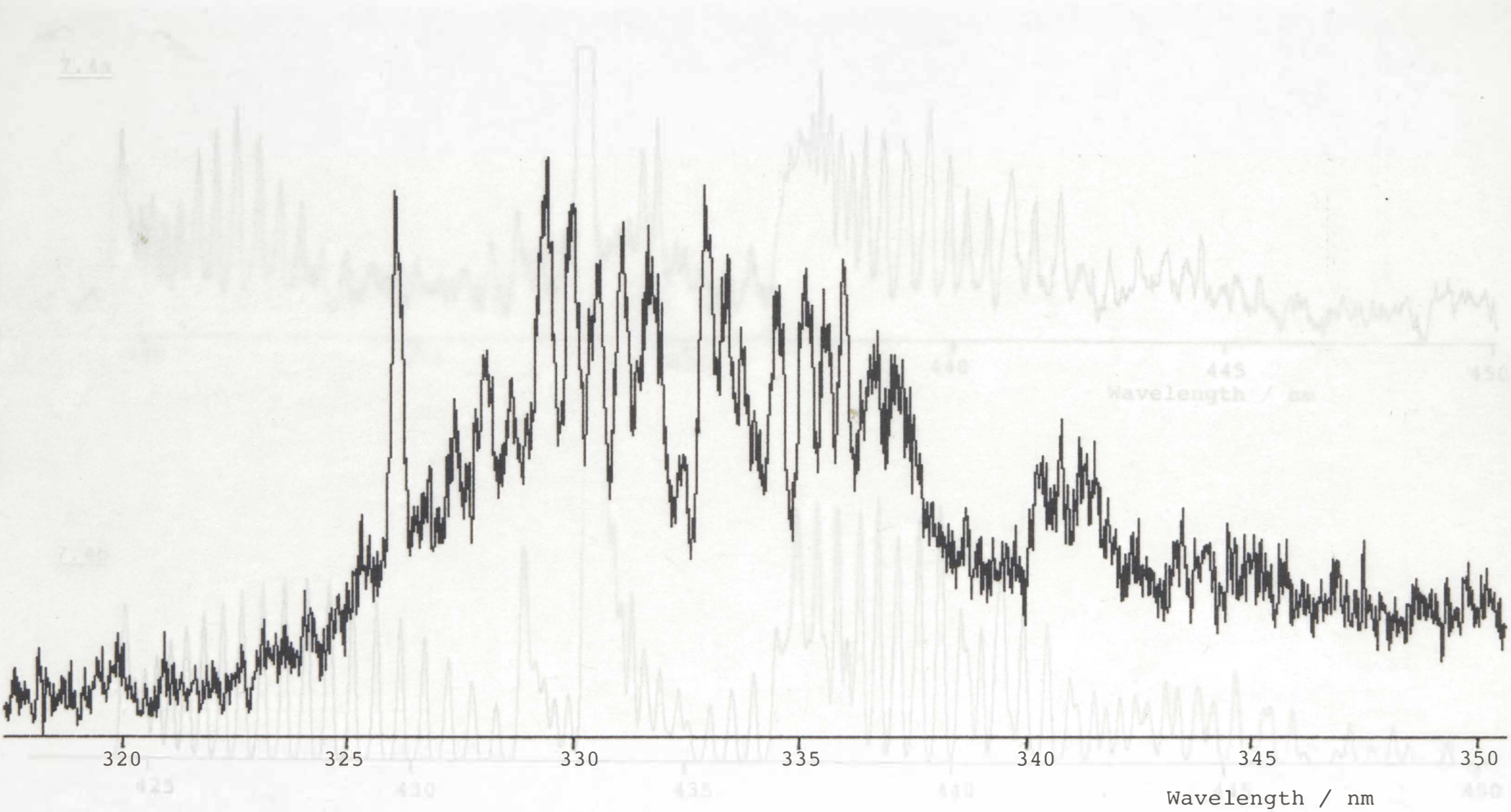

Figure 7.3 Higher resolution scan of the BH_2 emission band between 325 and 350 nm.

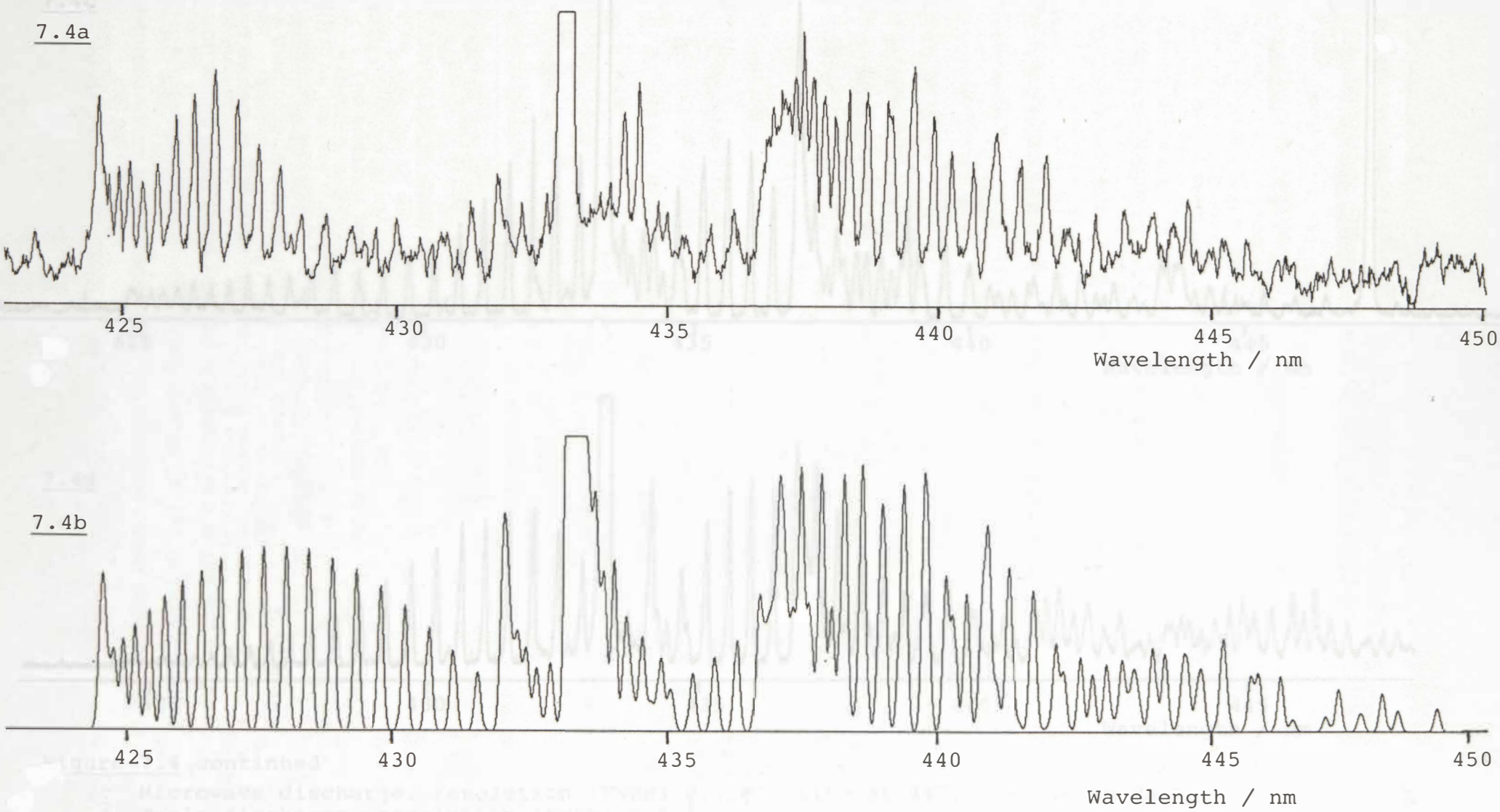

Figure 7.4 BH A-X emission bands.
a 193.3 nm laser generated spectrum, resolution (FWHM) 0.9 Å.
b Calculated spectrum for T = 2750 K, resolution (FWHM) 0.9 A.

7.4c

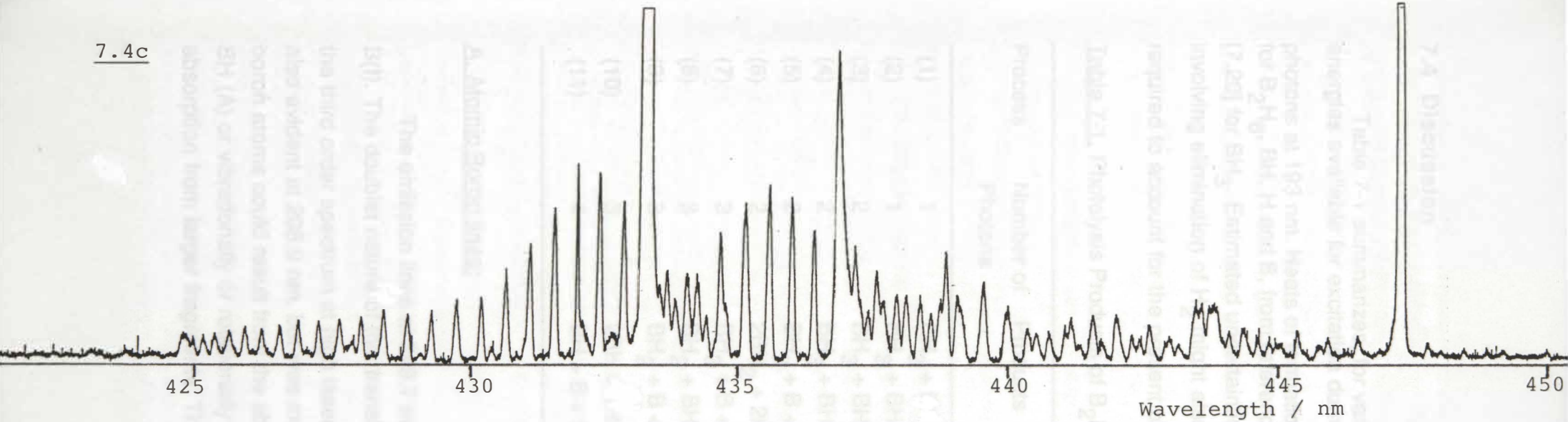

7.4d

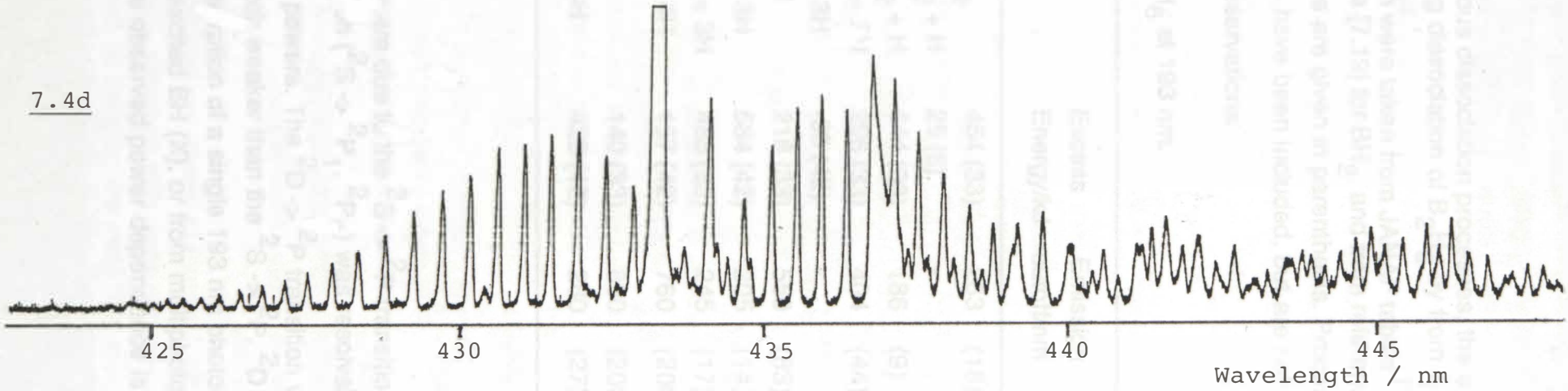

Figure 7.4 continued

c Microwave discharge, resolution (FWHM) 0.7 Å. Line at 447.2 is due to He.
d Tesla discharge, resolution (FWHM) 0.7 Å.

7.4 Discussion

Table 7-1 summarizes, for various dissociation processes, the excess energies available for excitation during dissociation of B_2H_6 by from 1 to 4 photons at 193 nm. Heats of formation were taken from JANAF tables [7.18] for B_2H_6, BH, H and B, from reference [7.19] for BH_2, and from reference [7.20] for BH_3. Estimated uncertainties are given in parenthesis. Processes involving elimination of H_2 might also have been included, but are not required to account for the present observations.

Table 7-1. Photolysis Products of B_2H_6 at 193 nm.

Process	Number of Photons	Products	Excess Energy/kJ	Emission cutoff/nm	
(1)	1	$BH_3 + BH_3$	454 (33)	263	(18)
(2)	1	$BH_3 + BH_2 + H$	25 (8)	-	
(3)	2	$BH_3 + BH_2 + H$	644 (33)	186	(9)
(4)	2	$BH_3 + BH + 2H$	296 (33)	404	(44)
(5)	2	$BH_3 + B + 3H$	-35 (42)	-	
(6)	2	$2BH_2 + 2H$	218 (33)	550	(83)
(7)	3	$BH_3 + B + 3H$	584 (42)	205	(14)
(8)	3	$BH_2 + BH + 3H$	488 (33)	245	(17)
(9)	3	$BH_2 + B + 4H$	157 (42)	760	(200)
(10)	3	$2BH + 4H$	140 (33)	850	(200)
(11)	4	$BH + B + 5H$	428 (42)	280	(27)

A. Atomic Boron lines:

The emission lines at 249.7 nm are due to the $^2S \rightarrow {}^2P$ transition of B(I). The doublet nature of this transition ($^2S \rightarrow {}^2P_1$, $^2P_2$) was resolvable in the third order spectrum at high laser powers. The $^2D \rightarrow {}^2P$ transition was also evident at 208.9 nm, but was much weaker than the $^2S \rightarrow {}^2P$. ^2D or ^2S boron atoms could result from the absorption of a single 193 nm photon by BH (A) or vibrationally or rotationally excited BH (X), or from multiphoton absorption from larger fragments. The observed power dependence is

consistent with process 7 of Table 7-1, although a contribution from process 11 might be a minor channel.

B. BH:

The observed power dependence of the BH A -> X emission band is that expected for process 4 of Table 7-1. A typical Tesla discharge spectrum of this transition is shown in Figure 7.4.c. The BH A -> X emission resulting from a microwave discharge through pure diborane is shown in Figure 7.4.d. The anomalous relative intensity of the P and R branches of the microwave discharge spectrum is due to the formation of an absorbing polymer on the window of the discharge lamp over the acquisition time of approximately 20 minutes. The apparent Boltzmann type distributions of these spectra are in obvious contrast to the laser generated spectrum. A simulated spectrum for the transition ^{11}BH A -> X is shown in Fig. 7.4.b. This simulated spectrum was generated by assuming a Boltzmann temperature of 2750 K for the upper state, which represents the closest match obtainable to the laser generated spectrum. Honl - London factors were calculated from the formulae in Herzberg [7.21] and Franck - Condon factors were not included in the calculation. Line positions used were those listed by Johns et al [7.16].

The features noted are :

1) The rotational population generated by the photolysis is distinctly non-Boltzmann.

2) The emitting population is both rotationally and vibrationally excited.

3) The emission breaks off at J' = 26 of the (0,0) band and the (3,3) band is entirely absent from the spectrum.

This last observation is consistent with other emission studies of this transition [7.16]. Observations 1 and 2 have also been made in studies of the generation of NH (A $^3\Pi$) from the 193 nm photolysis of ammonia [7.4,7.22-7.24].

C. BH2:

The band lying between 320 and 345 nm shown in Figure 7.3, has an apparent origin at 334 nm and evident K structure with peak separations averaging 52 cm^{-1} on the blue side and 42 cm^{-1} on the red. This spacing

(which is approximately 2(A' - B') of a near symmetric top) seems more reasonable for BH_2 (A" = 41.6 cm^{-1}, B", C" = 6.6 cm^{-1}) than for BH_3 (A" = B" = 8 cm^{-1}, C" = 4 cm^{-1}). Phillips [7.25], in his simulations of this band as a perpendicular transition of a near symmetric top, found it necessary to use an extremely non-Boltzmann distribution over initial rotational levels and a rotational temperature of 1250 K for the high rotational levels. Considering that this type of behaviour was observed for the A-X transition of BH, as discussed above, this does not seem unreasonable. Because of the notable absence of any detectable long progressions in this transition, the geometry of the upper state is probably quite close to that of the lower state. There have been no theoretical calculations on any of the states of BH_2 higher than the A state, making it impossible to identify either of the two states involved. The observed power dependence is consistent with process 3. Due to the very low detection sensitivity above 700 nm the possibility that other bands were present in this region cannot be ignored. In particular the A-X transition of BH_2 is almost certain to occur in such a system.

D. BH3:

The remaining two emission bands between 366 and 386 nm and the line - like series between 254.5 and 326.0 nm, are attributed to transitions of BH_3 on the basis that the intensities of both these bands depend linearly on the intensity of the ArF laser (process 1 of Table 7-1).

The intensity distribution of the progression of peaks between 254.5 and 326.0 nm is typical of a Franck - Condon envelope for a transition involving a significant change of geometry. The first peak at 254.5 nm was very weak and close to the intense atomic boron line at 249.7 nm, and consequently the position is uncertain to the extent of ± 0.5 nm. The spacings between the peaks of the strongest progression are 2297, 2031, 1944, 1455, and 841 cm^{-1}, with the last peak overlapping the band attributed to BH_2. From Figure 7.2 it can be seen that there are two smaller peaks 259 cm^{-1} and 296 cm^{-1} to the blue of the third and fourth line of the strong series. The overall shape of this series is consistent with a transition from a C_2v upper state, where the molecule has two BH bonds of equal length and the third is longer, as in the B_2H_6 precursor, to a planar D_3h ground state. The intervals then correspond to successive levels of an asymmetric stretching mode and the smaller levels to an out of plane mode

of the electronic ground state. Phillips [7.25] has simulated the sharp features themselves as perpendicular transitions of a rotationally cold symmetric (or near symmetric) top. The rotational temperatures required to give the narrow bands observed are around 50 K or less. The short wavelength limit of the emission corresponds to a maximum available excitation energy of 470 kJ/mol in good agreement with the value of 454 ± 33 kJ/mol in Table 7-1. This implies that one of the two BH_3 fragments produced contains most, if not all, of the excess energy. If the shortest wavelength peak at 254.5 nm is taken as the (0,0) transition of the lowest vibrational level of the ground state, we obtain a value of 149 kJ/mol for the dissociation energy of B_2H_6 to $2BH_3$. This compares well with the best ab-initio value from ref. [7.20] of 165.7 and the two most recent experimental estimates of Mappes et al (149 kJ/mol) [7.26] and Ruscic et al (154±18 kJ/mol) [7.13] . Due to the planar nature of the ground state and non-planar excited state this transition will be allowed in emission but not in absorption, in which regard it is analogous to the equivalent transition of CH_3, as discussed by Herzberg [7.27].

The separations of the peaks in the band between 366 and 386 nm are about 200 cm^{-1}, which is reasonable for an out of plane vibration of BH_3. The increased width of these bands, by comparison with the system just described, implies that the emitters of this system have a greater amount of rotational excitation. The absence of any long progression, other than that associated with the out of plane vibration, is indicative of a small change in geometry between the upper and lower states.

Schaefer et al [7.28] predict the lowest excited singlet state of BH_3 to be a $^1E"$ state of D_3h symmetry at 587 kJ/mol, and note that this state would be subject to Jahn-Teller distortion to $^1A_2$ and $^1B_2$ states of point group C_2v. The simplest interpretation of our two BH_3 emission bands is that the $^1E"/^1A_2, ^1B_2$ surface is being populated in two distinct regions during the initial photolysis event.

7.5 Summary

Emission spectra observed during the 193 nm ArF laser photolysis of diborane have been assigned on the basis of known thermochemistry and observed laser power dependence.

The emissions observed are:

B atom $^2S \rightarrow {}^2P$ 208.9 nm

B atom $^2D \rightarrow {}^2P$ 249.7 nm

BH $A(^1\Pi) \rightarrow X(^1\Sigma)$ 433.0 nm

New transitions observed are:

BH_2 320 - 340 nm

BH_3 254 - 326 nm

BH_3 366 - 388 nm

Both the BH and BH_2 bands arise from absorption of two photons and show extremely non-Boltzmann rotational populations in the upper state. The BH_3 bands arise from single photon absorption and are due to two different populations in the upper state (tentatively the $^1E''$, lowest lying electronic state), one of which is rotationally cold. This is the first observation of an electronic transition of BH_3. The enthalpy for dimerisation at room temperature inferred from the low wavelength threshold of the bands we attribute to BH_3, is 149 kJ/mol. This value is in excellent agreement with the most recent experimental measurements, and the best ab-initio values.

This work has been reported as reference [7.25].

CHAPTER 8

AB-INITIO POTENTIAL ENERGY SURFACE OF THE REACTION OF BH WITH NO

8.1 Introduction

The rate of reaction between BH($^1\Sigma$) and NO($^2\Pi$) is extremely fast, essentially proceeding at the dipole - dipole capture rate. The products of this reaction are unknown as are the relative thermodynamics of most of the possible intermediates and products. Presented here is an ab-initio study of the energies, optimised geometries, and harmonic vibrational frequencies of a variety of species conceivably involved in the reaction.

8.2 Details of Calculations

The geometries of the species that could be involved in the reaction of BH with NO were optimised at the HF/6-31G* level (U.H.F. for open shell /R.H.F. for closed shell species) and harmonic vibrational frequencies and MP2 to MP4SDQ energies were calculated at these optimised geometries with the same basis set. The MP2 energies quoted include core contributions while the MP4SDQ energies do not. The 6-31G* basis set is of double zeta quality and includes a set of d polarisation functions on the non-hydrogen elements. All calculations were done using the Gaussian 82 program [8.1].

8.3 Results and Discussion

A summary of the optimised HF/6-31G* geometries is given in Table 8.1. Of these species, all 6 diatomics and the two triatomics HBO and HNO have been observed experimentally. Comparison with the experimental data available on the geometries of these species indicates that the HF/6-31G* level of theory tends to underestimate the lengths of bonds by as much as 3%. These findings are in accord with the findings of Pople et al [8.2] for the HF/6-31G* geometries of molecules containing first row elements.

The harmonic vibrational frequencies calculated at the HF/6-31G* level are too high and comparison with the known experimental frequencies indicates the scaling factor recommended by DeFrees and McLean [8.3] will yield frequencies much closer to the experimental ones.

The HF/6-31G*, MP2/6-31G*, and MP4SDQ/6-31G* energies, calculated at the HF/6-31G* geometries, for all possible species involved are given in Table 8-2. The corresponding energies for the various species involved are given in Table 8-3 with the MP4SDQ+ZPVE results potted in Figure 8.1. From Figure 8.1 it can be seen that both possible association products are stable with respect to dissociation to BH and NO and that there are 5 stable sets of products. Of these 5 sets, two are spin forbidden and one involves production of electronically excited N(^{2}D) atoms. As yet there has been no experimental determination of the products of this reaction although HBO has been observed in conditions where BH is certain to be produced in reasonable quantity while in the presence of NO [8.4,8.5].

Analysis of the HF/6-31G* electronic structure for the initial association product HBNO indicates that both the hydrogen and boron atoms are slightly electron deficient with the excess electron density almost totally on the oxygen atom. For HBON both the boron and nitrogen atoms are electron deficient with the excess electron density on both the hydrogen and oxygen atoms. The HBNO association

Table 8-1. HF/6-31G* Optimised Geometries for HBON species.

BH($^1\Sigma$)	BH 1.225		
NH($^3\Sigma$)	NH 1.024		
OH($^2\Pi$)	OH 0.959		
BN($^3\Pi$)	BN 1.293		
BO($^2\Sigma$)	BO 1.187		
NO($^2\Pi$)	NO 1.143		
HBN($^2\Pi$)	HB 1.167	BN 1.292	
HBN-HNB TS($^2\Sigma$)	HB 1.228	BN 1.290	HBN 81.8°
HNB($^2\Sigma$)	HN 0.982	BN 1.228	
HOB(^{1}A')	HO 0.951	OB 1.300	HOB 121.5°
HBO($^1\Sigma$)	HB 1.167	BO 1.185	
HON(^{3}A")	HO 0.954	ON 1.316	HON 108.7°
HNO(^{1}A)	HN 1.032	NO 1.175	HNO 108.8°
BNO(^{3}A")	BN 1.422	NO 1.180	BNO 143.4°
BON(^{3}A")	BO 1.327	ON 1.327	BON 130.2°
HBON(^{2}A") cis	HB 1.189	BO 1.360	ON 1.328
	HBO 122.7°	BON 116.7°	HBON 0.0°
HBON TS_1	HB 1.191	BO 1.364	ON 1.305
	HBO 122.2°	BON 130.3°	HBON 89.5°
HBON(^{2}A") trans	HB 1.186	BO 1.356	ON 1.325
	HBO 118.8°	BON 120.2°	HBON 180°
HBON-BO+NH TS_2	HB 1.433	BO 1.348	ON 1.374
	NH 1.334	HBO 91.2°	BON 88.3°
	HBON 0.0°		
HBNO($^2\Pi$)	HB 1.164	BN 1.231	NO 1.241

Table 8-2. HF/6-31G*//HF/6-31G*, MP2/6-31G*//HF/6-31G* and MP4SDQ/6-31G*//HF/6-31G* energies for BHNO species. (hartree)

	HF	MP2	MP4SDQ
$H(^2S)$	- 0.49823	- 0.49823	- 0.49823
$B(^2P)$	-25.52204	-24.55872	-24.57562
$N(^4S)$	-54.38544	-54.45945	-54.47280
$O(^3P)$	-74.78393	-74.88200	-74.89528
$BH(^1\Sigma)$	-25.11826	-25.17585	-25.19253
$NH(^3\Sigma)$	-54.95942	-55.06125	-55.07669
$OH(^2\Pi)$	-75.38228	-75.52281	-75.53453
$BN(^3\Pi)$	-78.99016	-79.17562	-79.18574
$BO(^2\Sigma)$	-99.51995	-99.76092	-99.75808
$NO(^2\Pi)$	-129.24788	-129.56298	-129.56652
$HBN(^2\Pi)$	-79.63309	-79.83793	-79.85122
HBN-HNB TS($^2\Sigma$)	-79.56144	-79.77288	-79.79877
$HNB(^2\Sigma)$	-79.64644	-79.86919	-79.87231
$HOB(^1A')$	-100.09077	-100.33656	-100.34703
$HBO(^1\Sigma)$	-100.16615	-100.43044	-100.43064
$HON(^3A'')$	-129.79722	-130.08444	-130.09842
$HNO(^1A)$	-129.78607	-130.12436	-130.13082
$BNO(^3A'')$	-153.83665	-154.20279	-154.21299
$BON(^3A'')$	-153.86240	-154.20175	-154.21997
HBON-BO+NH TS_2	-154.38397	-154.76664	-154.78342
HBON TS_1	-154.44438	-154.78776	-154.80297
$HBON(^2A'')$ cis	-154.45826	-154.79981	-154.81503
$HBON(^2A'')$ trans	-154.45858	-154.79992	-154.81527
$HBNO(^2\Pi)$	-154.47717	-154.87374	-154.88198

product is very similar to the HNNO association product formed by the reaction of NH + NO, as discussed in chapter 5. The structure of the transition state for the interconversion of HBN and HNB has also been calculated and found to be 137.7 kJ mol^{-1} above HBN. The barrier to interconversion of the two isomers of HBON (TS_1) and the transition state energy for the conversion of HBON to BO + NH (TS_2) have been calculated. The level of theory used is not the most appropriate for this transition state structure. A MCSCF calculation would probably lead to a lower activation barrier for this step. The N(^{2}D) state cannot be represented by a single determinant with real orbitals. Therefore calculations on the transition state to HBO + N(^{2}D) could not be attempted.

The inclusion of correlation energy to the MP4SDQ level alters the relative stablilty of the products by anything between -30 and +160 kJ mol^{-1} when compared to the HF relative energies. The addition of zero point vibrational energies to the MP4SDQ energies does not alter the relative stabilities significantly for any of the possible sets of products, or the two intermediates. The general trends evident with inclusion of correlation effects on the energies are:

1) A stabilisation of HBNO and a destabilisation of the HBON isomers with respect to BH and NO. At the MP4SDQ level both HBNO and HBON are strongly bound intermediates and this would not be expected to change with a move to a higher level of theory.

2) At the HF level HBNO has three exothermic product channels. These are BN + OH (-16.65 kJ mol^{-1}), HBN + O (-133.6 kJ mol^{-1}) and BNH + O (-168.6 kJ mol^{-1}). At the MP4SDQ level only the BNH + O channel is still exothermic.

3) HBON also has three spin-allowed exothermic sets of products at the HF level: BO + NH (-297 kJ mol^{-1}), HBO + N(^{2}D) (-256.9 kJ mol^{-1}) and HOB + N(^{2}D) (-59 kJ mol^{-1}). Both the BO + NH and HBO + N(^{2}D) channels remain exothermic at the MP4SDQ level,and the magnitude of the exothermicities of these two product channels, indicates that further inclusion of correlation effects to a level higher than MP4SDQ would not affect the relative energies enough to make them endothermic. While the trans form of HBON is slightly more stable, the barrier to rotation is calculated to be only 29 kJ mol^{-1} at 0 K. The transition state corresponding to the formation of BO and NH from HBON, lies 75.2 kJ mol^{-1} above the cis isomer at 0 K. Hydrogen atom tunnelling rates would, almost certainly be significant through such a barrier.

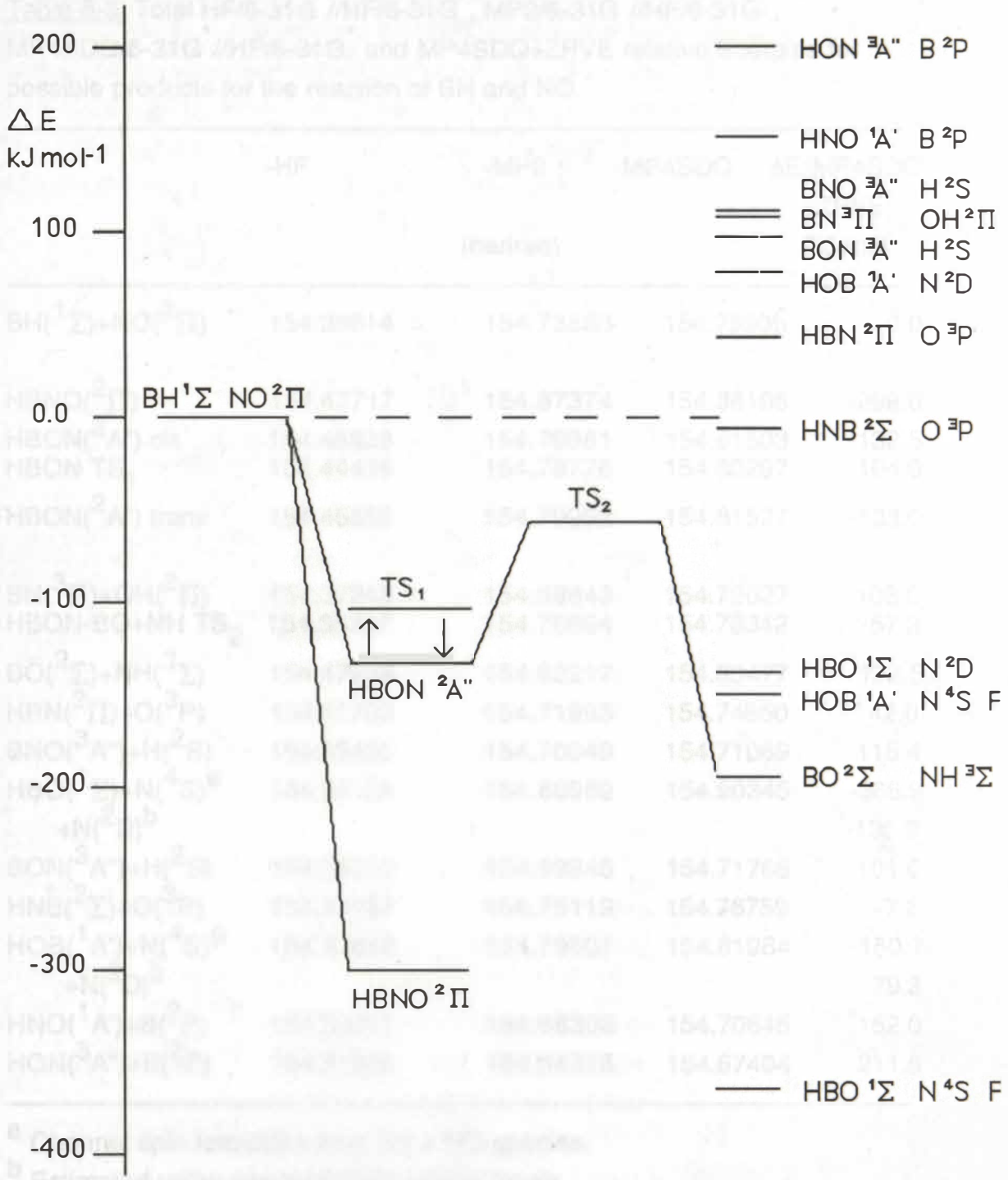

Figure 8.1. Relative MP4SDQ+ZPVE Energies for the Reaction of BH with NO.
F = Spin Forbidden.

Table 8-3. Total HF/6-31G*//HF/6-31G*, MP2/6-31G*//HF/6-31G*, MP4SDQ/6-31G*//HF/6-31G* and MP4SDQ+ZPVE relative energies for possible products for the reaction of BH and NO.

	-HF	-MP2	-MP4SDQ	ΔE(MP4SDQ +ZPVE)
		(hartree)		(kJ mol^{-1})
$BH(^1\Sigma)+NO(^2\Pi)$	154.36614	154.73883	154.75905	0.0
$HBNO(^2\Pi)$	154.47717	154.87374	154.88198	-299.0
$HBON(^2A")$ cis	154.45826	154.79981	154.81503	-132.5
HBON TS_1	154.44438	154.78776	154.80297	-104.0
$HBON(^2A")$ trans	154.45858	154.79992	154.81527	-133.0
$BN(^3\Pi)+OH(^2\Pi)$	154.37243	154.69843	154.72027	108.0
HBON-BO+NH TS_2	154.38397	154.76664	154.78342	-57.3
$BO(^2\Sigma)+NH(^3\Sigma)$	154.47938	154.82217	154.83477	-193.5
$HBN(^2\Pi)+O(^3P)$	154.41702	154.71993	154.74650	42.0
$BNO(^3A")+H(^2S)$	154.33435	154.70049	154.71069	115.4
$HBO(^1\Sigma)+N(^4S)$[a]	154.55159	154.88989	154.90345	-366.9
$+N(^2D)$[b]				-136.9
$BON(^3A")+H(^2S)$	154.36010	154.69945	154.71766	101.0
$HNB(^2\Sigma)+O(^3P)$	154.43037	154.75119	154.76759	-7.2
$HOB(^1A')+N(^4S)$[a]	154.47622	154.79601	154.81984	-150.7
$+N(^2D)$[b]				79.3
$HNO(^1A')+B(^2P)$	154.30811	154.68308	154.70645	152.0
$HON(^3A")+B(^2P)$	154.31926	154.64315	154.67404	211.6

[a] Channel spin forbidden from BH + NO species.

[b] Estimated using spectroscopic energy levels.

Table 8-4. HF/6-31G* harmonic vibrational frequencies and zero-point energies for BHNO species.

	Vibrational frequencies (cm^{-1})			ZPVE ($kJ\ mol^{-1}$)
BH($^1\Sigma$)	2513			15.0
BN($^3\Pi$)	1767			10.6
BO($^2\Sigma$)	2093			12.5
NH($^3\Sigma$)	3527			21.1
OH($^2\Pi$)	3997			23.9
NO($^2\Pi$)	2221			13.3
HBN($^2\Pi$)	Π 774	Σ 1696	Σ 3014	37.4
HNB($^2\Sigma$)	Π 586	Σ 1992	Σ 4114	43.5
HBN-HNB TS($^2\Sigma$)	a' 1099i	a' 1694	a' 2554	25.4
HBO($^1\Sigma$)	Π 854	Σ 2021	Σ 3049	40.5
HOB(^{1}A')	a' 671	a' 1471	a' 4082	37.2
HNO(^{1}A')	a' 1736	a' 1970	a' 3343	42.2
HON(^{3}A")	a' 1286	a' 1372	a' 4011	39.9
BNO(^{3}A")	a' 355	a' 1049	a' 2016	16.8
BON(^{3}A")	a' 286	a' 1102	a' 1412	20.7
HBNO($^2\Pi$)	Π 331	Π 878	Σ 1184	52.0
	Σ 2049	Σ 3040		
HBON(^{2}A") cis	a' 374	a' 541	a' 1083	42.8
	a' 1172	a' 1346	a' 2766	
HBON TS_1	a' 321	a' 473	a' 1017	42.9
	a' 1206	a' 1374	a' 2784	
HBON(^{2}A") trans	527i	281	1024	39.6
	1126	1451	2738	
HBON BO+NH TS_2	2412i	656	876	35.1
	1009	1336	1984	

Dipole - dipole attractive forces between BH and NO would favour the formation of HBON over HBNO. From Figure 8.1, if the reaction proceeds through the channel corresponding to initial formation of HBON then the reaction should proceed at the dipole - dipole collision rate. If the barrier to dissociation of HBON to HBO + N(^{2}D) is small, or if, as suggested above, the tunnelling rate through the barrier leading to BO + NH is large, then the dynamics of the dipole - dipole attraction would dominate the temperature dependence, rather than anything occurring on the PES. Hence a small negative temperature dependence is observed, within experimental error of Phillip's calculated dipole - dipole capture rates for this system (see chapter 9). HBNO has a single exothermic product channel, that of HNB($^2\Sigma$) + O(^{3}P) arising from a 1,2-H shift and loss of O. This channel is barely exothermic and would be expected to have a substantial barrier to H migration (of the order of 138 kJ mol^{-1} calculated for the HNB HBN interconversion) and loss of O such that the most favourable decomposition channel would be dissociation back to BH and NO. If the reaction did proceed through HBNO, then a pressure and positive temperature dependence would be predicted for the rate; this does not agree with the experimental findings to date.

8.4. Conclusion

The initial association reaction between BH($^1\Sigma$) and NO($^2\Pi$) can give rise to two stable intermediates, HBNO($^2\Pi$) and HBON(^{2}A"). Formation of HBON is favoured over formation of HBNO as the former is the result of the initial dipole - dipole attraction. HBON has two spin allowed, exothermic product channels available. Both the product channels to HBO + N(^{2}D) and BO + NH are more stable than HBON and although the barriers to rearrangement would not be negligible, it is unlikely that both barriers would be higher than the energy of the reactants, BH + NO. The overall bimolecular rate should be fast and show little pressure or temperature dependence, as observed.

This work has been previously reported as ref. [8.6].

CHAPTER 9

REACTIONS OF BH WITH NO, C_2H_4, CH_4, C_2H_6 AND O_2

9.1 Introduction

Boron Hydrides have long been of interest as high energy fuels [9.1] but, despite several studies of the properties of diborane/O(^{3}P),N atom [9.2-9.4], diborane/air and diborane/nitric oxide flames [9.5], virtually nothing is known about the rates of fundamental processes involving boron hydride radicals. In these studies BH was assumed to play a key role in the overall reaction scheme. The reactions of BH with O atom containing species are thought to be the source of the intense BO^* and BO_2^* emission observed in the oxidation of Boron containing compounds. Pasternak et al [9.6] have measured room-temperature rate constants over the pressure range of 6 to 620 Torr (of N_2 buffer) for reactions of BH_3 with CO, NO and C_2H_4, and found upper limits for the rate constants for reactions with O_2 and H_2O. In the study reported here, the rate constants for the reactions of BH with NO and C_2H_4 and upper limits for the rate of reaction with CH_4, C_2H_6, CO and O_2 were measured. The BH radicals were generated by excimer laser photolysis, as described in chapter 7, and monitored by laser induced fluorescence of the Q(0,0) branch of the A - X system at 433.4 nm. The experiments were performed at pressures around 1 Torr of various buffer gases, and at temperatures between 250 and 350 K. The rate of reaction of BH with NO is discussed in terms of the ab-initio results of the preceding chapter.

9.2 Experimental

The experimental design is similar to that used in the measurement of rates of reaction of the NH radical described in chapter 6. Gas flows were measured with Tylan mass flowmeters (section 2.1G) and allowed to mix before entering the cell. Typical concentration ratios buffer:diborane:reactant were 2000:1.0:0-7 at around 1 Torr cell pressure. The single-photon absorption cross-section of diborane at 193 nm is only 4.4×10^{-20} cm^2 [9.7] and hence the absorption of 193 nm radiation is less than 1% for the path length and pressure used. The reactions of BH thus obeyed pseudo first-order kinetics. The method of generation of BH from the ArF photolysis and the processes involved are discussed in chapter 7. The cell temperature was controlled by circulating liquid from a thermostated bath through the cell's outer jacket and gas temperatures were measured just below the viewing region by a copper constantin thermocouple. The cell is shown in Figure 9.1.

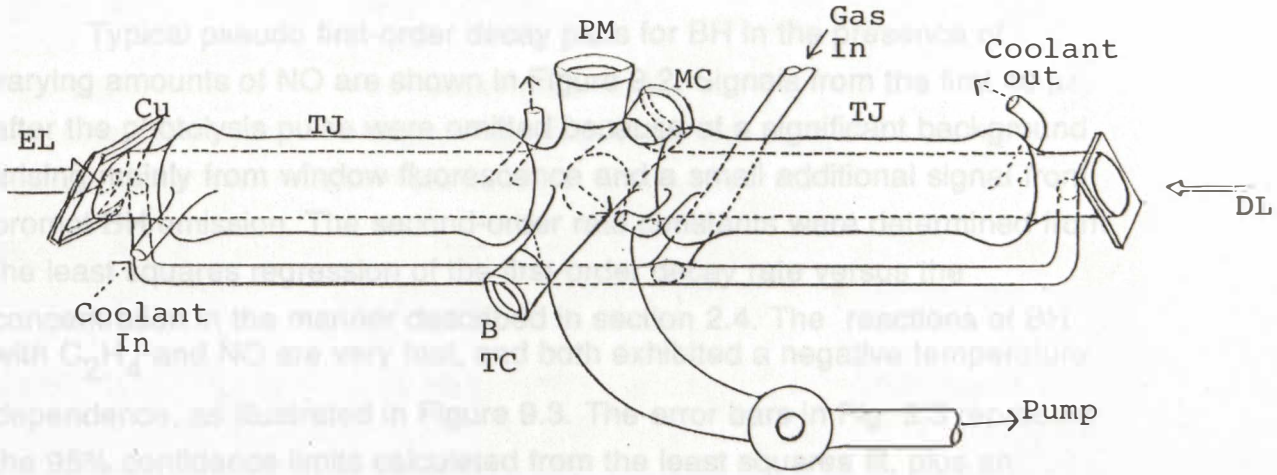

Figure 9.1 Photolysis Cell

EL Excimer Laser pulse
Cu Copper Shield
TJ Temperature Jacket
B Baratron (0-10 Torr)
TC Thermocouple
PM Photomultiplier
MC Monochromator
DL Dye Laser pulse

The pressure was monitored by a type 222CA 0-10 Torr MKS Baratron gauge. The range of pressures was limited due to fluorescence quenching of the LIF signal (above 2.5 Torr of buffer) or required reactant flows that were too small to be accurately measured (below 0.3 Torr total pressure). For this reason the effect of pressure was investigated by varying the nature of the buffer gas rather than the pressure.

The sources, purities, preparation and subsequent handling of the gases involved are described in section 2.2. Diborane was photolysed with the focussed output (lens focal length 50 cm) of the Lumonics TE-861T excimer laser at 193 nm and operating at 17 Hz. The low repetition rate ensured the contents of the cell were swept out between laser pulses. BH fluorescence was excited with the AVCO C5000 nitrogen-pumped dye laser (dye: Stilbene 420 - section B.1) and observed through Corning 7-69 and 3-73 filters (combined bandpass 410-490 nm, peak transmission 37% at 430 nm) with an EMI 9813QA photomultiplier. The output of the photomultiplier was taken through a preamplifier to a computer controlled PAR model 160 boxcar integrator.

9.3 Results

Typical pseudo first-order decay plots for BH in the presence of varying amounts of NO are shown in Figure 9.2. Signals from the first 40 μs after the photolysis pulse were omitted because of a significant background arising mainly from window fluorescence and a small additional signal from prompt BH emission. The second-order rate constants were determined from the least squares regression of the first-order decay rate versus the concentration in the manner described in section 2.4. The reactions of BH with C_2H_4 and NO are very fast, and both exhibited a negative temperature dependence, as illustrated in Figure 9.3. The error bars in Fig. 9.3 represent the 95% confidence limits calculated from the least squares fit, plus an additional 6% arising from measurements of gas pressure and time. The results given in Table 9-1. show the effect of changing the nature of the buffer gas.

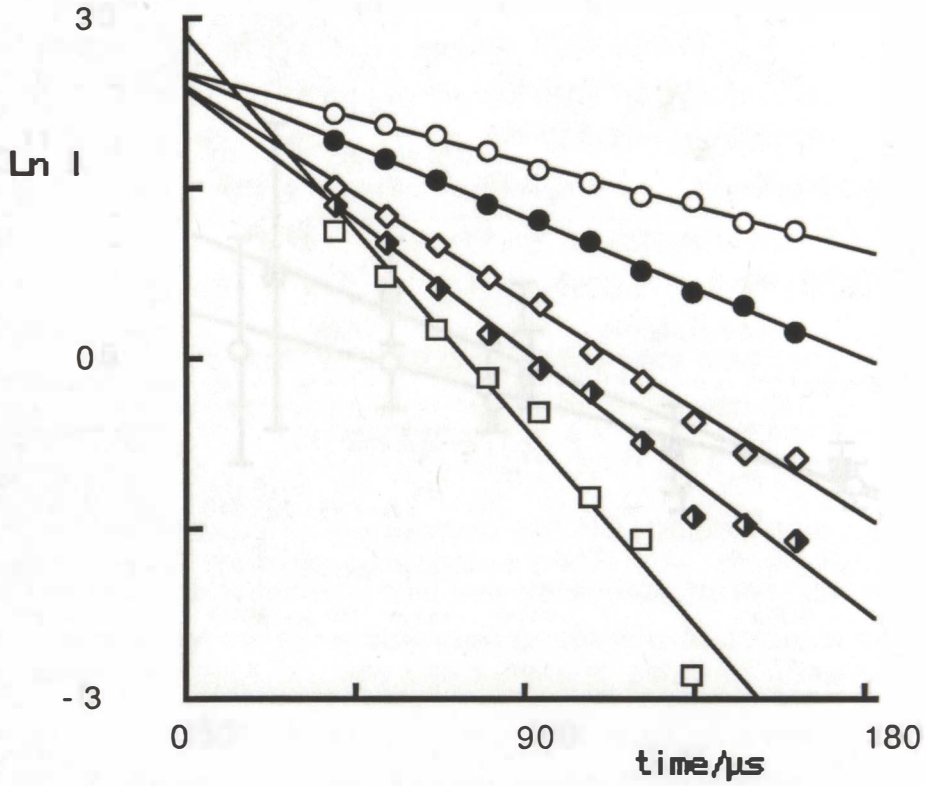

Figure 9.2. Sample first order decay plots for BH in 1 Torr He at room temperature. [NO]/10^{14} molecule cm^{-3}: open circles zero; filled circles 0.45; diamonds 0.92; half-shaded diamonds 1.12; squares 1.51.

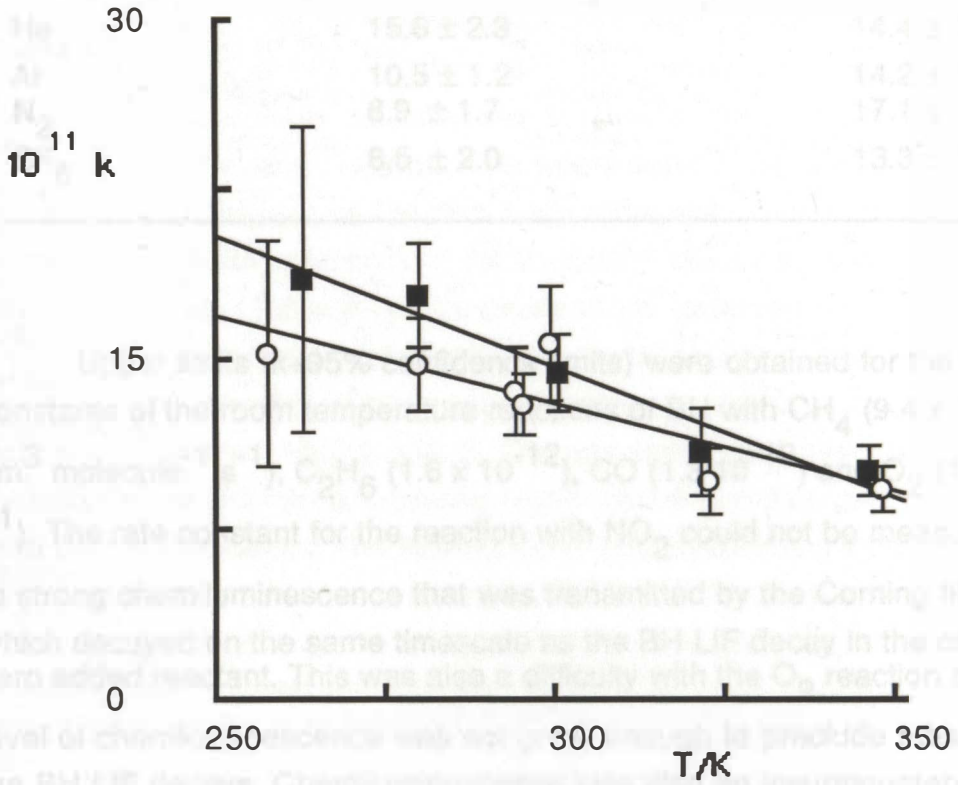

Figure 9.3. Observed variation of rate constants with temperature. Squares: BH + C_2H_4; Circles: BH + NO.

Table 9-1. Variation of measured bimolecular rate constant with buffer gas at room temperature and 1 Torr total pressure. (All 10^{-11} cm^3 $molecule^{-1}$ s^{-1}).

Buffer	k(BH+NO)	k(BH+C_2H_4)
He	15.6 ± 2.3	14.4 ± 1.7
Ar	10.5 ± 1.2	14.2 ± 1.7
N_2	8.9 ± 1.7	17.1 ± 1.9
SF_6	6.5 ± 2.0	13.3 ± 1.3

Upper limits (k+95% confidence limits) were obtained for the rate constants of the room temperature reactions of BH with CH_4 (9.4×10^{-13} cm^3 $molecule^{-1}$ s^{-1}), C_2H_6 (1.6×10^{-12}), CO ($1.3\ 10^{-13}$) and O_2 (1.1×10^{-11}). The rate constant for the reaction with NO_2 could not be measured due to strong chemiluminescence that was transmitted by the Corning filters and which decayed on the same timescale as the BH LIF decay in the case of zero added reactant. This was also a difficulty with the O_2 reaction but the level of chemiluminescence was not great enough to preclude measuring the BH LIF decays. Chemiluminescence was also an insurmountable problem with the use of N_2O as buffer. The emissions observed in these cases can be attributed to the formation of BO^* or BO_2^* by reactions of $B(^2P)$ with the oxygen-containing species, as described by Davidovits et al [9.8-9.10].

9.4 Discussion

A BH + NO:

The rate constant at room temperature (He, 1 Torr) of (15.6 ± 2.3) x 10^{-11} cm^3 $molec^{-1}$ s^{-1} compares favourably with the later determination by Nelson et al [9.11] of (13.5 ± 0.6) x 10^{-11} cm^3 $molec^{-1}$ s^{-1} (He, 5 - 100 Torr). Nelson's measurements indicated that the rate constant is independent of pressure over the range studied. This would seem to be contrary to the dependence of the rate on the third body observed in our study, where an increase in collision efficiency of the third body seems to have an inhibiting effect on the rate (Table 9-1). The cause of the observed dependence on the nature of the third body is attributed to a depletion in the viewing region of NO by a chain reaction involving such species as atomic boron, and other diborane fragments, NH, N, and O. The rate observed is then dependent on the diffusion of NO into the viewing region and would thus give the observed third body dependence. The rate constant measured in our system was observed to be constant over the range 0.3 to 3 Torr of He, indicating that in this pressure range, with He as the buffer gas, the rate was not diffusion limited. Nelson's measurements were carried out at 5, 20, 100 Torr of He and with an excess of at least 100:1 NO reactant:BH_3CO precursor. Due to our system limitations and the smaller absorption cross section at 193 nm of Diborane compared with borane carbonyl, the NO reactant:B_2H_6 precursor had to be at most 10:1 in order to obtain measurable signals over the timebase used. The chain reaction explanation is supported by the observation that the lifetime of the BH in our system (at zero NO concentration) was an order of magnitude less than that observed by Nelson. Any effects due to chain reactions involving the BH precursor would thus be more noticeable in our system, especially if the other fragments produced in the photolysis event are considered. The 193 nm photolysis of borane carbonyl produces mainly BH_3 and CO, whereas at the fluence used to produce BH from diborane, H, B, BH_2 and BH_3 are also produced.

The results of the ab initio study of chapter 8 indicate the following four processes could be of importance in this reaction.

$$BH + NO \rightarrow [HBNO]^* \rightarrow HBNO \qquad \Delta H = -299 \text{ kJ mol}^{-1} \quad (1)$$

$$\rightarrow HNB+O \qquad \Delta H = -7.2 \text{ kJ mol}^{-1} \quad (2)$$

$$\rightarrow [HBON]^* \rightarrow BO+NH \qquad \Delta H = -193.5 \text{ kJ mol}^{-1} \quad (3)$$

$$\rightarrow HBO+N(^2D) \qquad \Delta H = -136.9 \text{ kJ mol}^{-1} \quad (4)$$

Dipole-dipole attraction would result in the formation of HBON whereas formation of HBNO would require sufficient energy to overcome the dipole-dipole barrier or rearrangement of the collision complex. If HBNO were to form, the adduct could be stabilised (1) or could dissociate back to reactants. For the reasons discussed in chapter 8, channel (2) would be expected to have a significant activation barrier, and would thus be closed to HBNO dissociation. HBON is predicted to have the two spin-allowed exothermic channels (3) and (4) open to it. The barrier of 136.2 kJ mol^{-1} estimated for channel (3) is 57.3 kJ mol^{-1} below the energy of the reactants and thus this channel can proceed without an activation barrier and the adduct HBON would be expected to proceed via either (3) or (4) rather than be stabilised by collisions. The reaction rate measured should then exhibit no dependence on pressure, as observed by Nelson.

Phillips [9.12] has calculated the dynamical dipole-dipole capture rate of BH + NO --> HBON. The rate constants calculated using this model are essentially independent of temperature over the range 200 to 400 K and are very close to the experimental values. Inclusion of the barrier crossing rates, calculated by a statistical theory, was found to lower the overall rate constant such that the predicted rate was equal to or slightly smaller than the observed rate. Given the experimental uncertainties of the measured rates, this model adequately accounts for both the absolute magnitude of the rate constants and the temperature dependence observed.

Although no products have been experimentally observed for this reaction, the two most probable product sets are those resulting from (3) and (4). HBO has been observed in an AC discharge of Diborane/O_2 and Diborane/NO mixtures by Hirota et al [9.13,9.14] using IR diode laser absorption.

B $BH + C_2H_4$:

The room temperature rate (T = 300 K; P = 1 Torr He) was measured to be $(14.4 \pm 1.3) \times 10^{-11}$ cm^3 $molec^{-1}$ s^{-1}, in reasonable agreement with Nelson et al's value of $(11.7 \pm 0.4) \times 10^{-11}$ cm^3 $molec^{-1}$ s^{-1} (T = 298 K; P = 11, 50 Torr He). The rate was found to be independent of the buffer gas used and exhibited a negative temperature dependence, as shown in Figure 9.3. Nelson has speculated that the reaction proceeds first by addition of BH to the C-C double bond in a manner analogous to that observed in the isoelectronic reaction of C atoms with ethylene. The increased rate ($(1.87 \pm 0.07) \times 10^{-10}$ cm^3 $molec^{-1}$ s^{-1}) for the related reaction of BH with $(CH_3)_2C=C(CH_3)_2$ over that for ethylene, measured by Nelson et al, was attributed, by these workers, to the greater electron donating ability of the CH_3 substituents. This implies that the major mechanism for the reaction of BH with double bond containing species is the initial addition to the double bond, rather than a H extraction to form BH_2 or BH_3. The relative thermodynamics of the possible products and intermediates involved are unknown, but it seems likely that the initial adduct may will be stabilised before fragmentation occurs.

C $BH + CH_4$, C_2H_6, O_2, and CO:

The upper limits of the reactions of BH with O_2, CO and CH_4 ($k < 1.1 \times 10^{-11}$, 1.3×10^{-13}, 9.4×10^{-13} cm^3 $molec^{-1}$ s^{-1}) compare favourably with the more recent measurements of Nelson et al (k, O_2 = $(8.08 \pm 0.18) \times 10^{-13}$; k, CO, 10 Torr He = $(3.94 \pm 0.52) \times 10^{-13}$; k, CH_4 < $(1.71 \pm 0.28) \times 10^{-16}$ cm^3 $molec^{-1}$ s^{-1}). The upper limit for ethane of 1.6×10^{-12} cm^3 $molec^{-1}$ s^{-1} is likely to be inflated by the presence of ethylene, which is the major trace impurity.

O_2:

For the reaction of BH with oxygen, Nelson's rate constant is clearly consistent with our upper limit. Possible exothermic pathways for this reaction are:

1	$BH + O_2$ -->	$HBO + O$	$\Delta H = -448$ kJ mol^{-1}
2	-->	$BOH + O$	$\Delta H = -247$ kJ mol^{-1}
3	-->	$BO + OH$	$\Delta H = -402$ kJ mol^{-1}
4	-->	$BO_2 + H$	$\Delta H = -502$ kJ mol^{-1}
5	-->	$HOBO$	$\Delta H = -996$ kJ mol^{-1}

Shaub and Lin [9.15] in their modelling study of Diborane/O_2 flames assumed that channel 3 was the dominant pathway and estimated k to be 6×10^{-14} cm^3 $molec^{-1}$ s^{-1}. The higher value measured would not qualitatively affect Shaub et al's results as it was their intention to model the observed features of the combustion qualitatively, and because the most important reaction governing the induction time of the explosion was the homolytic cleavage of the diborane into BH_3 units, a change of the above rate constant would not affect any conclusions they may have formed.

CO:

The rate constant for the reaction of BH with CO was found by Nelson et al to be pressure dependent over the range 10 to 400 Torr in He, SF_6 or CF_4, varying from $(58.0 \pm 1.5) \times 10^{-13}$ (404 Torr, He) to $(3.94 \pm 0.26) \times 10^{-13}$ cm^3 $molec^{-1}$ s^{-1} (10 Torr, He). Our upper limit of 1.3×10^{-13} cm^3 $molec^{-1}$ s^{-1} for the reaction in 1 Torr of He essentially coincides with an extrapolated value from Nelson's data. Nelson modelled his data assuming that the reaction proceeds through a HBCO complex, which is subsequently stabilised by the bath gas. To obtain agreement between the TST - RRKM type model and their observed data, a B-C bond strength of 167 kJ mol^{-1} had to be assumed in the calculation.

CH_4:

The upper limit determined by Nelson is in agreement with our own value. The much smaller error limits quoted by Nelson reflect the greater sensitivity of their production and detection system over our own.

9.5 Summary

The previously unmeasured rate constants of BH with NO, C_2H_4, O_2, CH_4, C_2H_6 and CO have been determined by the method of laser photolysis of B_2H_6 / laser induced fluorescence of BH. The rate constants, pressure and temperature dependences measured were :

BH + NO - negative temperature dependence. Rate dependent on third body (= He, Ar, N_2, SF_6) at 1 Torr, independent of pressure of He between 0.3 - 3.0 Torr.

k (T = 298 K, 1 Torr He) = $(15.6 \pm 2.3) \times 10^{-11}$

BH + C_2H_4 - negative temperature dependence. Rate independent of third body at 1 Torr

k (T = 298 K, 1 Torr He) = $(14.4 \pm 1.7) \times 10^{-11}$

BH + O_2 $< 1.1 \times 10^{-11}$

BH + CH_4 $< 9.4 \times 10^{-13}$

BH + C_2H_6 $< 1.6 \times 10^{-12}$

BH + CO $< 1.3 \times 10^{-13}$

(all cm^3 $molecule^{-1}$ s^{-1}; 1 Torr He; T = 298 K)

All results agree with the later measurements of Nelson et al.

This work has been previously reported as reference [9.12].

CHAPTER 10

AB-INITIO POTENTIAL ENERGY SURFACES OF THE REACTION OF BH_2 WITH NO

10.1 Introduction

The reactions of BH_2 with other species have not received a great deal of attention. This is in part due to the lack of spectroscopic data available on BH_2 with the only recorded spectroscopic study that of Johns et al [10.1]. Nor, until recently, has there been a convenient method of generation of BH_2. The study of chapter 7 has shown that BH_2 fragments are produced in the 193 nm photolysis of diborane and quite probably in other borane containing compounds such as borane carbonyl. Small boron-hydride fragments, such as BH_2, have been proposed to play pivotal roles in the oxidation of diborane and other possible boron containing fuels. Within the last two years experimental kinetic studies have been reported on BH [10.2, 10.3], and BH_3 [10.4] and one theoretical study on the reaction of BH with NO [10.5].

The reactions of boron and boron containing substances with oxidising agents are characterised by very high flame velocities and large exothermicities, to give, amongst others, BO and BO_2. Many of the intermediate species, such as HBO, have remained until recently hypothetical entities only. With the advent of extremely sensitive laser based detection methods there is great potential for detecting most, if not all, of the products, and indeed possible intermediates, from such reactions like those of BH_2 with other species. Ab-Initio calculations are particularly valuable in these situations and are indeed, the most reliable source of thermochemical data for small, experimentally unknown molecules. In this study the ab-initio structures, frequencies and energies of intermediates and possible products in the reaction of BH_2 with NO are presented.

10.2 Details of Calculations

All molecules were optimised at the HF/6-31G* level before calculation of the harmonic vibrational frequencies and the MP4SDQ/6-31G* energies. All calculations were done using the standard routines of Gaussian 82.

10.3 Results and Discussion

The total energies for the species involved are given in Table 10-1 with the relative MP4SDQ+ZPVE/6-31G*//HF/6-31G* energies plotted in Figure 10.1. Geometries and frequencies are listed in Tables 10-2 and 10-3 respectively. From Figure 10.1 there are two possible initial adducts corresponding to either insertion into the NO PI bond (H_2BON) or end-wise addition to the N (H_2BNO). The former method of attack would be expected from dipole - dipole attraction of the B to the O end of the NO and subsequent rearrangement to give the long BN (1.507) and BO (1.615) bonds of H_2BON. H_2BNO could result from rearrangement of the H_2BON adduct. These initial adducts can then rearrange or dissociate into the many channels shown. This potential surface may be contrasted with that of the NH_2 + NO potential surface where the H atoms were found to be able to move freely around the NNO skeleton. Although energy barriers have not been calculated, it would appear that there is the additional possibility of a "scrambled egg" arrangement for the BON skeleton as well. On exothermicities alone the most likely product channels would be those leading to HBO + NH and NH_2 + BO, whereas it is questionable that the barriers to the other channels would be above the energy of BH_2 + NO. One interesting feature of figure 10.1 is the extremely stable HNBOH molecule. Although it is difficult to imagine this molecule as a direct product of the BH_2 + NO reaction it could arise from secondary reactions of initial products.

The IR spectrum of HBNH has recently been studied by Hirota et al [10.6] from a discharge plasma of diborane/NH_3 or diborane/NO mixtures. HBO has also recently been studied by the same group [10.7, 10.8] in the gas phase. Most of the other possible boron containing products have yet to be studied. From Figure 10.1 the reaction between BH_2 and NO would be expected to proceed at the dipole - dipole capture rate and the existence of a large number of product channels (at least some of which are likely to have

energy barriers below the reactants, in view of the large exothermicities of the intermediates and products) would imply a pressure independent rate. This is entirely analogous to the rate predicted for the reaction of BH with NO.

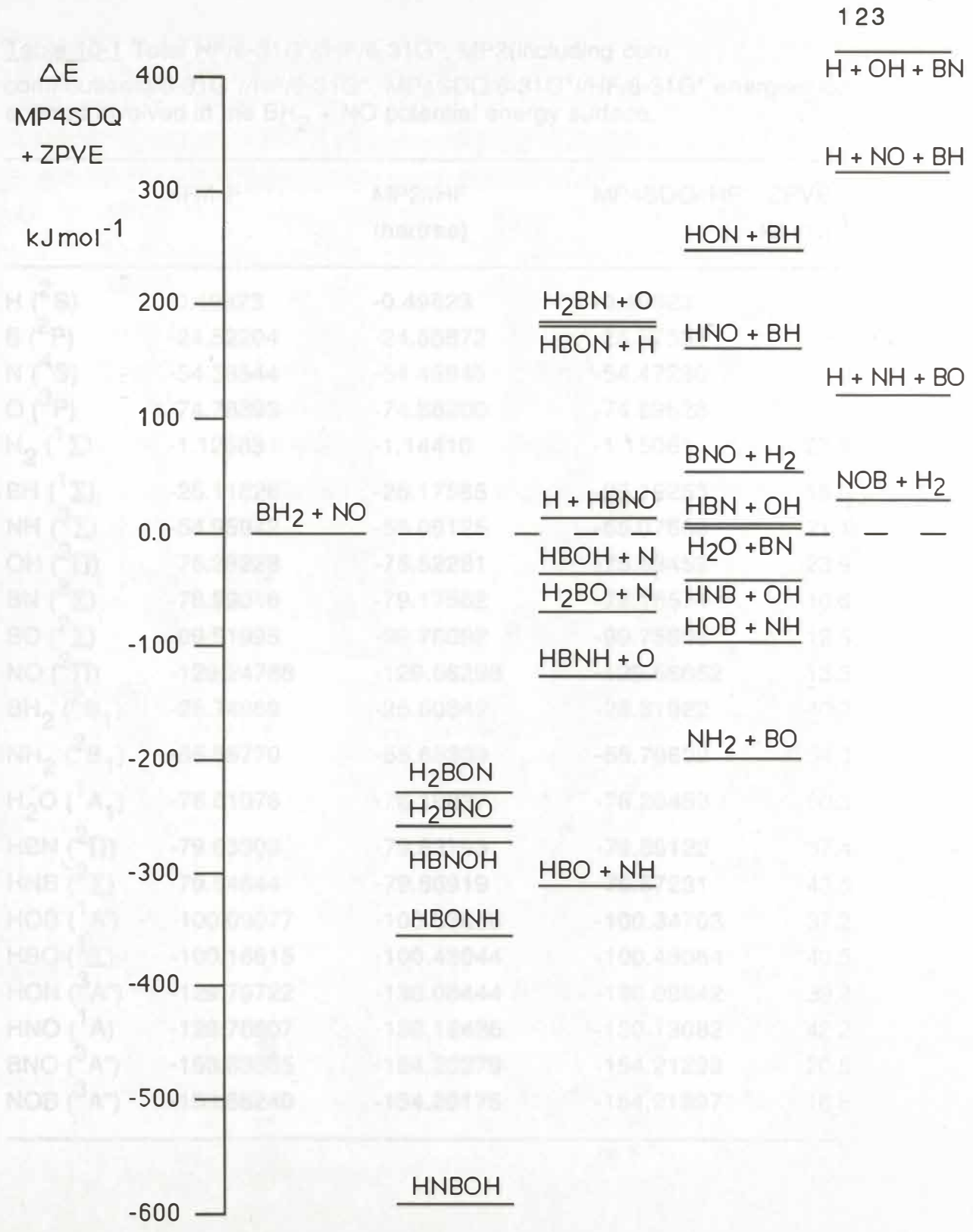

Figure 10.1. Relative MP4SDQ+ZPVE/6-31G*//HF/6-31G* energies for the reaction of BH_2 + NO.

Table 10-1 Total HF/6-31G*//HF/6-31G*, MP2(including core contributions)/6-31G*//HF/6-31G*, MP4SDQ/6-31G*//HF/6-31G* energies for species involved in the BH_2 + NO potential energy surface.

	HF//HF	MP2//HF	MP4SDQ//HF	ZPVE
		(hartree)		kJ mol^{-1}
H (^2S)	-0.49823	-0.49823	-0.49823	
B (^2P)	-24.52204	-24.55872	-24.57562	
N (^4S)	-54.38544	-54.45945	-54.47280	
O (^3P)	-74.78393	-74.88200	-74.89528	
H_2 ($^1\Sigma$)	-1.12683	-1.14410	-1.15081	27.8
BH ($^1\Sigma$)	-25.11826	-25.17585	-25.19253	15.0
NH ($^3\Sigma$)	-54.95942	-55.06125	-55.07669	21.1
OH ($^2\Pi$)	-75.38228	-75.52281	-75.53453	23.9
BN ($^3\Sigma$)	-78.99016	-79.17562	-79.18574	10.6
BO ($^2\Sigma$)	-99.51995	-99.76092	-99.75808	12.5
NO ($^2\Pi$)	-129.24788	-129.56298	-129.56652	13.3
BH_2 ($^2B_1$)	-25.74969	-25.80842	-25.81922	40.2
NH_2 ($^2B_1$)	-55.55770	-55.69339	-55.70802	54.0
H_2O ($^1A_1$)	-76.01076	-76.19837	-76.20459	60.3
HBN ($^2\Pi$)	-79.63309	-79.83793	-79.85122	37.4
HNB ($^2\Sigma$)	-79.64644	-79.86919	-79.87231	43.5
HOB ($^1A'$)	-100.09077	-100.33656	-100.34703	37.2
HBO ($^1\Sigma$)	-100.16615	-100.43044	-100.43064	40.5
HON ($^3A''$)	-129.79722	-130.08444	-130.09842	39.9
HNO (^1A)	-129.78607	-130.12436	-130.13082	42.2
BNO ($^3A''$)	-153.83665	-154.20279	-154.21299	20.5
NOB ($^3A''$)	-153.86240	-154.20175	-154.21997	16.8

Table 10-1. Continued.

	HF//HF	MP2//HF (hartree)	MP4SDQ//HF	ZPVE kJ mol^{-1}
H_2BN ($^3A_2$)	-80.22585	-80.39987	-80.42203	58.9
HBNH	-80.29187	-80.54036	-80.54559	71.8
HBOH ($^2A'$)	-100.68093	-100.92509	-100.93253	67.1
H_2BO ($^2B_2$)	-100.70327	-100.92418	-100.94177	60.2
HBON ($^2A''$)	-154.45826	-154.79981	-154.81503	43.6
HBNO ($^2\Pi$)	-154.47717	-154.87374	-154.88198	50.9
H_2BON ($^1A'$)	-155.04516	-155.47245	-155.48176	77.6
H_2BNO ($^1A'$)	-155.05454	-155.48434	-155.49309	76.1
HBNOH ($^1A'$)	-155.06695	-155.49716	-155.50159	84.8
HBONH ($^1A'$)	-155.09922	-155.52970	-155.53516	85.2
HNBOH ($^1A'$)	-155.19809	-155.62155	-155.62360	86.9

Table 10-2. Optimised HF/6-31G* geometries. (All distances in Å, angles in degrees)

H_2 ($^1\Sigma$)	0.730		
BH ($^1\Sigma$)	1.225		
NH ($^3\Sigma$)	1.024		
OH ($^2\Pi$)	0.958		
BN ($^3\Sigma$)	1.293		
BO ($^2\Sigma$)	1.187		
NO ($^2\Pi$)	1.127		
BH_2 ($^2B_1$)	BH 1.186	HBH 126.6	
NH_2 ($^2B_1$)	NH 1.013	HNH 104.3	
H_2O ($^1A_1$)	OH 0.947	HOH 105.5	
HBN ($^2\Pi$)	HB 1.167	BN 1.292	HBN 180.0
HNB ($^2\Sigma$)	HN 0.982	NB 1.228	HNB 180.0
HOB ($^1A'$)	HO 0.951	OB 1.300	HOB 121.5
HBO ($^1\Sigma$)	HB 1.167	BO 1.185	HBO 180.0
HON ($^3A''$)	HO 0.954	ON 1.316	HON 108.7
HNO (^1A)	HN 1.032	NO 1.175	HNO 108.8
BNO ($^3A''$)	BN 1.422	NO 1.180	BNO 143.4
NOB ($^3A''$)	NO 1.327	OB 1.327	NOB 130.2
H_2BN ($^3A_2$)	HB 1.189	BN 1.472	HBN 119.2
HBNH (linear)	HB 1.167	BN 1.223	NH 0.981
HBOH ($^2A'$)	HB 1.192	BO 1.335	OH 0.947
	HBO 120.7	BOH 114.4	HBOH 180.0
H_2BO ($^2B_2$)	HB 1.189	BO 1.325	HBO 117.6
HBON ($^2A''$,cis)	HB 1.189	BO 1.360	ON 1.328
	HBO 122.7	BON 116.7	HBON 180
HBNO ($^2\Pi$,linear)	HB 1.433	BN 1.231	NO 1.241

Table 10-2. Continued.

H_2BON ($^1A'$)[a]	HB 1.183	BO 1.616	ON 1.209
	BN 1.507	OBH 113.4	HBH_1 125.0
	BON 62.6	BNO 72.0	NBO 45.4
	NOBH 104.9	$NOBH_1$ 194.9	
H_2BNO ($^1A'$)[b]	HB 1.182	BN 1.345	NO 1.157
	HBN 116.0	BNO 180.0	HBH 148.0
HBNOH ($^1A'$)[c]	HB 1.166	BN 1.214	NO 1.325
	OH 0.950	HBN 179.0	BNO 174.5
	NOH 106.5	HBNO 0.0	BNOH 0.0
HBONH ($^1A'$)[d]	NO 1.534	BO 1.312	BN 1.425
	BH 1.175	NH 1.005	HBO 142.9
	OBN 68.1	BNO 52.5	NOB 59.5
	HNO 104.4	BONH 108.2	
HNBOH ($^1A'$)[e]	HN 0.979	NB 1.228	BO 1.330
	OH 0.947	HNB 178.0	NBO 180.0
	BOH 115.4	HNOH 180	

Key to structures a-e.

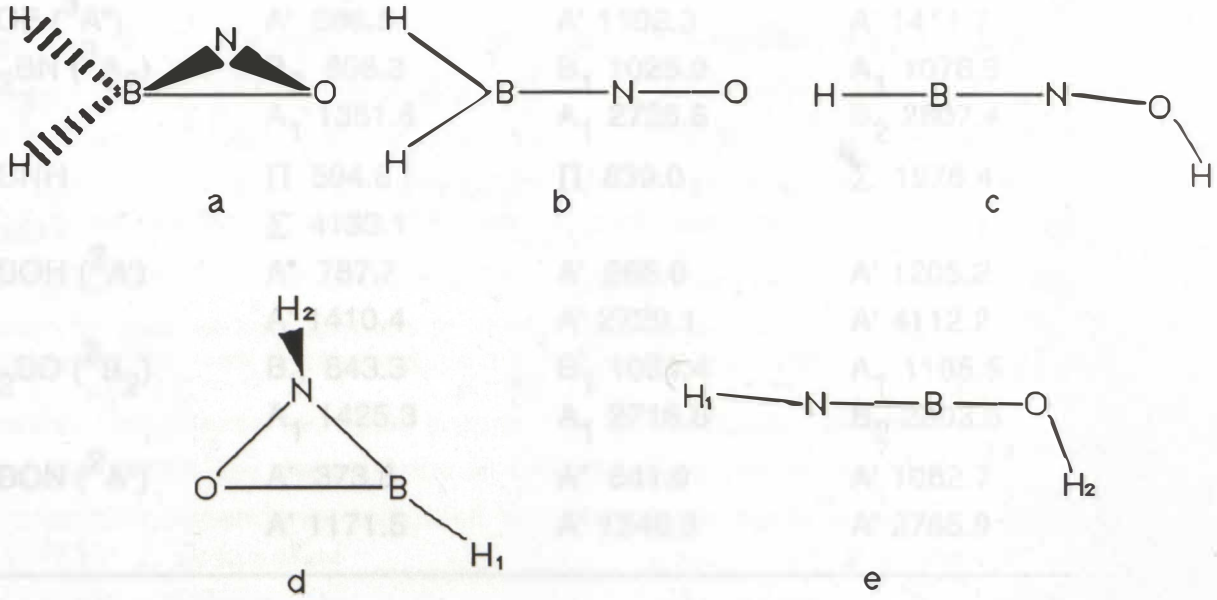

Table 10-3. HF/6-31G* harmonic vibrational frequencies. (cm^{-1})

H_2 ($^1\Sigma$)	Σ 4650.5		
BH ($^1\Sigma$)	Σ 2513.0		
NH ($^3\Sigma$)	Σ 3526.6		
OH ($^2\Pi$)	Σ 3997.0		
BN ($^3\Sigma$)	Σ 1766.6		
BO ($^2\Sigma$)	Σ 2092.5		
NO ($^2\Pi$)	Σ 2221.5		
BH_2 ($^2B_1$)	A_1 1126.8	A_1 2727.5	B_2 2866.4
NH_2 ($^2B_1$)	A_1 1711.9	A_1 3604.8	B_2 3705.0
H_2O ($^1A_1$)	A_1 1826.6	A_1 4070.5	B_2 4188.7
HBN ($^2\Pi$)	Π 777.2	Σ 1695.5	Σ 3013.7
HNB ($^2\Sigma$)	Π 585.6	Σ 1992.2	Σ 4114.2
HOB ($^1A'$)	A' 671.4	A' 1471.4	A' 4081.6
HBO ($^1\Sigma$)	Π 854.4	Σ 2020.6	Σ 3048.6
HON ($^3A''$)	A' 1285.6	A' 1371.6	A' 4011.0
HNO (^1A)	A' 1735.7	A' 1970.0	A' 3343.3
BNO ($^3A''$)	A' 354.9	A' 1048.9	A' 2015.5
NOB ($^3A''$)	A' 286.5	A' 1102.3	A' 1411.7
H_2BN ($^3A_2$)	B_2 858.3	B_1 1025.0	A_1 1078.9
	A_1 1351.6	A_1 2726.6	B_2 2807.4
HBNH	Π 594.8	Π 839.0	Σ 1976.4
	Σ 4133.1		
HBOH ($^2A'$)	A'' 787.7	A' 966.0	A' 1205.2
	A' 1410.4	A' 2729.1	A' 4112.2
H_2BO ($^2B_2$)	B_2 843.3	B_1 1084.4	A_1 1185.5
	A_1 1425.3	A_1 2716.6	B_2 2803.6
HBON ($^2A''$)	A' 373.8	A'' 541.0	A' 1082.7
	A' 1171.5	A' 1346.3	A' 2765.9

Table 10-3 Continued.

HBNO ($^2\Pi$)	PI 331.0	PI 878.0	Σ 1184.3
	Σ 2049.5	Σ 3040.4	
H_2BON ($^1A'$)	399.0	786.2	983.9
	984.5	1125.3	1323.4
	1773.9	2749.7	2853.6
H_2BNO ($^1A'$)	B_1 198.4	B_2 403.4	B_2 959.4
	B_1 964.5	A_1 1048.2	A_1 1308.9
	A_1 2207.1	A_1 2763.3	B_2 2865.5
HBNOH ($^1A'$)	A' 288.8	A" 342.4	A" 773.4
	A' 801.9	A' 1095.5	A' 1566.0
	A' 2201.5	A' 3040.1	A' 4060.1
HBONH ($^1A'$)	765.4	793.4	913.5
	1066.4	1124.5	1382.4
	1544.9	2922.9	3730.6
HNBOH ($^1A'$)	A" 377.9	A' 455.1	A' 520.3
	A" 530.6	A' 1056.3	A' 1076.9
	A' 2221.1	A' 4127.7	A' 4155.8

10.4 Summary

The reaction between BH_2 and NO has been investigated at the MP4SDQ/6-31G*//HF/6-31G* level. The reaction can proceed through a variety of intermediate adducts to one of several exothermic product channels. The most likely products are NH_2 + BO and HBO + NH. The reaction rate is expected to be around that for the dipole - dipole capture rate, not exhibit any dependence on total pressure and show only the weak temperature dependence expected from the dipole-dipole attraction.

CHAPTER 11

CONSTRUCTION AND CHARACTERISATION OF A PULSED SUPERSONIC MOLECULAR BEAM

11.1 Introduction

Since Kantrowitz and Grey's [11.1] first design and Kistiakowsky's [11.2] pioneering experiments of a supersonic nozzle source in 1951, there have been innumerable publications dealing with the theory of operation and possible improvements. Anderson [11.3] has reviewed the history of molecular beam development and the physics involved. The development of molecular beam equipment is very much an art form of its own, with its roots nested firmly in fluid mechanics and gas dynamics. The usefulness of a supersonic molecular jet as a source of rotationally and vibrationally cold molecules is evident from any recent spectroscopic or chemical physics publication. The principal advantages over conventional effusive sources are: an increase in the beam intensity by at least an order of magnitude; nearly monoenergetic, low temperature distributions can be obtained; and a reduction in the pumping speed necessary (pulsed systems in particular). As the University of Canterbury did not have such a facility, this project was undertaken to provide such an instrument for the spectroscopic and mass-spectrometric study of jet-cooled species. This chapter is devoted to the description of the construction of the pulsed supersonic molecular beam device and to the time-of-flight (TOF) techniques used to determine axial translational beam temperatures. It is hoped that studies of jet cooled species obtained using this equipment will be the subject of numerous future theses. Further development to a crossed beam system is envisioned.

The principles governing the production of a pulsed supersonic beam are well documented [11.4]. Basically, this involves expanding a gas from a high pressure reservoir through a small orifice into a high vacuum chamber. During the expansion the molecules move from a region where they

experience many collisions and the expansion is essentially isentropic (at the source orifice) to one where collisions do not occur and the flow is described as free molecular. The shock wave resulting from the expansion of the gas into the vacuum attaches to an axially located skimmer, which allows the supersonic portion of the beam to pass into another, separate chamber, undegraded. The process of expansion is a non-equilibrium process, although for a monatomic gas, it may be assumed to be essentially isentropic. Because the characteristics of the beam produced depend on many factors, such as nozzle to skimmer distance and geometry, the only reliable method of determining the resulting energy distribution of the molecules within the beam, is to measure it experimentally. The most useful and easily implemented technique for determining the translational velocity distribution along the beam axis is the time-of-flight method. Here the beam is initially chopped (section 11.2C) and the resulting pulse of molecules travels down a flight tube with the resulting characteristic arrival-time distribution measured downstream by a mass spectrometer. Recent implementations of this technique have been reported for systems similar to this one [11.5,11.6].

The velocity distribution is generally assumed to be a Maxwellian distribution, superimposed on the mean flow velocity. Thus if the arrival time distribution is fitted to the following equation:

$$I(v) = A\, v^2 \exp(-m(v-u)^2/(2kT)) \qquad 11\text{-}1$$

where: A = normalisation constant
v = velocity
m = mass of molecule
u = mean flow velocity
k = Boltzmann constant
T = beam temperature

the axial temperature and mean velocity can be obtained (section 11.3). To obtain the internal energy distribution of non-atomic molecular beams, it is necessary to probe the beam spectroscopically to obtain the population of each state. Infra-red diode laser absorption and UV-visible laser induced fluorescence measurements have yet to be undertaken in this laboratory.

11.2 Design and Construction

The system was designed as two distinct chambers, joined only by the 0.5 mm hole in the skimmer. The source chamber housed the moveable source assembly and necessarily had the largest pumping capacity of the two chambers. The second chamber contained the rotating disk chopper assembly, the flight tube, along with the quadrupole mass spectrometer.

A Vacuum System.

A schematic of the differentially pumped vacuum chambers is shown in Figure 11.1. All chambers were of stainless steel construction and connected via o'ring or copper-gasket sealed conflat joints. The diffusion pumps and their respective chambers were mounted on rails to enable speedy disassembly and trouble free maintenance.

1. The Source Chamber.

Pumping of the source chamber was provided by two oil diffusion pumps; one VHS 6 (3000 l s^{-1}) and one VHS 4 (1500 l s^{-1}), oriented as indicated in Fig. 11.1. Both pumps were backed by a tandem arrangement of two stage rotary pumps: an Edwards E2M40 (700 l min^{-1}) and an Edwards EDM20 (342 l min^{-1}). The pressure inside the chamber was monitored by a standard ion gauge connected to an MKS type 290 ion gauge controller. The foreline pressure was measured using thermocouple gauges (MKS TC1) connected to an MKS type 286 controller. The diffusion pumps could be isolated from the backing mechanical pumps using a selection of o'ring or diaphragm type valves in the foreline assembly. Additional cryogenic pumping was provided by a custom built liquid nitrogen trap located in the stainless steel elbow above the source. This trap resembled a hollow pipe of about 100 mm diameter and 100 mm in length into which liquid nitrogen could be poured. This particular design of trap proved to be extremely effective without demonstrably affecting the flow through the diffusion pumps. Typical background pressure was 1×10^{-7} Torr (without liq. N_2 trap operating).

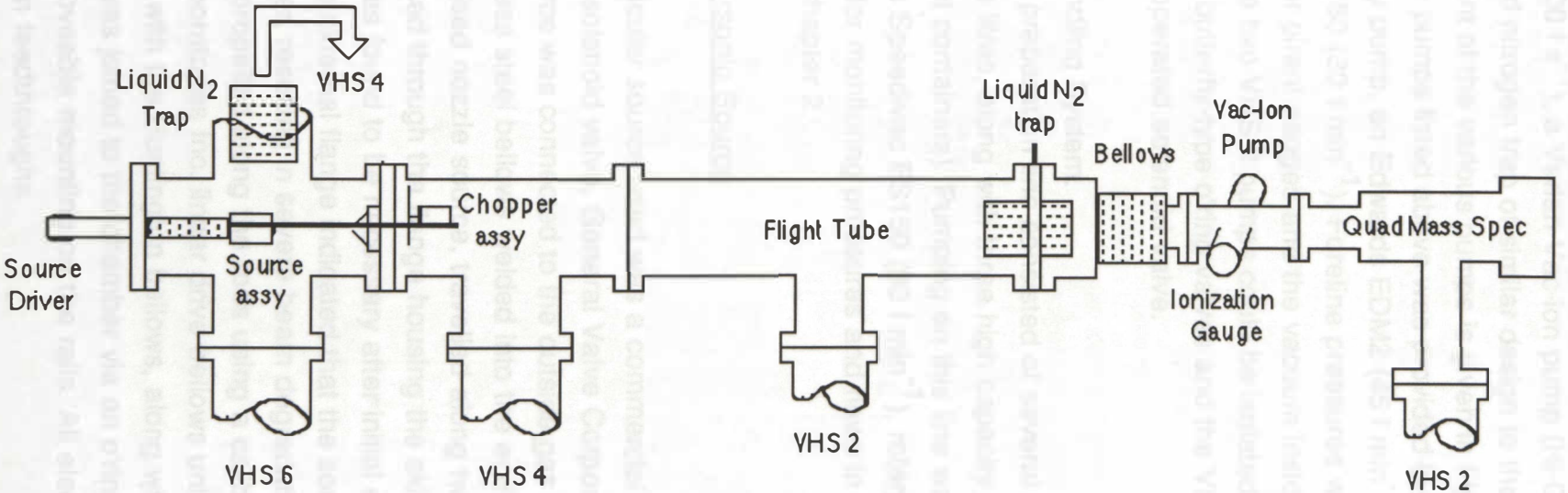

Figure 11.1 Side schematic of the molecular beam. Rails, window ports, diffusion pumps and mounting brackets not shown for clarity.

2. The Flight Chamber.

Pumping for this chamber was provided by a VHS 4 (1500 l s^{-1}), two VHS 2 (each 200 l s^{-1}), a Varian Vac-ion pump (Hi-Q model 911-5041, 20 l s^{-1}) and a liquid nitrogen trap of similar design to the one described above. The arrangement of the various pumps is given in Fig. 11.1. Backing vacuum for the diffusion pumps listed above was provided by an Alcatel (75 l min^{-1}) two stage rotary pump, an Edwards EDM2 (45 l min^{-1}) and an Edwards Speedivac ED150 (30 l min^{-1}). Foreline pressures were monitored with thermocouple or pirani gauges and the vacuum inside the chamber, by two ion gauges. The two VHS 2 pumps could be isolated from the vacuum chamber using butterfly-type o'ring valves and the VHS 4 was isolated by a pneumatically operated solenoid valve.

3. The Gas Handling System.

The gas preparation line consisted of several bulbs ranging in size from one to five litres, along with three high capacity storage vessels (old freon refrigerant containers). Pumping on this line was provided by a single stage, Edwards Speedivac ES150 (30 l min^{-1}), rotary pump. Descriptions of the equipment for monitoring pressures and flows in the source line have been given in chapter 2.

B Pulsed Supersonic Source

The particular source used was a commercial beam source (model 9-181, axial flow solenoid valve, General Valve Corporation, 0.030 inch orifice, 24 V). The source was connected to the outside gas supply using a 1/4 inch diameter stainless steel bellows welded into the end flange. The carriage housing the pulsed nozzle source, travelled along two parallel stainless rods that were pressed through the flange housing the skimmer assembly. This arrangement was found to be necessary after initial experiments with rods mounted on the external flange indicated that the source was not aligned with the skimmer, resulting in severe beam degradation. The source carriage assembly was propelled along the rods using a calibrated Huntington Mechanical Laboratories Inc. linear drive bellows unit (model VF-156). The external flange with the Huntington bellows, along with the gas and electrical feedthroughs, was joined to the chamber via an o'ring seal and had an independent moveable mounting on the rails. All electrical connections were via high vacuum feedthroughs.

C Chopper and Skimmer Assembly.

A schematic of the chopper and skimmer assembly is given in Figure 11.2. The diameter of the hole in the first skimmer was 0.5 mm. The motor used was a 400 Hz synchronous motor (TRW Electronic Components, Globe Motors). The chopper disk dimensions were: 30 mm radius at the point of transmission of the beam with a 2 mm wide slot. The placing of the optical switch directly below the skimmer ensured that the error in measuring the time when the slot passed the skimmer, was minimised. The chopper motor was cooled by a copper block fastened to the motor housing, through which cold water flowed. Large holes were bored through the aluminium mounting flanges to avoid any stagnation areas. After the beam has passed through the slotted disk it is further collimated by a skimmer with a 1.5 mm orifice.

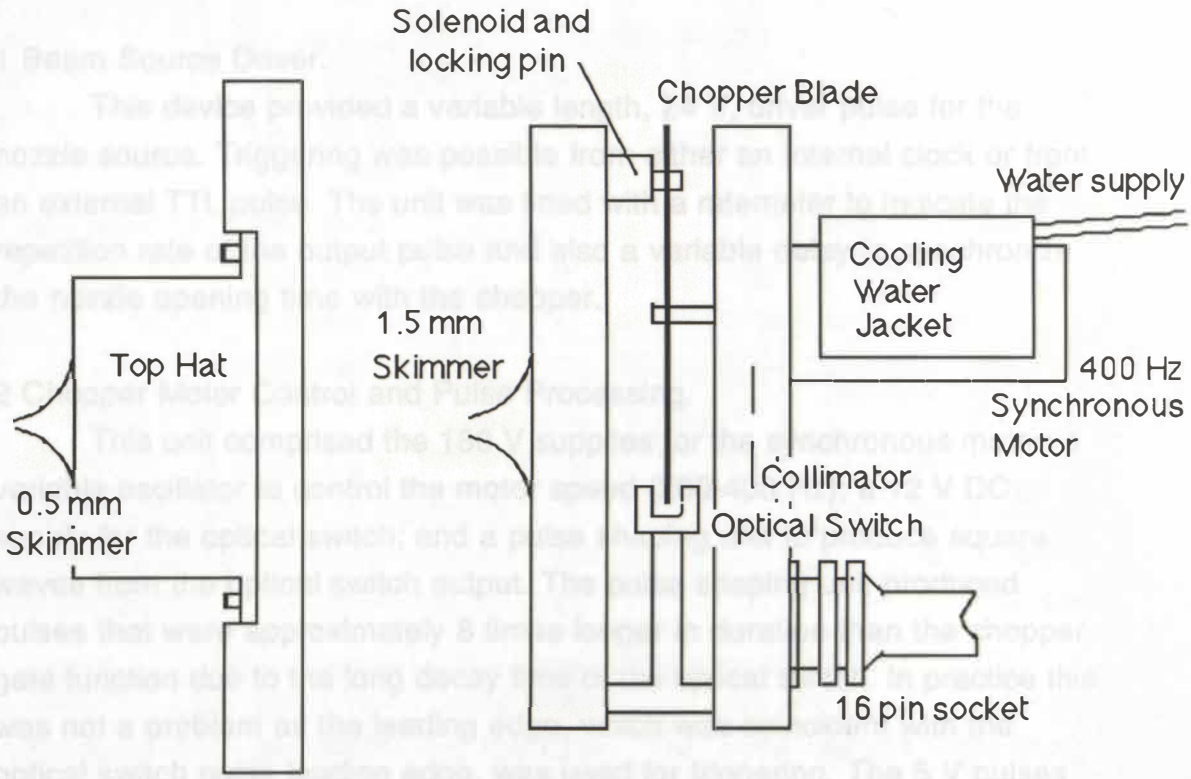

Figure 11.2. Skimmer and Chopper assembly
(Mounting Rods not shown for clarity)

The detector used for the time of flight measurements was a V. G. Gas Analysis Limited, SXP 300 quadrupole mass spectrometer. The response time of the in-built amplifier of this instrument was not sufficient to avoid convolution of the true ATD with the electronic response time of the amplifier. To overcome this, a 100 kHz pre-amplifier was connected directly to the channeltron and the output was then digitized by the LeCroy.

E Electronics

Apart from the dedicated commercially obtained equipment already described, a number of purpose built supplies and logic circuits were used to control the various facets of timing and signal detection. The three most important of these were: the beam source driver; the chopper motor control and pulse processing unit; and the pulse rejection circuit. The pulse logic is shown in Figure 11.3.

1 Beam Source Driver.

This device provided a variable length, 24 V, driver pulse for the nozzle source. Triggering was possible from either an internal clock or from an external TTL pulse. The unit was fitted with a ratemeter to indicate the repetition rate of the output pulse and also a variable delay to synchronize the nozzle opening time with the chopper.

2 Chopper Motor Control and Pulse Processing.

This unit comprised the 180 V supplies for the synchronous motor; a variable oscillator to control the motor speed (200-400 Hz); a 12 V DC supply for the optical switch; and a pulse shaping unit to produce square waves from the optical switch output. The pulse shaping unit produced pulses that were approximately 8 times longer in duration than the chopper gate function due to the long decay time of the optical switch. In practice this was not a problem as the leading edge, which was coincident with the optical switch pulse leading edge, was used for triggering. The 5 V pulses produced were fed to the pulse dividing unit and to the LeCroy 6103 amplifier. This unit also housed the solenoid power supply for the chopper locking mechanism. To align the slot in the chopper blade with the locking pin, the motor could be pulsed slowly around until the disk set LED indicated that the slot was in the correct position.

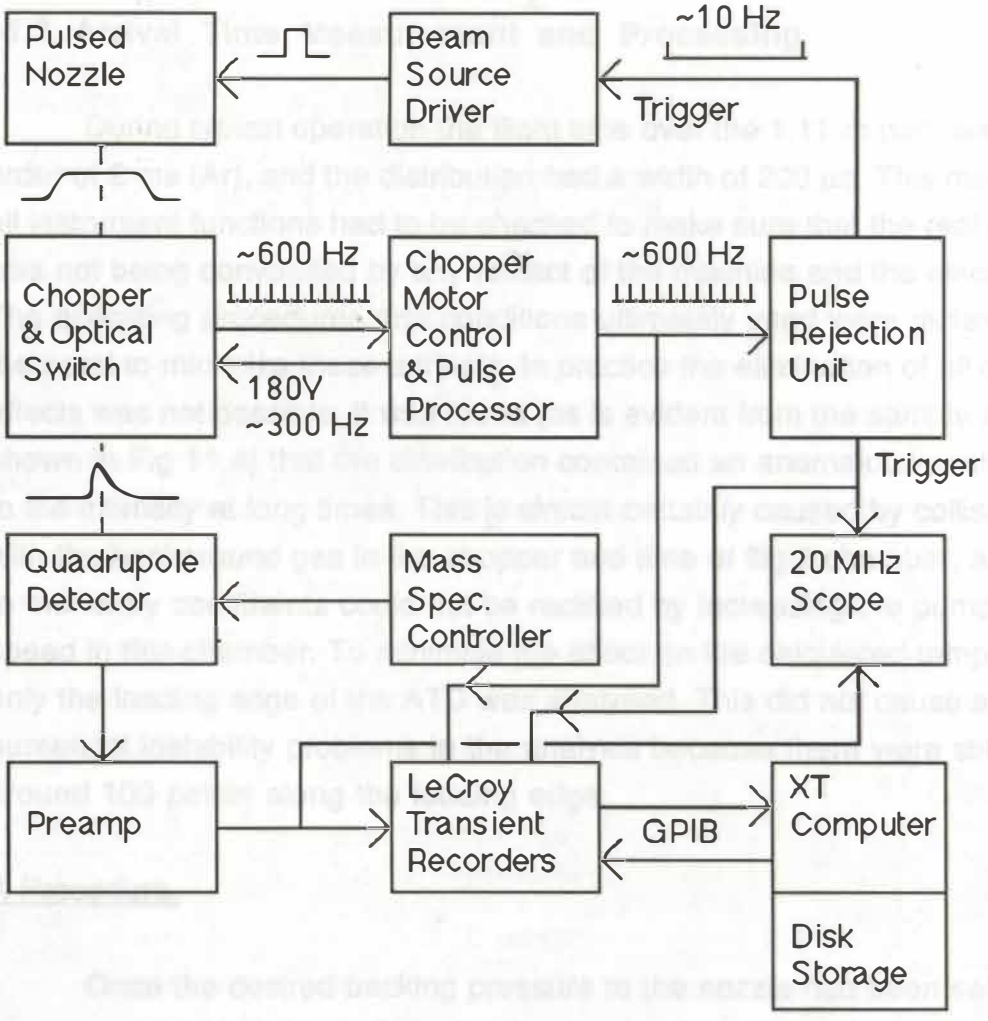

Figure 11.3. Block diagram of the molecular beam pulse and detection logic.

3 Pulse Rejection Circuitry

The pulse train from the pulse processing unit was divided by the pulse rejection circuitry from between 400 and 800 Hz to about 10. This was necessary because the nozzle could not operate at such high repetition rates and if the rate was too high the build up of thermalised gas interfered with the subsequent pulse.

11.3 Arrival Time Measurement and Processing

During typical operation the flight time over the 1.11 m path was of the order of 2 ms (Ar), and the distribution had a width of 200 μs. This meant that all instrument functions had to be checked to make sure that the real ATD was not being convoluted by any artifact of the machine and the electronics. The operating procedures and conditions ultimately used were dictated by the need to minimize these artifacts. In practice the elimination of all of these effects was not possible. It was found (as is evident from the sample ATD shown in Fig 11.4) that the distribution contained an anomalous contribution to the intensity at long times. This is almost certainly caused by collisions with the background gas in the chopper and time of flight chamber, and due to monetary constraints could not be rectified by increasing the pumping speed in this chamber. To minimise the effect on the calculated temperature only the leading edge of the ATD was analysed. This did not cause any numerical instability problems in the analysis because there were still around 100 points along the leading edge.

A Procedure.

Once the desired backing pressure to the nozzle had been selected, the mass spectrometer and electronics powered on, the arrival-time signal was optimised by adjusting the delay of the beam source driver with respect to the chopper pulse. The nozzle to skimmer distance could be varied at any time during the experiment to obtain an optimal beam. The LeCroy Waveform-Catalyst acquisition parameters were set up for the two LeCroy 8837F transient digitisers and for the LeCroy 6103 Amplifier. The chopper pulses from the output of the pulse processing unit and the preamplified channeltron signal were averaged and stored to disk as unformatted fortran files with names *.tim and *.dat respectively. Files thus stored were then processed by the program ATD, described below.

B ATD Software.

The arrival time data (*.dat) is read into the program along with any chopper data present (*.tim). If chopper data is present then the leading edge of the pulse occurring before the maximum in the ATD data can be used as the t=0 point. The average background signal is then calculated by computing the average signal of the data between the trigger point and the t=0 point (the beam passes through the second chopper pulse recorded due to the delay in triggering the nozzle). The range of data points used in calculating the beam temperature is then selected. All data points on the leading edge of the ATD that have intensity at least 5% above the background signal level are included in the analysis. These points are then transformed from the time domain to the velocity domain and the v^2 term of equation 11-1 is divided out. The log of the intensity is then taken and the data is least squares analysed, yielding the beam temperature. As the value of u is not known accurately from the ATD the values of u and T are refined in an iterative manner. The theoretical ATD is then calculated and both distributions are plotted on the screen of the PC-XT in high resolution (EGA), along with a summary of the analysis.

The fortran source contains over 800 lines of code and hence will not be included in this thesis. The program was based on a modular design that enabled further routines to be added without disturbing existing code.

C Results.

A sample output of the ATD program is shown in Figure 11.4 for Ar at a nozzle-skimmer distance of 32 mm, 700 torr backing pressure, 280 Hz chopper speed, 10 Hz source repetition rate, and 100 averages. Typical temperatures obtained for the gases H_2, He and Ar were 10 K, 10 K, and 2 K, respectively. The particular example shown in Figure 11.4 is a nearly isentropic expansion with 85% of the initial thermal (300 K) energy included in the combination of kinetic energy along the axis and random molecular motion (as measured by the beam temperature). Experiments using seeded beams have yet to be completed, however initial results are encouraging; with translational temperatures approaching that of the diluent gas.

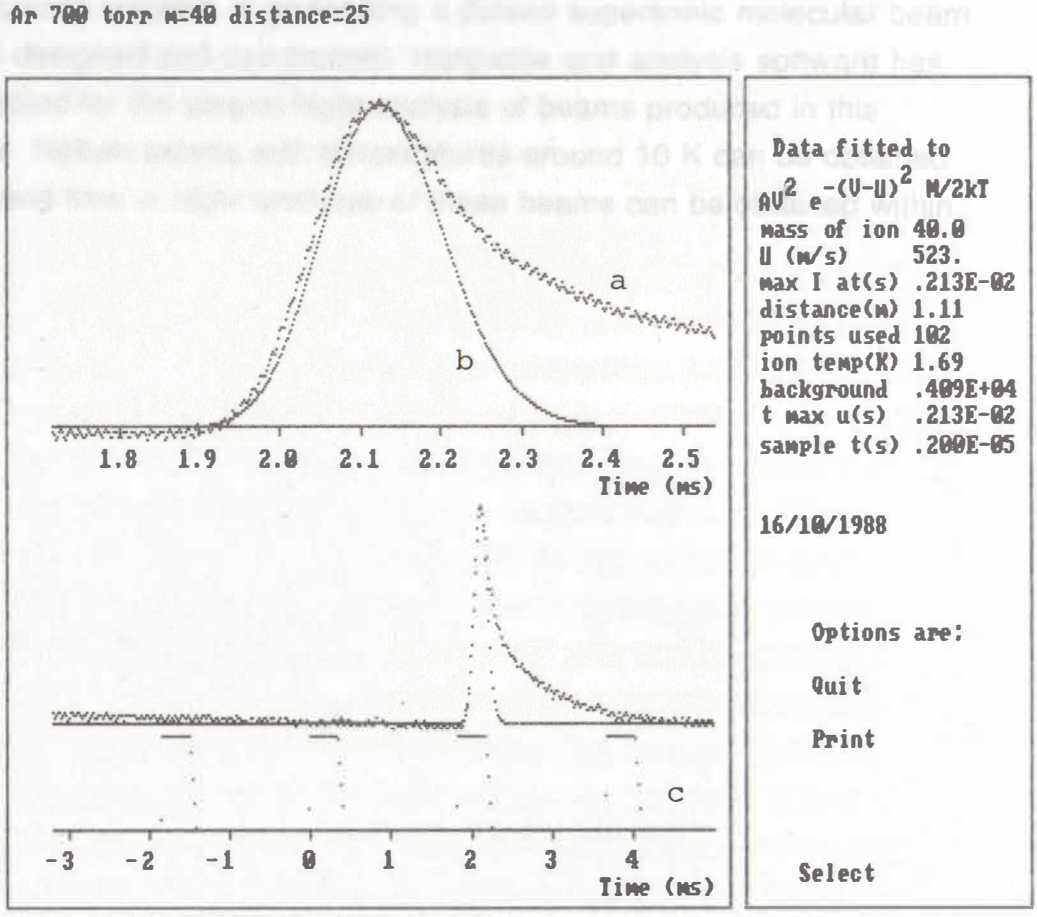

Figure 11.4 Sample output of ATD program.

Conditions were:

700 Torr nozzle backing pressure (Ar)
280 Hz chopper speed
10 Hz source repetition rate
100 averages

Trace a: Experimental Arrival Time Distribution
Trace b: Fitted curve
Trace c: Optical switch output

11.4 Summary

A device capable of generating a pulsed supersonic molecular beam has been designed and constructed. Hardware and analysis software has been installed for the time-of-flight analysis of beams produced in this apparatus. Helium beams with temperatures around 10 K can be obtained routinely and time of flight analyses of these beams can be obtained within minutes.

CHAPTER 12

CONCLUSION

From the information presented here it is apparent that although it is not possible to calculate the entire potential surface for reactions involving several atoms, the calculation of the critical points corresponding to the intermediates, transition states and products can reveal a great deal about the reaction. If the reaction can proceed with no energy barrier then the reaction rate is dominated by dynamical effects such as the rate of crossing the centrifugal barrier in a dipole - dipole potential curve. From these studies it is apparent that the level of theory is of critical importance to the quality of the results obtained. The results at the Hartree-Fock level are not of sufficient accuracy to draw any conclusion from them and inclusion of correlation effects to quite a high level is necessary before the calculations may be used for more quantitative analysis of the results.It would appear that it is desirable to apply the highest level of theory to such problems rather than use a carefully selected basis set with moderate inclusion of correlation effects to e.g. MP2 level in the hope that cancellation of systematic errors will produce meaningful results. This means that considerable computer time and disk space are needed for a reasonable calculation. Currently it is not feasible for most experimenters without access to large computer facilities to do calculations at any high level of theory, but this is changing rapidly. The information gained from the ab-initio studies is of great help to the experimenter and modeller and hence such studies are definitely worthwhile where possible. From the experimental viewpoint any study of a reactive molecule is a major undertaking, even with the growing arsenal of experimental weapons available to the physical chemist and hence any information on the potential energy surface is likely to be of benefit to the experimentalist.

The potential energy surface of the reaction between NH_2 and NO has been studied using ab-initio methods, in order to provide data for

modeling this reaction and to suggest reasons for the discrepancies evident in the literature. Our results are consistent with N_2 and H_2O as the major products with the channel to N_2H + OH (N_2 + OH + H) as, at most, a secondary pathway, in agreement with the most recent determinations of the branching coefficient. Despite the large amount of rearrangement needed to form N2 + H2O from the reactants, the MP4SDQ/6-31G*//HF/6-31G* results suggest these products can be formed without significant energy barriers. H atom tunneling is likely to be an important factor on surfaces such as these. The minimum energy structure for nitrosamide was found to be that with the H atoms out of the NNO plane, whereas previous studies did not seem to have considered this possibility or used a particular level of theory that would be expected to lead to a planar structure. The non-planar structure has some tentative supporting evidence from recent matrix isolation experiments where the observed spectrum could be explained as a combination of a site effect and inversion doubling. The optimised HF/6-31G* structure of the related molecule, Nitramide, is in excellent agreement with the experimentally determined structures. Both the reactions of NH_2 with NO and NO_2 show an anomalous difference of a factor of two between the rate constants determined in discharge flow experiments and those measured in flash photolysis systems. This difference has in the past been assigned to the formation of a stable intermediate which can diffuse out of the viewing region before dissociating back to reactants in a flash experiment, but which can redissociate on the timescales of the discharge experiments. From the experimental evidence and calculations arising from the ab-initio data this would appear unlikely for the reaction of NH_2 + NO but could occur for the corresponding reaction with NO_2. There is thus scope for further studies to determine the longevity of the intermediates and the exact nature of the products for both these reactions.

The ab-initio studies in chapter 5 of the potential energy surfaces for the reactions of NH + NO and NO_2 predict that the reaction with NO can proceed without barriers to N_2O and H or with a small or zero barrier to N_2 + OH. The reaction with NO2 is predicted to proceed with an energy barrier and is thus expected to be slower as observed. The experimental studies suggest (mostly from inference) that the major products of the NH + NO reaction are N_2 + OH rather than the favoured ab-initio products of N_2O + H. This may be attributed to dynamical processes occurring on the surface, although experimental confirmation of the products needs to be established.

The absolute values of the rates measured are in accord with the theoretical predictions and for NH + NO the temperature dependence is that expected, for the reaction with NO_2 it is not. The ab-initio data for NH + NO_2 is consistent with a reaction that exhibits a positive temperature dependence rather than the observed negative dependence. The possibility of other channels not considered in the $HNNO_2$ PES can not be discounted as the source of the difference and further studies are continuing.

Chapter 6 describes the experimental studies on the kinetics of the reactions of NH + NO and NO_2. The temperature dependences for both reactions between 270 and 380 K and the effects of variation of the nature of the third body were investigated. For NH + NO the reaction exhibited no significant temperature dependence as expected for a reaction whose rate is determined by the rate of crossing the centrifugal barrier of a dipole - dipole potential. The reaction with NO_2 is significantly slower than that expected from the dipole - dipole capture rates and exhibited a negative temperature dependence. The rates measured for both reactions were not affected by altering the nature of the third body.

The prompt emissions resulting from the 193 nm photolysis of diborane were recorded and analysed in chapter 7. The assignment was based on the observed power dependence of the emission intensity on the incident laser power.

The emissions observed are:

B atom $^2S \rightarrow {}^2P$ 208.9 nm

B atom $^2D \rightarrow {}^2P$ 249.7 nm

BH $A(^1\Pi) \rightarrow X(^1\Sigma)$ 433.0 nm

including the new transitions:

BH_2 320 - 340 nm

BH_3 254 - 326 nm

BH_3 366 - 388 nm

Both the BH and BH_2 bands appear to arise from absorption of two 193 nm photons and show extremely non-Boltzmann rotational populations in the upper state. The BH_3 bands arise from single photon absorption and are due to two different populations in the upper state (^1E"?), one of which is rotationally cold. This is the first observation of an electronic transition of BH_3 and the enthalpy for dimerisation at room temperature inferred from the low wavelength threshold of the bands is 149 kJ/mol, in excellent agreement

with the most recent experimental measurements, and the best ab-initio values. The spectroscopic transitions of BH_2 and BH_3 are important as these species are among the lightest polyatomics for which electronic spectra have been measured. The observation of emission from BH_2 suggests that the 193 nm photolysis of diborane should be an adequate source of BH_2 for kinetic studies and work along these lines is currently underway in this laboratory.

The MP4SDQ/6-31G*//HF/6-31G* ab-initio study of chapter 8 predicts the reaction between BH and NO to proceed at the dipole - dipole rate to products via the intermediate HBON. The two most likely product sets are HBO + N(^{2}D) and BO + NH although there has yet to be any experimental confirmation of either of these channels. The magnitude of the rate measured in chapter 9 for the reaction of BH + NO is consistent with a dipole - dipole capture rate as is the temperature dependence. Other reactions to be measured for the first time are the reactions of BH with ethylene, and upper limits established for O_2, CH_4, C_2H_6, and CO. The reaction chemistry of boron hydrides has been a largely unexplored field although a detailed knowledge of the elementary reactions involved is necessary for any serious attempt at understanding the combustion of Boron containing fuels. Chapter 10 presents an ab-initio study of the reactants, intermediates and products that could potentially be involved in the reaction of BH_2 and NO. This study indicates that a variety of intermediates could be formed directly or from rearrangement of one of the initial collision complexes with the channels to NH_2 + BO and HBO + NH favoured as the major product sets.

A differentially pumped pulsed supersonic molecular beam device has been constructed for the spectroscopic and mass spectrometric study of jet cooled species. Hardware and analysis software has been installed for the Time-of-Flight analysis of beams produced. Routine TOF analysis of the beams can take place within minutes of obtaining a suitable vacuum. Beams of translationally cold He atoms have been produced with temperatures of around 10 K. Further expansion to a crossed beam system is currently underway. These equipment expansions include facilities for IR diode laser studies of species present.as well as LIF. It is hoped that photolysis of mixtures in these beams will generate cold reaction intermediates which can subsequently be studied by the methods available before dissociation.

REFERENCES

Chapter 1:

1.1 W. Demtroder, *"Laser Spectroscopy"*, Springer Series in Chemical Physics, 5, (1982)

1.2 W. H. Green Jr, I. C. Chen and C. B. Moore, *Ber. Bunsenges. Phys. Chem.*, 92 (1988) 389.

1.3 M. J. Rosker, T. S. Rose and A. H. Zewail, *Chem. Phys. Lett.*, 146 (1988) 175.

1.4 E. J. Heller, *Acc. Chem. Res.*,14 (1981) 368.

1.5 P. R. Brooks, *Chem. Rev.*,88 (1988) 407.

1.6 R. J. Donovan, in *"Gas Kinetics and Energy Transfer"*, P. G. Ashmore and R. J. Donovan eds. Specialist Periodical Report. R. S. C. Lond, 4 (1981) 117.

1.7 H. M. Gillespie and R. J. Donovan, *Ann. Rep. Prog. Chem. Sect. C.*, 78 (1981) 173.

1.8 D. G. Truhlar, R. Steckler and M. S. Gordon, *Chem. Rev.*, 87 (1987) 217.

1.9 H. B. Schlegel, in *"Advances in Chem. Phys."*, I. Prigogine and S. A. Rice eds., 67 (1987) 249.

1.10 T. Clark, *"A Handbook of Computational Chemistry"*, J. Wiley & Sons, (1985).

1.11 W. J. Hehre, L. Radom, P. vR. Schleyer and J. A. Pople, *"Ab-Initio Molecular Orbital Theory"*, John Wiley & Sons, (1986).

1.12 R. N. Zare, *Science*, 185 (1974) 739.

1.13 J. B. Anderson, in *"Molecular Beams and Low Density Gas Dynamics"*, P. P. Wegener Ed., M. Dekker, New York, (1966) 1.

1.14 D. H. Levy, *Ann. Rev. Phys. Chem.*,31 (1982) 197; R. E. Smalley, L. Wharton and D. H. Levy, *Acc. Chem. Res.*, 10 (1977) 139.

1.15 J. C. Polanyi, *Angew. Chem. Int. Ed. Engl.* 26 (1987) 952.

1.16 Y. T. Lee, *Angew. Chem. Int. Ed. Engl.* 26 (1987) 939.

1.17 W C Gardiner ed., *"Combustion Chemistry"*, Springer-Verlag, New York, 1984.

1.18 W. M. Jackson, *J. Photochem*, 17 (1981) 509.

Chapter 2:

2.1 W. Jeffers, *Chem & Ind.*, April 8, 1961.

2.2 J. W. Mellors, *"Comprehensive Treatise on Inorganic and Theoretical Chemistry"*, Supplement Series Vol V, Supplement I, pp 65-68, Longman (1980).

Chapter 3:

3.1 I. N. Levine, *"Quantum Chemistry"*, Allyn and Bacon Inc., Massachussetts, Third Ed., 1983.

3.2 A. Szabo and N. S. Ostlund, *"Modern Quantum Chemistry"*, Macmillan Publishing Co. Inc., New York, 1982.

3.3 J. S. Binkley, M. J. Frisch, D. J. DeFrees, K. Raghavachari, R. A. Whiteside, H. B. Schlegel, E. M. Fluder and J. A. Pople, *Gaussian 82*, Carnegie-Mellon University, Pittsburgh (1983).

3.4 L. Radom, W. J. Hehre and J. A. Pople, *J. Chem. Soc. (A)*, (1971) 2299.

3.5 J. A. Pople, B. T. Luke, M. J. Frisch and J. S. Binkley, *J. Phys. Chem.*, 89 (1985) 2198.

3.6 J. A. Pople, M. J. Frisch, B. T. Luke and J. S. Binkley, *Int. J. Quant. Chem., Quant. Chem. Symp.*, 17 (1983) 307.

3.7 J. S. Binkley and M. J. Frisch, *Int. J. Quant. Chem., Quant. Chem. Symp.*, 17 (1983) 331.

3.8 J. A. Pople, H. B. Schlegel, R. Krishnan, D. J. DeFrees, J. S. Binkley and J. A. Pople, *Int. J. Quant. Chem., Quant. Chem. Symp.*, 15 (1981) 269.

3.9 J. A. Pople, . S. Binkley and R Seeger. *Int. J. Quant. Chem., Quant. Chem. Symp.*, 10 (1976) 1.

3.10 R. Ditchfield and K. Seidman, *Chem. Phys. Lett.*, 54 (1978) 57.

3.11 D. J. DeFrees, B. A. Levi, S. K. Pollack, W. J. Hehre, J. S. Binkley and J. A. Pople, *J. Am. Chem. Soc.*, 101 (1979) 4085; 102 (1980) 2513.

3.12 P. C. Hariharan and J. A. Pople, *Theor. Chim. Acta.*, 28 (1973) 213.

3.13 D. J. DeFrees and A. D. McLean, *J. Chem. Phys.*, 82 (1985) 333.

Chapter 4:

4.1 C. H. Bamford, *Disc. Faraday Soc.*, 35 (1939) 568.

4.2 A. Serewicz and W. A. Noyes, *J. Phys. Chem.*, 63 (1959) 843.

4.3 R. Srinivasan, *J. Phys. Chem.*, 64 (1960) 579.

4.4 C. P. Fenimore and G. W. Jones, *J. Phys. Chem.*, 65 (1961) 298.

4.5 S. Gordon, W. Mulac and P. Nangia, *J. Phys. Chem.*, 75 (1971) 2087.

4.6 L. Radom, W. J. Hehre and J. A. Pople, *J. Amer. Chem. Soc.*, 93 (1971) 289.

4.7 M. Gehring, K. Hoyermann, H. Schacke and J. Wolfrum, *Fourteenth Symp. (Int.) on Combustion*, (The Combustion Institute , Pittsburgh, 1972) 99.

4.8 G. Hancock, W. Lange, M. Lenzi and K. H. Welge, *Chem. Phys. Lett.*, 33 (1975) 168.

4.9 R. Lesclaux, P. V. Khe, P. Dezauzier and J. C. Soulignac, *Chem. Phys. Lett.*, 35 (1975) 493.

4.10 R. K. M. Jayanty, R. Simonaitis and J. Heicklen, *J. Phys. Chem.*, 80 (1976) 433.

4.11 R. K. Lyon, *Int. J. Chem. Kin.*, 8 (1976) 315.

4.12 C. Thomson, D. Provan and S. Clark, *Int. J. Quant. Chem, Quant. Biology Symp.*, 4 (1977) 205.

4.13 R. Cimiraglia, M. Persico and J. Tomasi, *J. Phys. Chem.*, 81 (1977) 1876.

4.14 O. M. Sarkisov, S. G. Cheskis and E. A. Sviridenkov, *Izvestiya Akademii Nauk SSSR, Seriya Khimicheskaya*, (Eng. Trans.) 11 (1978) 2612.

4.15 R. K. Lyon and D. Benn, *Seventeenth Symp. (Int.) on Combustion*, (The Combustion Institute , Pittsburgh, 1979) 601.

4.16 W. Hack, H. Schacke, M. Schroter and H. Gg. Wagner. *Seventeenth Symp. (Int.) on Combustion*, (The Combustion Institute , Pittsburgh, 1979) 505.

4.17 J. A. Miller, M. C. Branch and R. J. Kee, *Comb. and Flame*, 43 (1981) 853.

4.18 T. R. Roose, R. K. Hanson and H. C. Kruger, *Eighteenth Symp. (Int.) on Combustion*, (The Combustion Institute , Pittsburgh, 1981) 853.

4.19 L. J. Steif, W. D. Brobst, D. F. Nava, R. P. Borkowski and J. V. Michael, *J. Chem. Soc. Faraday Trans. II.*, 78 (1982) 1391.

4.20 J. A. Silver and C. E. Kolb, *J. Phys. Chem.*, 86 (1982) 3240.

4.21 L. J. Steif, W. D. Brobst, D. F. Nava, R. P. Borkowski and J. V. Michael, *Nasa Technical Memorandum 83928*, April 1982.

4.22 P. Andresen, A. Jacobs, C. Kleinermanns and J. Wolfrum, *Nineteenth Symp. (Int.) on Combustion*, (The Combustion Institute , Pittsburgh, 1982) 11.

4.23 C. J. Casewit and W. A. Goddard III, *J. Amer. Chem. Soc.*, 104 (1982) 3280.

4.24 J. A. Miller, M. D. Smooke, R. M. Green and R. J. Kee, *Comb. Sci. and Tech.*, 34 (1983) 149.

4.25 A. R. Whyte and L. F. Phillips, *Chem. Phys. Lett.*, 102 (1983) 451.

4.26 J. B. Jeffries, J. A. McCaulley and F. Kaufman, *Chem. Phys. Lett.*, 106 (1984) 111.

4.27 T. K. Ha, M. T. Nguyen and P. Ruelle, *J. Mol. Struct. (Theochem).*, 109 (1984) 339.

4.28 K. H. Gericke, L. M. Torres and W. A. Guillory, *J. Chem. Phys.*, 80 (1984) 6134.

4.29 H. Abou-Rachid, C. Pouchan and M. Chaillet, *Chem. Phys.*, 90 (1984) 243.

4.30 C. F. Melius and J. S. Binkley, *Twentieth Symp. (Int.) on Combustion*, (The Combustion Institute , Pittsburgh, 1984) 575.

4.31 T. Dreier and J. Wolfrum, *Twentieth Symp. (Int.) on Combustion*, (The Combustion Institute , Pittsburgh, 1984) 695.

4.32 H. Abou-Rachid and C. Pouchan, *J. Mol. Struct. (Theochem)*, 121 (1985) 299.

4.33 R. G. Gilbert, A. R. Whyte and L. F. Phillips, *Int. J. Chem. Kin.*, 18 (1986) 721.

4.34 J. L. Hall, D. Zeitz, J. W. Stephens, J. V. V. Kasper, G. P. Glass, R. F. Curl and F. K. Tittel, *J. Phys. Chem.*, 90 (1986) 2501.

4.35 M. A. Kimball-Linne and R. K. Hanson, *Comb. and Flame*, 64 (1986) 337.

4.36 J. A. Harrison, A. R. Whyte and R. G. A. R. Maclagan, *Chem. Phys. Lett.*, 135 (1986) 6714.

4.37 D. A. Dolson, *J. Phys. Chem.*, 90 (1986) 6714.

4.38 L. F. Phillips, *Chem. Phys. Lett.*, 135 (1987) 269.

4.39 J. N. Crowley and J. R. Sodeau, *J. Phys. Chem.*, 91 (1987) 2024.

4.40 J. A. Silver and C. E. Kolb, *J. Phys. Chem.*, 91 (1987) 3713.

4.41 J. A. Harrison, A. R. Whyte and R. G. A. R. Maclagan, *J. Phys. Chem.*, 91 (1987) 6683.

4.42 J. N. Crowley, Ph.D. Thesis, University of East Anglia, (1988).

4.43 H. Kurasawa and R. Lesclaux, *Chem. Phys. Lett.*, 66 (1979) 602.

4.44 T. X. Xiang, L. M. Torres and W. A. Guillory, *J. Chem. Phys.*, 83 (1985) 1623.

4.45 C. A. Beevers and A. F. Trotman-Dickenson, *Acta. Cryst.*, 10 (1957) 34.

4.46 K. Kaya, K. Kuwata and S. Nakaguma, *Bull. Chem. Soc. Japan*, 37 (1964) 1055.

4.47 J. Stals, C. G. Barraclough and A. S. Buchanan, *Trans. Faraday Soc.*, 65 (1969) 904.

4.48 J. K. Tyler, *J. Mol. Spectry.*, 11 (1963) 39.

4.49 M. Nonella, R. P. Muller and J. R. Huber, *J. Mol. Spectry.*, 112 (1985) 142.

4.50 E. N. P. Spence, New Zealand Meteorological Service. Personal Communication. (1988).

4.51 J. S. Binkley, M. J. Frisch, D. J. DeFrees, K. Raghavachari, R. A. Whiteside, H. B. Schlegel, E. M. Fluder and J. A. Pople. *Gaussian 82,* Carnegie-Mellon University, Pittsburgh (1983).

4.52 E. B. Wilson, J. C. Decius and P. C. Cross, *"Molecular Vibrations"*, McGraw - Hill, New York, 1955.

4.53 C. A. Reynolds and C. Thomson, *J. Chem. Soc. Faraday Trans. II*, 83 (1987) 485.

4.54 U. Kaldor and I. Shavitt, *J. Chem. Phys.*, 45 (1966) 888.

4.55 R. M. Stevens, *J. Chem. Phys.*, 55 (1971) 1725.

4.56 A. Daoudi and C. Pouchan, *J. Mol. Struct.*, 92 (1983) 31.

4.57 D. J. DeFrees, B. A. Levi, S. K. Pollack, W. J. Hehre, J. S. Binkley and J. A. Pople, *J. Amer. Chem. Soc.*, 101 (1979) 4085; 102 (1980) 2513.

4.58 D. J. DeFrees and A. D. McLean, *J. Chem. Phys.*, 82 (1985) 333.

4.59 L. A. Curtiss, D. L. Drapcho and J. A. Pople, *Chem. Phys. Lett.*, 103 (1984) 437.

4.60 R. K. Lyon, U. S. Patent No. 3,900.544, August 1975.

4.61 R. A. Perry and D. L. Siebers, *Nature,* 324 (1986) 657.

4.62 E. Tannenbaum, R. J. Myers and W. D. Gwinn, *J. Chem. Phys.*, 25 (1956) 42.

4.63 R. L. Collin and W. N. Lipscomb, *Acta Cryst.*, 4 (1951) 10.
4.64 P. R. Raddemaker and W. Luttke, *Ber. Bunsenges Phys. Chem.*, 78 (1974) 1353.
4.65 E. C. Hunter and J. R. Partington, *J. Chem. Soc.*, (1933) 309.

Chapter 5:

5.1 L. F. Phillips, *J. Chem. Soc., Faraday Trans. II*, 83 (1987) 857.
5.2 J. S. Binkley, M. J. Frisch, D. J. DeFrees, K. Raghavachari, R. A. Whiteside, H. B. Schlegel, E. M. Fluder and J. A. Pople, *Gaussian 82*, Carnegie-Mellon University, Pittsburgh, Pa., 1983.
5.3 J. N. Mulvihill and L. F. Phillips, *Chem. Phys. Lett.*, 35 (1975) 327.
5.4 A. R. Whyte and L. F. Phillips, *J. Phys. Chem.*, 88 (1984) 5670.
5.5 P. Marshall, A. Fontijn and C. F. Melius, *J. Chem. Phys.*, 86 (1987) 5540.
5.6 J. A. Silver and C. E. Kolb, *J. Phys. Chem.*, 91 (1987) 3713.
5.7 C. F. Melius and J. S. Binkley, Twentieth Symp. (Int.) on Combustion, (The Combustion Institute, Pittsburgh, 1984) 575.
5.8 T. Fueno, M. Fukuda and K. Yokoyama, *Chem. Phys.*, 124 (1988) 265.

Chapter 6:

6.1 I. Hansen, K. Hoinghaus, C. Zetsch and F. Stuhl, *Chem. Phys. Lett.*, 42 (1976) 370.
6.2 J. W. Cox, H. H. Nelson and J. R. McDonald, *Chem. Phys.*, 96 (1985) 175.
6.3 S. Gordon, W. Mulac and P. Nangia, *J. Chem. Phys.*, 75 (1971) 2087.
6.4 C. Zetsch and F. Stuhl, *Ber. Bunsenges Physik. Chem.*, 82 (1978) 836.
6.5 W. Hack, H. Kurzke and H. G. Wagner, *J. Chem. Soc. Faraday Trans. I I*, 81 (1985) 949.
6.6 P. G. Pagsberg, J. Erikson and H. C. Christensen, *J. Phys. Chem.*, 83 (1979) 582.
6.7 C. Zetsch and F. Stuhl, *Ber. Bunsenges Phys. Chem.*, 85 (1981) 564.
6.8 G. M. Meaburn and S. Gordon, *J. Phys. Chem.*, 72 (1968) 1592.
6.9 M. Clerc, M. Schmidt, J. Hagege-Temman and J. Belloni, *J. Phys. Chem.*, 75 (1971) 2908.

6.10 A. G. Gaydon and H. G. Wolfhard, "*Flames*", Chapman and Hall, London, 4th Ed, (1976)

6.11 R. W. B. Pearse and A. G. Gaydon, *"The Identification of Molecular Spectra"*, Chapman and Hall, London, 4th Ed, (1976)

6.12 C. F. Melius and J. S. Binkley, *Twentieth Symp. (Int.) on Combustion*, (The Combustion Institute, Pittsburgh, 1984) 575.

6.13 T. Fueno, M. Fukuda and K. Yokoyama, *Chem. Phys.*, 124 (1988) 265.

6.14 P. Marshall, A. Fontijn and C. F. Melius, *J. Chem. Phys.*, 86 (1987) 5540.

6.15 D. W. Scott, G. D. Oliver, M. E. Gross, W. N. Hubbard and H. M. Huffman, *J. Am. Chem. Soc.*, 71 (1949) 2293.

6.16 C. Willis, R. A. Back and J. G. Purdon, *Int. J. Chem. Kin.*, 9 (1977) 787.

6.17 R. K. Hanson and S. Salimian, in *"Combustion Chemistry"*, W. C. Gardiner Jr, ed. Springer-Verlag, New York, 1984.

6.18 L. F. Phillips, *J. Chem. Soc. Faraday Trans. II*, 83 (1987) 857.

6.19 J. N. Mulvihill and L. F. Phillips, *Chem. Phys. Lett.*, 35 (1975) 327.

6.20 A. R. Whyte and L. F. Phillips, *J. Phys. Chem.*, 88 (1984) 5670.

6.21 J. A. Harrison, A. R. Whyte and L. F. Phillips, *Chem. Phys. Lett.*, 129 (1986) 346.

Chapter 7:

7.1 R. D. Kenner, F. Rohrer, R. K. Browarzik, A. Kaes and F. Stuhl, *Chem. Phys.*, 118 (1987) 141.

7.2 V. M. Donnelly, A. P. Baronavski and J. R. McDonald, *Chem. Phys.*, 43 (1979) 271.

7.3 P. Lindberg, D Raybone, J. A. Salthouse, T. M. Watkinson and J. C. Whitehead, *Mol. Phys.*, 62 (1987) 1297.

7.4 R. D. Kenner, R. K. Browarzik and F. Stuhl, *Chem. Phys.*, 121 (1988) 457.

7.5 K. Kawaguchi, J. E. Butler, C. Yamada, S. H. Bauer, T. Minowa, H. Kanamori and E. Hirota, *J. Chem. Phys.*, 87 (1987) 2438.

7.6 G.Herzberg and J. W. C. Johns, *Proc. Roy. Soc. A*, 298 (1966) 142 ; M. Peric, S. D. Peyerimhoff and R. J. Buenker, *Can. J. Chem.*, 59 (1981) 1318.

7.7 E. Blum and G. Herzberg, *J. Phys. Chem.*, 41 (1937) 91.

7.8 W. C. Price, *J. Chem. Phys.*, 16 (1948) 894 .

7.9 T. Hirata and H. E. Gunning, *J. Chem. Phys.*, 27 (1957) 477.

7.10 W. C. Kreye and R. A. Marcus, *J. Chem. Phys.*, 37 (1962) 419.
7.11 M. Bufalini and J. E. Todd, *J. Phys. Chem.*, 72 (1968) 3367.
7.12 J. H. Clark and R. G. Anderson, *Appl. Phys. Lett.*, 32 (1978) 46.
7.13 B. Ruscic, C. A. Mayhew and J. Berkowitz, *J. Chem. Phys.*, 88 (1988) 5580.
7.14 M. P. Irion and K. L. Kompa, *J. Chem. Phys.*, 76 (1982) 2338.
7.15 M. P. Irion and K. L. Kompa, *J. Photochem.*, 32 (1986) 139.
7.16 J. W. C. Johns, F. A. Grimm and R. F. Porter, *J. Mol. Spectry.*, 22 (1967) 435.
7.17 J. Dufayard and O. Nedelec, *J. Chem. Phys.*, 69 (1978) 4708; G. H. F. Diercksen, N. E. Gruner, J. R. Sabin and J. Oddershede, *Chem. Phys.*, 115 (1987) 15.
7.18 JANAF Thermochemical Tables, 2nd ed. D. R. Stull, H. Prophet et al., NSRDS-NBS37, Washington D. C., 1971.
7.19 J. A. Pople, B. T. Luke, M. J. Frisch and J. S. Binkley, *J. Phys. Chem.*, 89 (1985) 2198.
7.20 M. Page, G. F. Adams, J. S. Binkley and C. F. Melius, *J. Phys. Chem.*, 91 (1987) 2675.
7.21 G. Herzberg, *"Molecular Spectra and Molecular Structure"*, vol 1, *" Spectra of Diatomic Molecules"*, (1950) 2nd Edition, Van Nostrand Reinhold Company N. Y., p.208.
7.22 T. Ni, S. Yu, X. Ma and F. Kong, *Chem. Phys. Lett.*, 126 (1986) 413.
7.23 A. Hofzumahaus and F. Stuhl, *J. Chem. Phys.*, 82 (1985) 5519.
7.24 H. K. Haak and F. Stuhl, *J. Phys. Chem.*, 88 (1984) 3627.
7.25 J. A. Harrison, R. F. Meads and L. F. Phillips, *Chem. Phys. Lett.*, 148 (1988) 125.
7.26 G. W. Mappes, S. A. Fridmann and T. P. Fehlner, *J. Phys. Chem.*, 74 (1970) 3307.
7.27 G. Herzberg, *"Molecular Spectra and Molecular Structure"*, vol 3, *" Electronic Spectra of Polyatomic Molecules"*, (1966), D Van Nostrand Company N.Y., p.513.
7.28 W. C. Swope, H. F. Schaefer III and D. R. Yarkony, *J. Chem. Phys.*, 73 (1980) 407.

Chapter 8:

8.1 J. S. Binkley, M. J. Frisch, D. J. DeFrees, K. Raghavachari, R. A. Whiteside, E. M. Fluder and J. A. Pople, *"Gaussian 82"*; Carnegie-Mellon University, Pittsburgh, Pa., (1983).

8.2 D. J. DeFrees, K. Raghavachari, H. B. Schlegel and J. A. Pople, *J. Am. Chem. Soc.*, 104 (1982) 5576.

8.3 D. J. DeFrees and A. D. McLean, *J. Chem. Phys.*, 82 (1985) 333.

8.4 Y. Kawashima, K. Kawaguchi and E. Hirota, *Chem. Phys. Lett.*, 131 (1986) 205.

8.5 Y. Kawashima, Y. Endo, K. Kawaguchi and E. Hirota, *Chem. Phys. Lett.*, 135 (1987) 441.

8.6 J. A. Harrison and R. G. A. R. Maclagan, *Chem. Phys. Lett.*, 146 (1988) 243.

Chapter 9:

9.1 A. G. Gaydon and H. G. Wolfhard, *"Flames, Their Structure, Radiation and Temperature"*. Second Edition, Chapman and Hall, London, (1970).

9.2 C. W. Hand and L. K. Derr, *Inorg. Chem.*, 13 (1974) 339.

9.3 G. K. Anderson and S. H. Bauer, *J. Phys. Chem.*, 81 (1977) 1146.

9.4 D. B. Borchardt, J. G. Choi, K. Suzuki and S. H. Bauer, *J. Chem. Phys.*, 88 (1988) 6282.

9.5 W. Roth, *J. Chem. Phys.*, 28 (1958) 668.

9.6 L. Pasternak, R. J. Balla and H. H. Nelson, J. Phys. Chem., 92 (1988) 1200.

9.7 M. P. Irion and K. L. Kompa, *J. Chem. Phys.*, 76 (1982) 2338.

9.8 J. DeHaven, M. T. O'Connor and P. Davidovits, *J. Chem. Phys.*, 75 (1981) 1741.

9.9 A. Brzychcy, J. De Haven, A. T. Prengel and P. Davidovits, *Chem. Phys. Lett.*, 60 (1978) 102.

9.10 G. J. Green and J. L. Gole, *Chem. Phys. Lett.*, 69 (1980) 45.

9.11 J. K. Rice, N. J. Caldwell and H. H. Nelson, *J. Phys Chem.*, submitted for publication.

9.12 J. A. Harrison, R. F. Meads and L. F. Phillips, *Chem. Phys. Lett.*, 150 (1988) 299.

9.13 Y. Kawashima, K. Kawaguchi and E. Hirota, *Chem. Phys. Lett.*, 131 (1986) 205.

9.14 Y. Kawashima, Y. Endo, K. Kawaguchi and E. Hirota, *Chem. Phys. Lett.*, 135 (1987) 441.

9.15 W. M. Shaub and M. C. Lin, *NBS Special Publication*, 561 (1979) 1249.

Chapter 10:

10.1 G. Herzberg and J. W. C. Johns, *Proc. Roy. Soc. A*, 298 (1966) 142.

10.2 J. A. Harrison, R. F. Meads and L. F. Phillips, *Chem. Phys. Lett.*, 150 (1988) 299.

10.3 J. K. Rice, N. J. Caldwell and H. H. Nelson, *J. Phys. Chem.*, submitted for publication.

10.4 L. Pasternak, R. J. Balla and H. H. Nelson, *J. Phys. Chem.*, 92 (1988) 1200.

10.5 J. A. Harrison and R. G. A. R. Maclagan, *Chem. Phys. Lett.*, 146 (1988) 243.

10.6 Y. Kawashima, K. Kawaguchi and E. Hirota, *J. Chem. Phys.*, 87 (1987) 6331.

10.7 Y. Kawashima, K. Kawaguchi and E. Hirota, *Chem. Phys. Lett.*, 131 (1986) 205.

10.8 Y. Kawashima, Y. Endo, K. Kawaguchi and E. Hirota, *Chem. Phys. Lett.*, 135 (1987) 441.

Chapter 11:

11.1 A. Kantrowitz and J. Grey, *Rev. Sci. Instrum.*, 22 (1951) 328.

11.2 A. Kistiakowsky and W. P. Slichter, *Rev. Sci. Instrum.*, 22 (1951) 333.

11.3 J. B. Anderson, in *"Molecular Beams and Low Density Gas Dynamics"*, P. P. Wegener, ed., Marcel Dekker, New York, (1974) 4.

11.4 J. B. Anderson, R. P. Andres and J. B. Fenn, *Advances in Chem. Phys.*, 10 (1966), Ross ed., J. Wiley and Sons Ltd.

11.5 B. D. Kay, T. D. Raymond and J. K. Rice, *Rev. Sci. Instrum.*, 57 (1986) 2266.

11.6 H. S. Carman Jr., Ph.D. Thesis, Rice University, (1986).

"Notice all the computations, theoretical scribblings, and lab equipment, Norm . . . . Yes, curiosity killed these cats."